REAL-TIME ORBIT IMPROVEMENT FOR GPS SATELLITES

M. C. dos SANTOS

November 1995

TECHNICAL REPORT
NO. 178

REAL-TIME ORBIT IMPROVEMENT FOR GPS SATELLITES

Marcelo Carvalho dos Santos

Department of Geodesy and Geomatics Engineering
University of New Brunswick
P.O. Box 4400
Fredericton, N.B.
Canada
E3B 5A3

November 1995

© Marcelo Carvalho dos Santos, 1995

PREFACE

This technical report is a reproduction of a dissertation submitted in partial fulfillment of the requirements for the degree of Doctor of Philosophy in the Department of Geodesy and Geomatics Engineering, May 1995. The research was supervised by Dr. Petr Vaníček, and funding was provided by Brazil's Conselho Nacional de Desenvolvimento Científico e Tecnológico.

As with any copyrighted material, permission to reprint or quote extensively from this report must be received from the author. The citation to this work should appear as follows:

Santos, M. C. (1995). *Real-Time Orbit Improvements for GPS Satellites*. Ph.D. dissertation, Department of Geodesy and Geomatics Engineering, Technical Report No. 178, University of New Brunswick, Fredericton, New Brunswick, Canada, 125 pp.

ERRATUM

Equation (5.13), on page 64, and equation (III.25), on page 122, should read:

$$\underline{A} = -\frac{GM}{r^3}\left(\underline{I} - 3\,\frac{\underline{r}\;\underline{r}^T}{r^2}\right)$$

Abstract

Many geodetic GPS applications require orbits of better accuracy than the predicted ones broadcast by the satellites themselves. However, orbits of high quality are available to users. Their generation is based on GPS data collected by dedicated tracking networks. Nevertheless, these orbits are available only after an interval of several days following data collection. For real-time positioning applications, one currently depends on the broadcast orbits.

An alternative, real-time approach for orbit improvement is described here. This approach is designed to yield, in real-time, the best representation of orbits based on all available observations from a network of fiducial stations. The algorithm design is based on a unit, called the update step, which defines the length of the orbital arc over which the improvement takes place. The initial conditions computed in one orbital arc are propagated into the following one.

The algorithm was implemented based on the UNB DIPOP software package, which was further modified to allow network adjustment including correlations between simultaneously observed baselines. The principle of the method has been tested using data collected by a network of 8 stations in Canada and the U.S., which are part of the IGS network. The orbital arcs generated with the method have been compared among themselves, in a test of orbit repeatability to test the orbit internal consistency, and also with the IGS orbits, in a test of external consistency. A subset of the 8-station network has been processed constraining the orbits generated by the real-time algorithm to assess their effect in geodetic positioning. These tests aimed to assess the quality of the orbits generated with the proposed method.

The results show that the real-time orbits are at or below the 1 metre level 3drms. Their use in geodetic positioning yield baselines with relative error varying from 0.05 to 0.02 ppm, over baselines of hundreds of kilometres. This represents an improvement

of 1 order of magnitude over the broadcast orbits, the only ones presently available for real-time applications.

Contents

Abstract **ii**

List of Tables **viii**

List of Figures **ix**

Resumo (in Portuguese) **xi**

Acknowledgements **xiii**

List of Abbreviations **xv**

List of Symbols **xviii**

1 Introduction **1**

1.1 Literature review 1

1.2 Statement of the problem 8

1.3 Contributions of the research 11

1.4 Outline of the dissertation 11

2 Space and time coordinate systems **13**

2.1 Introduction 13

2.2 Time systems 14

2.2.1 Rotational times 14

2.2.2 Atomic times 15
2.2.3 Dynamical times 17
2.3 Geocentric coordinate systems 18
2.3.1 Definitions 18
2.3.2 Transformations 19
2.3.3 Orbital system 20
2.4 Satellite-centered coordinate system 22

3 The Global Positioning System 24
3.1 GPS observation equations 25
3.2 Errors and biases 28
3.2.1 Clock biases 29
3.2.2 Selective Availability and Anti-Spoofing 29
3.2.3 Atmospheric effects 30
3.2.4 Antenna and receiver errors 31
3.2.5 Geometrical configuration of the satellites 32
3.2.6 Ambiguity and cycle slips 33

4 Modelling and solving the equations of motion 38
4.1 Introduction to the problem 38
4.2 Mathematical representation of the acceleration producing forces . . . 40
4.2.1 Earth's gravitational field 40
4.2.2 Solar, lunar, and planetary gravitational perturbation 43
4.2.3 Solar radiation pressure perturbation 43
4.2.4 Solid earth and ocean tidal perturbation 50
4.2.5 Relativistic perturbation 52
4.2.6 Other perturbations 52
4.2.7 Force model accuracy level 54
4.3 Solution of the equations of motion 54

4.3.1 Methods for numerical integration 55
4.3.2 Methods for first-order differential equations 56
4.3.3 Methods for second-order differential equations 57
4.3.4 Multi-step starting procedures 59

5 Real-time GPS orbit improvement 61

5.1 Principles of orbit improvement 61
5.1.1 Least-squares solution 65
5.1.2 Traditional approach for GPS orbit improvement 69
5.2 Real-time orbit improvement 71
5.2.1 The real-time algorithm 71
5.2.2 The screening of observations 74
5.3 A real-time orbit service 75
5.3.1 Monitor stations 75
5.3.2 Master Center 75
5.3.3 The transmitted information 76

6 Test of the algorithm and discussion of results 77

6.1 Assessing orbit precision and accuracy 77
6.2 Software implementation 80
6.3 Data set description 81
6.4 Testing the real-time orbits 85
6.4.1 Effect on geodetic positioning 86
6.4.2 Comparison with IGS orbits 90
6.5 Other tests 92
6.5.1 Relative error in baseline length 92
6.5.2 Orbit repeatability 93
6.5.3 Effect of cycle slips and predicted EOP 93

7 Conclusions and recommendations **97**

7.1 Summary and conclusions 97

7.2 Recommendations for future work 98

References **100**

Appendices

I Transformation between Keplerian elements and the OR-system **112**

I.1 Keplerian elements to the OR-system 112

I.2 OR-system to Keplerian elements 113

II Program PREDICT **115**

III Partial derivatives **118**

III.1 Station coordinates 119

III.2 Orbital parameters 119

III.3 Tropospheric zenith delay correction 123

III.4 Ambiguity 123

III.5 Misclosure 124

List of Tables

1.1 Relative error in baseline as a function of orbital error 2

1.2 Software suites with capability for orbit improvement. 8

2.1 Relationship between TAI, GPST and UTC since the beginning of GPS Time until July 1994. 16

3.1 Number of cycles added to L1 and L2 undifferenced carrier phases. . 35

4.1 Nominal mass of Block I GPS satellites. 48

5.1 Typical characteristics of short-arc and long-arc approaches. 69

6.1 IGS stations used in our analysis. 83

6.2 IGS station coordinates in the ITRF92 (epoch 1994.0) (F= fiducial stations). 83

6.3 Baseline lengths, based on ITRF92 (1994.0) input coordinates. 83

6.4 Receivers and antenna heights. 84

6.5 Comparison with IGS (values in metres). 92

6.6 Orbit repeatability (values in metres). 93

6.7 Nominal discontinuities (cm) in Lc caused by cycle slips. 94

List of Figures

2.1 Keplerian orbital elements 21

2.2 Equatorial close-up on i, Ω, ϖ and f 22

2.3 Satellite-centered coordinate system 23

3.1 Cycle slips detected by the ionospheric residual 34

3.2 Rate of change of the ionospheric residual 35

3.3 Cycle slip on the ionosphere-free linear combination double difference 36

3.4 Cycle slip on the wide lane linear combination double difference . . . 37

4.1 Satellite coordinate system 44

4.2 Störmer-Cowell; X-coordinate error 59

5.1 Difference between predicted orbit and reference orbit 66

5.2 Difference between improved orbit and reference orbit 67

5.3 Long-arc and short-arc strategies 70

5.4 Real-time orbit improvement flow-chart 72

6.1 Comparing overlapping arcs: (a) orbit repeatability; (b) extrapolation 78

6.2 North-American network (based on IGS stations). 82

6.3 Deviation of latitude and longitude with respect to ITRF92 87

6.4 Deviation of height with respect to ITRF92 88

6.5 Deviation of baseline components with respect to ITRF92 89

6.6 Relative error in baseline length 90

6.7 Orbital residuals with respect to IGS – PRN 3 91

6.8 Orbit repeatability for PRN 26 96

6.9 Percentage increase in orbit 3drms caused by cycle slips. 96
II.1 Program PREDICT flowchart 117

Resumo (in Portuguese)

Muitas das aplicações geodésicas requerem órbitas com precisão maior do que aquelas transmitidas pelos satélites GPS. Atualmente, órbitas de alta qualidade são determinadas a partir de dados coletados por redes geodésicas dedicadas a este fim. Porém, estas órbitas tornam-se disponíveis apenas após alguns dias. Aplicações em tempo real contam somente com as efemérides transmitidas.

Um método alternativo baseado na determinação da órbita dos satélites em tempo real é descrito nesta Dissertação de Doutorado. Este método busca fornecer, em tempo real, a melhor representação da órbita baseada nos dados coletados por uma rede fiducial até aquela epoca. O algorítmo baseia-se numa unidade, chamada "degrau de atualização", que define o arco orbital dentro do qual o ajustamento da órbita se efetua. As condições iniciais calculadas em um segmento orbital são propagadas para o próximo.

O algorítmo foi implementado utilizando como arcabouço o programa DIPOP, adicionalmente modificado de modo a permitir ajustamento em rede, incluindo-se correlações matemáticas entre as bases.

O principio do método foi testado utilizando-se dados coletados por uma rede de 8 estações, situadas no Canadá e nos EUA, estações estas que fazem parte da rede do IGS. As duas modalidades de órbitas geradas pelo método foram comparadas com elas próprias, em um teste de repetibilidade orbital visando quantificar sua consistencia interna, e tambem com as órbitas do IGS, visando mensurar sua consistencia externa. Um sub-conjunto desta rede foi processado utilizando as órbitas determinadas pelo

método, almejando verificar o impacto destas órbitas no posicionamento geodésico. Estes testes objetivam avaliar a qualidade das órbitas geradas usando-se o método proposto.

Os resultados obtidos mostram que o erro médio tri-dimensional das órbitas ajustadas é igual ou menor do que 1 metro. O emprego destas órbitas no posicionamento geodésico permite a determinação de bases geodésicas com erro relativo variando entre 0,05 e 0,02 ppm. As bases geodésicas utilizadas possuem comprimento na ordem da centena de quilômetros. Estes resultados são superiores aos encontrados usando-se as efemérides transmitidas, atualmente as únicas disponíveis em tempo-real.

Acknowledgements

I would like to thank the following persons and Institutions which helped me, in many different ways, in going through these long 4 years and 9 months in Canada, to arrive at this final stage of my academic life:

- My sponsoring agency, Brazil's Conselho Nacional de Desenvolvimento Científico e Tecnológico (CNPq);
- Dr. P. Vaníček, the academic supervisor, for his guidance and many stimulating discussions;
- Dr. R. B. Langley for his interest and many helpful discussions and suggestions. Also, for allowing me to join his GPS group which gave me opportunity to exchange ideas and experiences with its members. Among them, A. Komjathy, A. van der Wal and V. B. Mendes, with whom I interacted the most;
- Prof. D. Small, of Department of Mathematics and Statistics at UNB, Dr. G. Beutler, of the Astronomical Institute, University of Berne and Dr. Z. Martinec, Charles University, Czech Republic, for valuable discussions on various topics of my research;
- Dr. Denizar Blitzkow, of the University of São Paulo, who suggested the Department of Geodesy and Geomatics Engineering at UNB as the ideal place for my Ph.D. studies;

- All my Brazilian friends with whom I kept in contact throughout these years. Among them Leonardo C. Oliveira, of the Military Institute of Engineering, Edvaldo S. Fonseca Junior, of the University of São Paulo, Renato C. Guimarães, of the University of Brasília (UnB) and Claudio Bastos, of the National Observatory in Rio;

- All the international friends I have the opportunity to gain, among them James Carroll, Dianne Burns, Margo Watts (actually, the whole Watts family), and the bold indoor soccer team (UNB Intramural Champions of 1994);

- My wife, Denise, who changed her comfortable life in Rio de Janeiro for a harder one, of "student's wife" in this little town of Fredericton. She helped me in every aspect, including in typing part of this document, using her mastering of LaTeX. This dissertation is dedicated to her, to my mother Nilcéa, and to my god-daughters Madalena, Lia and Andréa.

List of Abbreviations

A-S	Anti-Spoofing
ACP	Active Control Points
ACS	Active Control System
BIPM	Bureau International de Poids and Measures
CANSPACE	Canadian Space Geodesy Forum
CI	Conventional Inertial
CIGNET	Cooperative International GPS Network
CNPq	Conselho Nacional de Desenvolvimento Cientifico e Tecnologico
CT	Conventional Terrestrial
DGPS	Differential GPS
DIPOP	Differential POsitioning Package
DOP	Dilution Of Precision
DoD	Department of Defense
EOP	Earth Orientation Parameters
GAST	Greenwich Apparent Sidereal Time
GEM	Goodard Earth Model
GIG	GPS IERS and Geodynamics
GMST	Greenwich Mean Sidereal Time
GPS	Global Positioning System
GPST	GPS Time
GRS	Geodetic Reference System

IAU	International Astronomical Union
IBGE	Instituto Brasileiro de Geografia e Estatistica
IERS	International Earth Rotation Service
IGS	International GPS Service for Geodynamics
IN	Inertial system adopted
ISDN	Integrated Services Digital Network
ISO	International Standards Organization
ITRF	IERS Terrestrial Reference Frame
JD	Julian Date
MCS	Master Control Station
MRA	Mean Right Ascension
NGS	National Geodetic Survey
NSWC	Naval Surface Warfare Center
OR	Orbital (system)
OTF	On-The-Fly
RBMC	Rede Brasileira de Monitoramento Continuo dos satelites GPS
RINEX	Receiver-Independent Exchange format
RTCM	Radio Technical Commission for Maritime Services
SA	Selective Availability
SIO	Scripps Institute of Oceanography
SLR	Satellite Laser Ranging
SOPAC	Scripps Orbit and Permanent Array
TAI	International Atomic Time
TCB	Barycentric Coordinate Time
TCG	Geocentric Coordinate Time
TDB	Barycentric Dynamical Time
TDT	Terrestrial Dynamical Time
TRA	True Right Ascension

TT	Terrestrial Time
UT	Universal Time
UTC	Coordinated Universal Time
OCS	Operational Control System
UNB	University of New Brunswick
VLBI	Very Long Baseline Interferometry
WADGPS	Wide Area Differential GPS

List of Symbols

A	spacecraft effective cross sectional area affected by solar radiation
$\underline{A}$	design matrix
a	major semi-axis of the orbital ellipse
a_{ES}	major semi-axis of the earth's orbit around the sun
a_e	major semi-axis of the ellipsoid
a_x, a_z	accelerations output from T10 and T20 formulae
B	baseline length
$\underline{B}^*$	matrix of variational partials
β	geocentric latitude
$\underline{C}_\ell$	covariance matrix of $\underline{\ell}$
C_{nm}, S_{nm}	geopotential coefficients of degree n and order m
$\underline{C}_p$	covariance matrix of $\underline{p}$
$\underline{C}_R$	covariance matrix of $\underline{R}$
C_r	reflectivity factor
$\underline{C}_s$	covariance matrix of $\underline{s}$
$\underline{C}_y$	covariance matrix of $\underline{y}$
$\underline{C}_{\nabla\Delta\Phi}$	covariance matrix of the double difference observations
$\underline{C}_\Phi$	covariance matrix of the undifferenced observations
c	speed of light in a vacuum
dB	baseline length error
dT	receiver clock offset from GPS Time

d_{ion}	ionospheric delay
dr	satellite position error
dt	satellite clock offset from GPS Time
d_{trop}	tropospheric delay
$\Delta \underline{C}_{\hat{x}}$	increment to the covariance matrix
$\Delta \hat{\underline{\delta}}_x$	increment to the solution vector
$\Delta\psi$	nutation in longitude
Δt	observation sampling step
$\Delta\tau$	length of orbital arc for orbit improvement
$\hat{\underline{\delta}}$	least-squares vector of corrections to the estimated parameters
$\underline{\delta}$	difference between reference and computed orbits
$\overline{\delta}$	average value of orbital residuals
$\delta\Phi$	ionospheric residual (in length unit)
E	eccentric anomaly
e	eccentricity of the orbital ellipse
$\underline{e}$	receiver-satellite unit vector
$\underline{e}_z, \underline{e}_y, \underline{e}_x$	unit vectors in the satellite coordinate system
ϵ'	true obliquity of the ecliptic
ϵ_Φ	random measurement errors with carrier phase
ϵ_p	random measurement errors with pseudorange
f	true anomaly
f_{L1}, f_{L2}	frequencies corresponding to L1 and L2 carriers
$\underline{G}$	rotation matrix for GAST
GM	earth's gravitational constant
G_x, G_z	solar pressure coefficient scaling factors
h	integration step size
$\underline{h}$	angular momentum of a satellite
i	inclination of the orbital plane

J_2	dynamic form factor
k	update step
k_2	second degree Love number
$\underline{\kappa}$	vector of Keplerian elements
$\underline{\ell}$	vector of observations
λ	carrier wavelength **or** longitude
M	mean anomaly
M_{tb}	the mass of the third body
m	mass of the satellite
m_p	error caused by code signal multipath
m_Φ	error caused by phase signal multipath
N	cycle ambiguity
$\underline{N}$	nutation matrix **or** normal matrix
$(\underline{N}^* \underline{P}^*)^T$	transformation from $J2000$ to initial epoch of the equations of motion
n	satellite's mean motion
$\underline{n}$	unit vector pointing from the sun to the spacecraft
$\nabla\Delta$	double difference operator
ν	eclipse factor
ξ^p	numerical integrator coefficient for predictor
ξ^c	numerical integrator coefficient for corrector
ξ^L	numerical integrator coefficient for the stater
$\underline{P}$	precession matrix
$P_{nm}(\sin\beta)$	associated Legendre functions
P_s	solar radiation pressure
p	pseudorange measurement
$\underline{p}$	vector of initial dynamical parameters
$\underline{p}^o$	vector of approximate values of $\underline{p}$
p_0	direct solar radiation pressure parameter

$\underline{\ddot{p}}$	sum of the perturbing accelerations that act on the satellite
$\underline{\ddot{p}}_{dir}$	direct acceleration due to solar radiation pressure
$\underline{\ddot{p}}_{r}$	relativistic perturbation
$\underline{\ddot{p}}_{se}$	perturbing acceleration vector due to the solid earth tides
$\underline{\ddot{p}}_{srp}$	acceleration due to solar radiation
$\underline{\ddot{p}}_{tb}$	gravitational perturbation induced by a third body
$\underline{\ddot{p}}_{y}$	y-bias parameter
$\underline{R}$	vector of station coordinates
$\underline{R}^o$	vector of approximate values of $\underline{R}$
$r = \parallel \underline{r} \parallel$	geocentric distance to the satellite
$\underline{r}$	geocentric position vector of the satellite
$\underline{\dot{r}}$	geocentric velocity vector of the satellite
$\underline{\ddot{r}}$	total acceleration vector of the satellite
$\underline{r}_s$	geocentric position vector of the sun
$\underline{r}_{tb}$	geocentric position vector of the third body
ρ	geometric satellite-receiver range
$\underline{s}$	initial state vector
$\underline{s}^o$	vector of approximate values of $\underline{s}$
t	an epoch
t_0	initial epoch for the solution of the equations of motion
$\underline{u}$	constant vector
$\underline{v}$	residual vector
$\underline{W}$	rotation matrix for polar motion
W_s	tidal bulge potential (at the satellite altitude)
W_g	earth's gravitational potential field
$\underline{w}$	misclosure vector
Φ	carrier beat phase observation (in length unit)
Φ_{Lc}	ionosphere-free linear combination (in length unit)

Φ_{Ln}	narrow lane linear combination (in length unit)
Φ_{Lw}	wide lane linear combination (in length unit)
X, Y	output of T10 and T20 formulae
X_{al}	orbital residual in the along-track direction
X_{rd}	orbital residual in the radial direction
X_{cr}	orbital residual in the cross-track direction
$\underline{x}$	vector of parameters of interest
x, y, z	components of the position vector $\underline{r}$
$\dot{x}, \dot{y}, \dot{z}$	components of the velocity vector $\dot{\underline{r}}$
$\ddot{x}, \ddot{y}, \ddot{z}$	components of the acceleration vector $\ddot{\underline{r}}$
$\underline{y}$	vector of nuisance parameters
$\underline{y}^o$	vector of approximate values of $\underline{y}$
Ω	right ascension of the ascending node
ϖ	argument of perigee

Chapter 1

Introduction

The level of accuracy of the ephemerides broadcast by the GPS satellites does not satisfy many geodetic requirements. To overcome this limitation, a network technique known as orbit improvement has been widely used in a post-processing mode. This implies that the availability of better orbits than the broadcast ones suffers a delay. A method which intends to furnish the best orbit representation possible at any given time has been investigated and tested. This chapter presents a review of how orbit improvement became a common approach in the GPS milieu. It also states the problems we have faced in this research. The contributions of this dissertation are summarized and its structure described.

1.1 Literature review

The two basic observables of the Global Positioning System (GPS), the pseudorange and the carrier phase, are affected by several different biases, such as orbital bias, clock biases, ionospheric and tropospheric delays. In the context of this dissertation, our concern is with the modelling of the orbital bias.

The orbits of the GPS satellites are of indispensable knowledge due to the fact that to compute the position of a GPS receiver's antenna at or near the earth's

surface we need to know the geometric range between the antenna and the satellite. This quantity is a function of both the satellite's and the antenna's position [*Langley*, 1991c]. A bias in the orbit of a satellite translates into positioning errors of the same order of magnitude in absolute positioning. In differential positioning the effect of the orbit bias can be assessed by the use of the "rule of thumb" first presented by *Bauersima* [1983] and later derived by *Vaníček et al.* [1985]:

$$\frac{dB}{B} = \frac{dr}{\rho}, \tag{1.1}$$

where dr represents the satellite position error, dB the resulting baseline length error, ρ the range to the satellite and B the baseline length. Table 1.1 shows the relative error in baseline $\frac{dB}{B}$ for varying values of dr assuming ρ with an average value of 22,500 km.

Table 1.1: Relative error in baseline as a function of orbital error

dr	$\frac{dB}{B}$
1 cm	4.4×10^{-10}
10 cm	4.4×10^{-9}
1 m	4.4×10^{-8}
10 m	4.4×10^{-7}

The rule of thumb can be regarded as a pessimistic approximation of the error provoked by an orbital error. This seems to be confirmed by results reported by *Ware et al.* [1986] in which the same baseline was processed using two different sets of orbits, with differences of up to 60 metres. The final solution showed agreement of the order of 0.4 ppm. Moreover, *Zieliński* [1989] based on a study of the covariance matrix of the measurements and simulation analysis presented an alternative expression intended to asses the effect of orbital bias in differential positioning. This alternative expression has the same form as eqn. (1.1), in which ρ is multiplied by a factor greater than 4 and less than 10. *Beutler et al.* [1995] suggest that Zieliński's expression seems more

appropriate for the propagation of orbit errors into baseline components, whereas eqn. (1.1) for the orbit errors into height.

The satellites' positions, or ephemerides, are available from the messages they broadcast. These broadcast ephemerides are a set of predicted orbital positions, computed and uploaded into a satellite's memory by the GPS Control Centre (see Chapter 3). As with every predicted orbit, the broadcast ephemerides have an inherent error that grows with time. On top of that there is the effect caused by the so-called Selective Availability (see Chapter 3). The bias in the broadcast ephemerides has been assessed by several authors [e.g., *Remondi & Hoffmann-Wellenhof*, 1990; *Rothacher*, 1992]. It is believed to be around the 3–20 metre level. At this level, accuracies not better than the 0.1 ppm should be expected when using the broadcast ephemerides.

More accurate orbits are computed by the U.S. Naval Surface Warfare Center (NSWC), based on a global network composed of ten sites. They are known as "precise ephemerides" and are supposed to be at the meter level or better [*Swift*, 1993]. These orbits, however, were originally intended for domestic consumption within the U.S. Department of Defense (DoD). (Currently, they are available upon request about 4–8 weeks after the observations.)

With the precision limit of the broadcast ephemerides and the initial unavailability of the precise ones, the geodetic community soon realized it had to look for alternatives. The alternative found was the use of a network technique known as "orbit improvement", also known as "orbit computation" or "orbit correction" [*Rizos et al.*, 1985]. This technique allows the estimation of corrections to the initial conditions and dynamical parameters at a reference time, usually the initial time of the campaign, along with other parameters of interest, such as station coordinates.

The use of this technique would serve two purposes. The first one would be to obtain better results in the network adjustment by allowing the initial conditions to "learn" about the satellite's trajectory defined by the observations, as extra parameters in the adjustment. The second purpose, a by-product of the first one, would be

to generate an orbit better than the one used in the network adjustment by using the adjusted (improved) initial conditions to solve the equations of motion of the satellite (see Chapter 4).

Orbit improvement is a technique that requires a large network to adequately work. Therefore, the first conclusive results of its application started appearing in the literature after the first campaigns using regional networks with baselines of about 1000 km in length. The processing of the first of these campaigns, the 1984 Alaska Spring Test and the 1985 High-Precision Baseline Test showed unequivocally the power of the orbit improvement technique. Using these data sets, network accuracy of 0.1 ppm was achieved by different groups [e.g., *Beutler et al.*, 1985; *Abbot et al.*, 1986; *Williams*, 1986], which represented a great improvement in the quality of baseline determination.

Two approaches were used for data processing, the "free-network" [*Beutler et al.*, 1985] and the "fiducial network" [*Davidson et al.*, 1985]. In the free-network approach, a combination of station and satellite coordinates are allowed to vary simultaneously in an adjustment by a way of imposing relatively strong a priori constraints on the orbits letting the terrestrial network adjust freely. In the fiducial network approach, the GPS orbits and determined baselines are defined in the framework of a few fiducial stations whose coordinates are accurately known from VLBI or SLR [*Delikaraoglou*, 1989]. A consideration regarding the length of the orbital arcs is somewhat fundamental. Two alternatives have been explored: the short-arc [e.g., *Parrot*, 1989] and the long-arc [e.g., *Chen*, 1991] approaches (see Chapter 5).

With the results of those campaigns at hand, the focus started to shift towards the generation of GPS orbits below the metre level. Orbits at this level of accuracy, along with a more sophisticated modelling of the troposphere, would allow baseline measurements with accuracy and precision at the order of 10 ppb or even better [*Beutler et al.*, 1988; *Lichten*, 1990].

At first, orbit improvement had to count on regional networks yielding the generation of orbits at the metre level within the region covered by the fiducial stations [*Lichten & Border*, 1987; *Lichten & Bertiger*, 1989; *Ashkenazi et al.*, 1990].

At this stage, the Geodetic Survey of Canada had already undertaken the development of the Active Control System (ACS) [*Delikaraoglou et al.*, 1986]. The ACS would establish a zero-order fiducial network of Active Control Points (ACP) covering the Canadian territory. The major task of the ACS would be the computation of accurate orbits. Moreover, the data colleted by the ACP would be made available to the geomatics community allowing an easy access to the geodetic reference frame. Other types of information would also be made available by the ACS such as differential corrections for single receiver users, which would have to be disseminated in real-time. A similar system, known by the acronym RBMC, has been proposed by the Brazilian Geodetic Institution (IBGE) [*Fortes*, 1993].

But since covariance analyses were showing that expanding the size of the network would increase orbit accuracy [*Wu et al.*, 1988], efforts started to be made towards the establishment of global networks.

The first global fiducial network established was the Cooperative International GPS Network (CIGNET) [*Schenewerk et al.*, 1990] with stations distributed over all continents but concentrated mostly in North America. The network had its reference frame defined by the International Earth Rotation Service (IERS) Terrestrial Reference Frame (ITRF). The objective behind CIGNET was to make available continuous GPS tracking data for crustal motion studies and for GPS orbit generation. Regional campaigns, such as the CASA Project [*Schutz et al.*, 1990] relied on data coming from CIGNET and further indicated the need for a global GPS tracking network. Another global GPS campaign was the First GPS IERS and Geodynamics experiment (GIG'91) [*Melbourne et al.*, 1993], with an overall goal to obtain a high quality data set to be used by the IERS for earth orientation monitoring and terrestrial reference frame control.

The need for a permanent civilian fiducial global network led to the establishment of the International GPS Service for Geodynamics (IGS), following Resolution No. 5 of the 20th General Assembly of the International Union of Geodesy and Geophysics (IUGG), in Vienna, Austria, in 1991. The IGS is the result of a cooperative effort among institutions of several countries, consisting of a Central Bureau, Analysis Centers, and Network Data (archiving) Centers. The IGS begun its operation in 1992 in an experimental mode by means of a test campaign. Two weeks of this campaign became known as the Epoch'92 campaign. The IGS remained as a pilot service until January 1, 1994, when the routine operations of IGS started. The primary objectives of the IGS are to provide the scientific community with high quality GPS orbits on a rapid basis, to provide earth orientation parameters (EOP) of high resolution (orbits and EOP are the IGS products), as well as to expand geographically the current ITRF, and to monitor global deformations of the earth's crust. [*Mueller & Beutler*, 1992; *Mueller*, 1993; *Beutler*, 1993a].

The GPS data collected by the IGS network is processed by the analysis centers. The goal of this processing is to compute orbits and EOP, the products procured. The accuracy of the orbits generated by these analysis centers are at the 10–20 cm level, for most of them, according to their own assessment. The products of each individual analysis center are then combined into the official IGS product. The time delay for an analysis center to release its orbit varies from center to center, but are at the order of a few days. The IGS releases its official orbit product 2 weeks after the GPS data collection.

Another approach, that among several objectives would also aim towards better orbits than the broadcast ones, is the technique of wide-area differential GPS (WADGPS). The WADGPS is a network technology which has grown in interest recently [*Mueller*, 1994]. It can be regarded as a further development of the conventional differential GPS (DGPS). The underlying idea of DGPS is that errors experienced at a reference station are, for the most part, identical to those experienced

by a user. This error would be translated into pseudorange corrections, determined by comparing computed ranges with observed pseudoranges at the reference station, and transmitted to users in real-time. There are two deficiencies with DGPS: the corrections contain errors of different sources (ephemerides biases, satellite clocks, atmospheric delays, and SA); and, there is a limit in the distance between the reference station and the user [*Brown*, 1989]. WADGPS tries to solve both deficiencies by means of a network of GPS reference stations, which increases the geographical coverage, and by separating the lumped correction into their component parts. The latter are then transmitted to users. The formats of these transmissions are usually inspired by the standards established by the Special Committee # 104 of the Radio Technical Committee for Maritime Services (RTCM) [*RTCM*, 1994]. Some of the algorithms for WADGPS found in the literature are those of *Brown*, [1989], *Kee et al.* [1991], *Ashkenazi et al.* [1993] and *Lapucha & Huff* [1993]. These authors report final horizontal positions with root means square (rms) errors at the 2 metre level. Ephemerides corrections are comparable to GPS broadcast ephemerides without SA.

Starting in January 1995, the Scripps Orbit and Permanent Array (SOPAC) has been making available via anonymous File Transfer Protocol (ftp) improved ephemerides with a 24 hour delay from the IGS data collection as well as a 24-hour predicted orbit from the improved ephemerides so that the latter is available in real-time (IGS Electronic Message # 851).

We conclude this section by saying that there are several software suites with orbit improvement capability. They have been developed by various universities and institutions based on different processing strategies, using different observable types, etc. The results reported in this section have been obtained with some of them. Table 1.2 presents the software's name and organization that has developed it. The '*' symbol indicates the ones capable of handling data from space-based systems other than GPS. Most of these software suites have had their characteristics summarized by a survey we carried out. This summary has been published electronically via the

Canadian Space Geodesy Forum (CANSPACE) File Archives.

Table 1.2: Software suites with capability for orbit improvement.

Name	Developed at
BAHN/GPSOBS (*)	European Space Agency/Operations Center
BERNESE	University of Berne, Switzerland
CGPS22	Geological Survey of Canada
DIPOP	University of New Brunswick, Canada
EPOS.P.V3	German Geodetic Research Institute
GAMIT/GLOBK	Massachusets Institute of Technology, USA
GAS	University of Nottingham, England
GEODYN II (*)	NASA/Goddard Space Flight Center, USA
GEONAP	University of Hannover, Germany
GEOSAT (*)	Norwegian Defence Research Establishment
GIPSY/OASIS (*)	Jet Propulsion Laboratory, USA
MSOP	National Aerospace Laboratory, Japan
OMNIS	Naval Surface Warfare Center, USA
PAGE3	National Geodetic Survey, USA
TEXGAP/MSODP	University of Texas, USA

1.2 Statement of the problem

Let us make clear at this point that orbit generation, via solution of the satellite equations of motion, is always a process of orbit prediction. In this dissertation we shall make a distinction between the orbit generated for the same time span encompassed by the GPS data collection, and the orbit generated for times beyond this time span. The former shall be called improved orbit (or improved ephemeride); the latter as predicted or extrapolated orbit. The technique of orbit improvement yields improved (adjusted) initial conditions (also referred to as the initial state vector). Let us also make clear that an orbit, or ephemerides, satisfying the satellite's equations of motion, can only reach the users in real-time (meaning, at the exact time a GPS observation is collected) as a result of extrapolation.

As seen in the previous section, a delay that may vary from days to weeks is imposed presently on those who want to have access to accurate orbits. That is because the orbit improvement takes place in a post-processing mode, i.e., only after all GPS data have been collected. Therefore, there is the time span of data collection (usually 24 hours) plus the processing time itself. Only after that can the ephemerides be generated. In this dissertation, orbit improvement in a post-processing mode has been called the "traditional approach for orbit improvement". Another characteristic of the traditional approach is that the initial conditions are estimated referring to the same reference epoch independent on whether it uses a batch or a sequential adjustment for the time covered by the data set used. But many types of applications would gladly accept orbits of much better accuracy than the broadcast ones if readily available. These applications include the monitoring of sudden crustal motions, such as earthquakes or volcanoes, data validation and ambiguity resolution in rapid static surveys and aircraft landing approaches. This has been the motivation which led us to investigate what we have called in this dissertation the "real-time approach for orbit improvement".

The purpose of this research as previously proposed [*Santos*, 1992] is to investigate the possibility of a real-time high accuracy GPS orbit determination, i.e., the possibility of obtaining at any time the best possible estimate of an orbit, based on all observations collected up to that time. This required the development of a sequential updating algorithm based upon a unit, called the update step. The update step defines the length of the orbital arc over which the improvement takes place. In the real-time approach, the update step equals the observation sampling step used by the sequential algorithm, e.g., 2 minutes. The initial conditions improved in one orbital arc are used for orbit generation covering the orbital arc in which the improvement took place and the next one where they are used as a priori orbits in the new improvement. New initial conditions are then established for the new orbital arc. The technique is actually making use of multiple (moving) expansion points for

the initial conditions, as opposed to the traditional approach for orbit improvement which uses only one for several arcs. The contribution of the previous observations are accumulated within the system.

Another characteristic to point out is that the orbital arc may be of different lengths. In this context by "length" of the orbital arc we refer to a "time interval". It will be shown (cf. Chapter 5) that the traditional approach is a particular case of the real-time one if the update step is very large, and if used in a post-processing mode. It can be correctly concluded that the algorithm generates orbits of two kinds: an improved orbit based on individual orbital arcs, and orbits predicted over the next orbital arcs.

The whole idea behind the algorithm can be used in an orbit service, in which GPS observations collected by a network of monitor stations are transmitted in real-time to a Master Center whose duty is to carry out the real-time orbit improvement and to make the real-time improved orbits available to subscribers as soon as they are ready. We have tried to envisage how such service would operate. Among the problems this service would have to handle is the screening of the observations and some thought has been dedicated towards this. We try to address important questions that arise, on whether this technique is capable of generating better quality orbits than the broadcast ones, and on what the effect on geodetic positioning the real-time orbits would have.

Real-time orbits were generated using GPS data, collected in January 1995, by a network of 8 stations in Canada and the U.S. Four days of data were used. The effect of the real-time orbits on geodetic positioning was assessed using a subset of this network.

1.3 Contributions of the research

The original contribution of the research is the development of a real-time algorithm for orbit improvement, based on a sequential updating algorithm, using the update step as a temporal unit. Two types of orbits can be generated: an orbit available in real-time which is extrapolated from the previous orbital arc, and the improved orbit, available with a delay (disregarding transmission time) equal to or less than the length of the orbital arc plus the time for the numerical integration, depending on the orbital arc definition. The research encompasses the development and testing of the algorithm. The questions asked at the end of the previous section are addressed.

As by-products of our main contribution we have:

- the development of an orbital integrator incorporating as much as possible the standards recommended by the IERS [*International Earth Rotation Service*, 1992];
- the description of a real-time orbit service;
- the establishment of criteria for automatic cycle slip detection in the context of a real-time static test case;
- the implementation of a new orbit improvement per se in the DIPOP software package; and,
- the implementation of network adjustment in DIPOP taking into account the correlations among baselines.

1.4 Outline of the dissertation

The dissertation is divided into 7 chapters.

Chapter 2 reviews the coordinate systems needed in the orbit improvement, including time, coordinate, and satellite-centered systems.

Chapter 3 overviews the GPS system and its errors and biases.

Chapter 4 explains how to go about solving the equations of motion of a satellite, describing the modelling of the forces that affect it, and the numerical technique used to solve them.

Chapter 5 describes the technique of orbit improvement and its least-squares solution. Most importantly it contains the description of the real-time algorithm. A discussion of the orbit service and screening of observations conclude this chapter.

Chapter 6 describes the tests we have carried out in order to check the quality of the several test orbits generated using the real-time algorithm, as well as their effect on geodetic positioning. Analysis of the results of these tests are presented.

Chapter 7 concludes this dissertation with final comments and suggestions for future work.

Throughout the dissertation matrices have been represented by underlined capital letters and vectors by underlined small letters. The inner product between two vectors is represented by '$\cdot$' and the cross product by '$\times$'. The norm of a vector $\underline{v}$ is represented by '$\| \underline{v} \|$'.

Chapter 2

Space and time coordinate systems

2.1 Introduction

Orbit determination is, in part, a process of coordinate transformation [*Escobal*, 1976]. This is due to the fact that the earth-bound stations and the orbiting satellites are usually 'attached' to different coordinate systems: the former to an earth-fixed coordinate system, the Conventional Terrestrial System (CT-system); the latter to an inertial coordinate system, the Conventional Inertial System (CI-system). The CT-system is in relative motion with respect to the CI-system. The satellite's trajectory is integrated in the CI-system whereas the orbit improvement is carried out in the CT-system. Hence, a relation between the two coordinate systems has to be established, based on rotation matrices. The choice of a geocentric coordinate system, i.e., one with its origin at the earth's center of mass, is the most convenient for the computation of earth orbiting satellites.

The GPS observations are fundamentally referred to the GPS Time scale. Relations between the GPS Time and the other time systems used in satellite geodesy have also to be defined.

This chapter overviews the space and time coordinate systems used in GPS orbit computations.

2.2 Time systems

Satellite geodesy makes use of three different systems of time, namely, Rotational Time, Atomic Time, and Dynamical Time.

2.2.1 Rotational times

Rotational time scales are the ones based on the daily rotation of the earth. They can be determined from observations of stars, artificial satellites and extragalactic radio-sources. There are two modalities of rotational times: Sidereal Time and Solar Time.

Sidereal Time is defined as being the hour angle of the vernal equinox. If the hour angle is measured using the Greenwich astronomic meridian as reference we have Greenwich Apparent Sidereal Time (GAST) and Greenwich Mean Sidereal Time (GMST). Their difference is due to the former refering to the true (or apparent) vernal equinox and the latter to the mean vernal equinox.

Solar Time is numerically defined by the hour angle of the sun. Of major importance in our context is Greenwich Mean Time or, as it is now usually called, Universal Time (UT), which is the hour angle of the fictitious (or mean) sun referred to the Greenwich mean astronomic meridian (plus 12^h) [*Moritz & Mueller*, 1988]. It is convenient for satellite geodesy to use UT corrected for polar motion, thus representing the true angular rotation of the earth. This modality of UT is known as UT1 [*Mueller*, 1969].

UT1, GMST and GAST are related by rigorous formulae. To begin with, GMST at 0^h UT1 (GMST1) is obtained from [*Aoki et al.*, 1982]:

$$\mathrm{GMST1} = 24110^s.54841 + 8640184^s.812866 T_u + 0^s.093104 T_u^2 - 6^s.2 \times 10^{-6} T_u^3, \quad (2.1)$$

where T_u is the number of centuries of 36525 days of universal time elapsed since 2000 January 1, 12^h UT1 (Julian Date 2451545.0 UT1). T_u is computed by [*Seidelmann*,

1992]:

$$T_u = \frac{JD - 2451545.0}{365.25}, \tag{2.2}$$

being JD the Julian Date of the epoch of interest at 0^h UT1.

The GMST of date is computed by [*Aoki et al.*, 1982]:

$$\text{GMST} = \text{UT1}\ \frac{1}{r'} + \text{GMST1}, \tag{2.3}$$

where the quantity r' can be thought of as the length of one sidereal day in units of solar days:

$$\frac{1}{r'} = 1.002737909350795 + 5.9006 \times 10^{-11} T_u - 5.9 \times 10^{-15} T_u^2, \tag{2.4}$$

with T_u given by eqn. (2.2) referring to UT1 of date.

The relation between GAST and GMST is given by the equation of the equinox:

$$\text{GAST} = \text{GMST} + \Delta\psi\ cos\epsilon', \tag{2.5}$$

where $\Delta\psi$ is the nutation in longitude and ϵ' the true obliquity of the ecliptic.

2.2.2 Atomic times

The name 'atomic time' comes from the fact that it is a time system kept by atomic clocks. The atomic time which defines the fundamental and continuous time scale for the time-keeping services is International Atomic Time (TAI[1]). Its unit interval is exactly one SI second at sea level. Being a uniform time scale, the TAI became mis-synchronized with the solar day. This problem was solved with the introduction of Coordinated Universal Time (UTC). By definition, the difference between TAI and UTC equals an integer number of seconds. This difference is altered, by the insertion of a leap second in UTC, whenever the difference between UT1 and UTC

[1]The acronym for this time scale obeys the French word order.

is projected to become larger than $0^s.9$ in absolute value. The decision to introduce a leap second in UTC to meet this condition is the responsibility of the International Earth Rotation Service (IERS), which works closely with the Bureau International de Poids and Mesures (BIPM).

The GPS Time (GPST) scale is realized by atomic clocks on board the GPS satellites and those at the GPS Operational Control System (OCS) monitor stations. It started at 0^h UTC on January 6, 1980 and keeps a constant difference at the integer second level of 19^s with TAI. The relation between GPST, UTC and UT1, since the start of GPS Time, is shown by Table 2.1 (compiled using the International Earth Rotation Service annual reports).

Table 2.1: Relationship between TAI, GPST and UTC since the beginning of GPS Time until July 1994.

Date at 0^h UTC		TAI-UTC	GPST-UTC
Calendar Date	Modified Julian Date	(seconds)	(seconds)
6 Jan 1980	44244.0	19	0
1 Jul 1981	44786.0	20	1
1 Jul 1982	45151.0	21	2
1 Jul 1983	45516.0	22	3
1 Jul 1985	46247.0	23	4
1 Jan 1988	47161.0	24	5
1 Jan 1990	47892.0	25	6
1 Jan 1991	48257.0	26	7
1 Jul 1992	48804.0	27	8
1 Jul 1993	49169.0	28	9
1 Jul 1994	49534.0	29	10

Very important quantities related to GPST are the GPS weeks, numbered with integer numbers. The first GPS week was numbered with 0. A particular epoch is identified in GPST as the number of seconds elapsed since the previous Saturday/Sunday midnight plus the corresponding GPS week number.

2.2.3 Dynamical times

Dynamical time is the uniform time scale used to describe the motion of bodies with respect to a certain reference frame obeying a particular gravitational theory. Barycentric Dynamical Time (TDB) is a dynamical time scale measured in an inertial reference frame with origin at the centre of mass of the solar system, the barycentre of the solar system. For satellite orbit computations, Terrestrial Dynamical Time (TDT) can be used. This time scale is valid for the motion of a body within the earth's gravitational field and has the same rate as an atomic clock at sea level. For this reason TAI is used as a practical implementation of TDT [*King et al.*, 1985]. They are related by [*Seidelmann*, 1992]:

$$\mathrm{TDT} = \mathrm{TAI} + 32^s.184. \tag{2.6}$$

The relation between TDB and TDT (neglecting higher-order terms) is [*Seidelmann*, 1992]:

$$\mathrm{TDB} = \mathrm{TDT} + 0^s.001658 \sin g + 0^s.000014 \sin 2g), \tag{2.7}$$

where g is the mean anomaly of the earth in its orbit around the sun:

$$g = 357^o.53 + 0^o.98560028(JD - 2451545.0), \tag{2.8}$$

and JD is the Julian Date in TDT.

The International Astronomical Union (IAU) Working Group on Reference Systems recommended the renaming of TDT as Terrestrial Time (TT) and defined new scales consistent with the SI second and the General Theory of Relativity. These scales are the Geocentric Coordinate Time (TCG) and the Barycentric Coordinate Time (TCB). They have their spatial origins at the center of the mass of the earth and the solar system barycentre, respectively. These time scales will be introduced into the astronomical almanacs when new fundamental theories and ephemerides based on these time scales are adopted by the IAU [*Hughes et al.*, 1991; *Nautical Alamanac Office*, 1995].

2.3 Geocentric coordinate systems

2.3.1 Definitions

The coordinate systems involved in the transformation between the CI-system and CT-system are right-handed orthogonal geocentric systems. The definition of such a coordinate system makes use of a fundamental plane of reference and principal axes, in which the X-axis has a fixed orientation in the fundamental plane and the Z-axis may be a rotation axis or not. The Y-axis is selected to make the system right-handed. These systems are [*Mueller*, 1969; *Vaníček & Krakiwsky*, 1986; *Torge*, 1991] the Conventional Terrestrial System (CT-system), the Instantaneous Terrestrial System (IT-system), the True Right Ascension System (TRA-system) and the Mean Right Ascension System (MRA-system).

Conventional terrestrial system, is an earth-fixed system, i.e., it rotates with the earth. Its Z-axis points towards the Conventional International Origin [*Moritz & Mueller*, 1988], the X-axis is in the mean equatorial plane, and the XZ-plane contains the mean Greenwich meridian.

Instantaneous terrestrial system, is akin to the CT-system but its Z-axis coincides with the instantaneous spin axis and the XZ-plane contains the instantaneous Greenwich meridian. Its fundamental plane is the instantaneous equatorial plane.

True right ascension system at epoch τ, TRA(τ), also known as "true equator and equinox" of date system, has its Z-axis coinciding with the earth's instantaneous spin axis (i.e., pointing towards the instantaneous north celestial pole) while its X-axis points towards the true vernal equinox at epoch τ. Its fundamental plane is the true celestial equator at epoch τ. The TRA(τ) and IT are related by a rotation matrix whose argument is the angle GAST. The TRA(τ) both precesses and nutates.

Mean right ascension system is akin to the TRA(τ) with the very important difference that its Z- and X- axes point toward the mean north celestial pole and the mean vernal equinox, respectively, at a certain specified epoch, and its fundamental plane is the mean celestial equator at the same epoch. If the effects of nutation are removed from the TRA(τ) we get the **mean right ascension system at** (the same) **epoch** τ, MRA(τ), also known as "mean equator and equinox" of date system. If the effects of precession are removed from MRA(τ) the resulting system refers to a particular epoch of reference τ_o and is called **mean right ascension system at epoch** τ_o, MRA(τ_o), or mean equator and equinox of date τ_o. The reference epoch τ_o used is $J2000.0$, which corresponds to 2000 January 1, 12^h TDB. MRA(τ_o) is the CI-system.

2.3.2 Transformations

The coordinate system transformation between the CI-system and CT-system is spelled out as:

$$\underline{r}^{CT} = \underline{W} \ \underline{G} \ \underline{N} \ \underline{P} \ \underline{r}^{CI}, \tag{2.9}$$

where $\underline{P}, \underline{N}, \underline{G}$ and $\underline{W}$ represent rotation matrices for precession, nutation, GAST and polar motion, respectively, and are defined by the *International Earth Rotation Service* [1992], and $\underline{r}$ is the position vector.

Inertial system adopted

The adopted inertial coordinate system (IN-system) for the numerical integration of the equations of motion is the true right ascension system at a reference epoch t_0, the initial epoch of the equations of motion. The IN-system keeps a constant orientation with respect to the CI-system at $J2000.0$. Then, the relation between the CT-system and the IN-system reads:

$$\underline{r}^{CT} = \underline{W} \ \underline{G} \ \underline{N} \ \underline{P} \ (\underline{N}^* \ \underline{P}^*)^T \ \underline{r}^{IN(t_0)}, \tag{2.10}$$

where $\underline{P}^*$ and $\underline{N}^*$ are the precession and nutation matrices used in the transformation between $J2000.0$ and the initial epoch of the equations of motion.

2.3.3 Orbital system

The motion of a satellite in a pure central force field is known as the Keplerian orbit or two-body problem. The satellite obeys Kepler's laws, traveling along an orbital ellipse in which the centre of mass of the earth is at one of the foci. This motion is described by the well-known Keplerian elements. These elements define the shape and size of the elliptic path (by the semi-major axis, a; and the eccentricity, e), the orientation of the orbital plane with respect to the inertial coordinate system adopted (by the inclination, i; the right ascension of the ascending node, Ω; and the argument of perigee, ϖ), and the position of the satellite on the orbital ellipse (by one of the anomalies: the true anomaly, f; the eccentric anomaly, E; or the mean anomaly, M). In a central force field, only the anomaly varies with time. In real life, all elements are functions of time due to the various perturbing forces [*Vaníček & Krakiwsky*, 1986].

The Keplerian elements are schematically depicted in Figure 2.1. In this figure, the velocity vector is represented by $\underline{v}$. Figure 2.2 concentrates on i, Ω, ϖ and f, shown in an equatorial projection, in which the great circles on the celestial sphere are represented as straight lines. The anomalies require further explanation. Odd as it may seem, the anomalies are nothing else but angles. They all refer to the line of apsides (the imaginary line joining the perigee – point of satellite's closest approach to earth, with the apogee – the point of farthest recession) and are reckoned from the perigee, or from the vernal point for polar orbits. The true anomaly f is the angle between the the line of apsides and the satellite, measured at the earth's centre of mass. The eccentric anomaly E is the angle between the line of apsides and the projection of the satellite on a circle of radius a coplanar and concentric with the orbital ellipse. The mean anomaly M is the true anomaly corresponding to the motion of an imaginary satellite of uniform angular velocity [*Vaníček & Krakiwsky*,

1986].

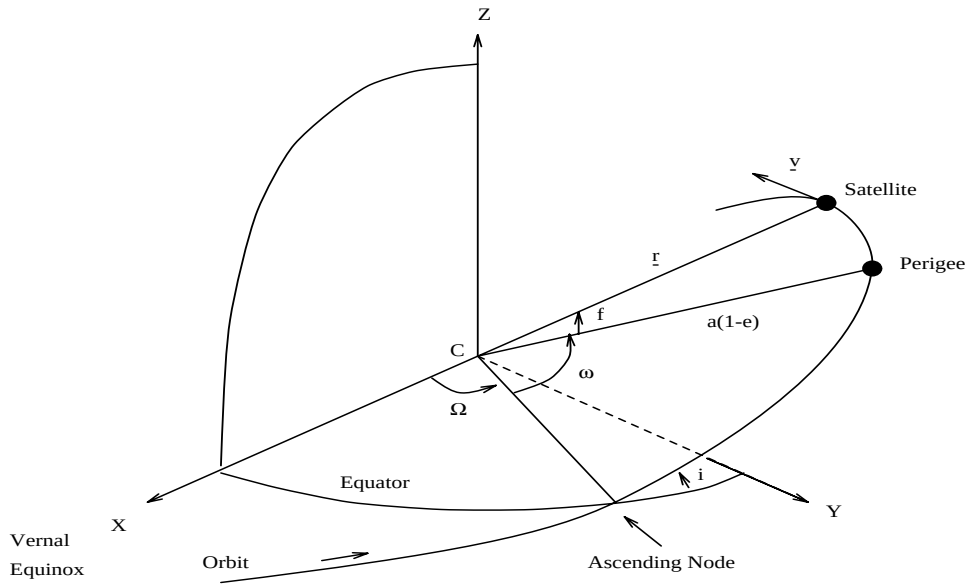

Figure 2.1: Keplerian orbital elements

The relation between the true and eccentric anomalies is given by:

$$\tan f = \frac{(1-e^2)^{1/2}\sin E}{\cos E - e}. \tag{2.11}$$

The relation between the eccentric and the mean anomalies is described by Kepler's equation [*Brouwer & Clemence*, 1961]:

$$M = E - e\sin E. \tag{2.12}$$

Equation (2.12) can be solved for E by iterations or by using a power series in e [*Krakiwsky & Wells*, 1971].

The Keplerian orbital elements are related to the orbital coordinate system (OR-system). This system has its X-axis coincident with the line of apsides, the Y-axis corresponds to $f = \pi/2$, and the Z-axis completes the right-handed system [*Vaníček & Krakiwsky*, 1986]. The relation between the Keplerian orbital elements and the OR-system is presented in Appendix I.

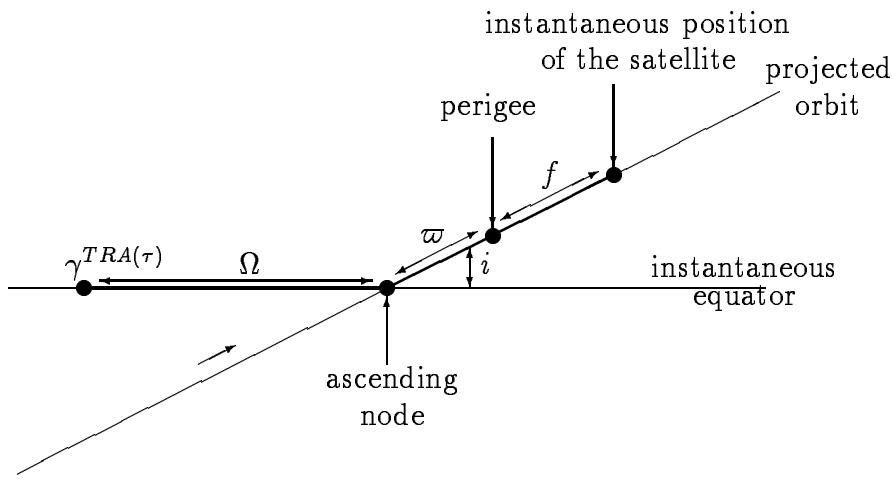

Figure 2.2: Equatorial close-up on i, Ω, ϖ and f

The OR-system is related to the TRA-system by the following matrix relations [*Wells et al.*, 1987]:

$$\left.\begin{array}{l} \underline{r}^{TRA} \\ \underline{\dot{r}}^{TRA} \end{array}\right\} = \underline{R}_3\,(-\Omega)\;\underline{R}_1\,(-i)\;\underline{R}_3\,(-\varpi)\left\{\begin{array}{l} \underline{r}^{OR} \\ \underline{\dot{r}}^{OR} \end{array}\right. , \tag{2.13}$$

where $\underline{r}$ and $\underline{\dot{r}}$ are position and velocity vectors, respectively.

2.4 Satellite-centered coordinate system

A very convenient way of representing the orbital motion of a satellite is by using a satellite-centered coordinate system. Such a system may be defined in many different ways, the most common in orbital analysis being the one with center at the satellite's center-of-mass and with the radial axis pointing towards the earth's center-of-mass, the along-track axis tangent to the satellite's trajectory and a third (cross-track) axis perpendicular to those, forming the coordinate system depicted by Figure 2.3.

This system is very useful for representing the departure between two orbits of the same satellite. For example, let's suppose that $\underline{r}$ and $\underline{\dot{r}}$ are the position and velocity

vectors of a satellite on a computed orbit, which has to be compared with that on a reference orbit given by the position vector $\underline{p}$. The departure can be computed, in a circular or near-circular orbit, as:

$$X_{al} = \frac{\dot{\underline{r}} \cdot \underline{\delta}}{\| \dot{\underline{r}} \|}, \tag{2.14}$$

$$X_{rd} = -\frac{\underline{r} \cdot \underline{\delta}}{\| \underline{r} \|}, \tag{2.15}$$

$$X_{cr} = \frac{\underline{h} \cdot \underline{\delta}}{\| \underline{h} \|}, \tag{2.16}$$

where:

$$\underline{\delta} = \underline{p} - \underline{r}, \tag{2.17}$$

$$\underline{h} = \underline{r} \times \dot{\underline{r}}, \tag{2.18}$$

and X_{al}, X_{rd} and X_{cr} are the departures in the along-track, radial and cross-track directions.

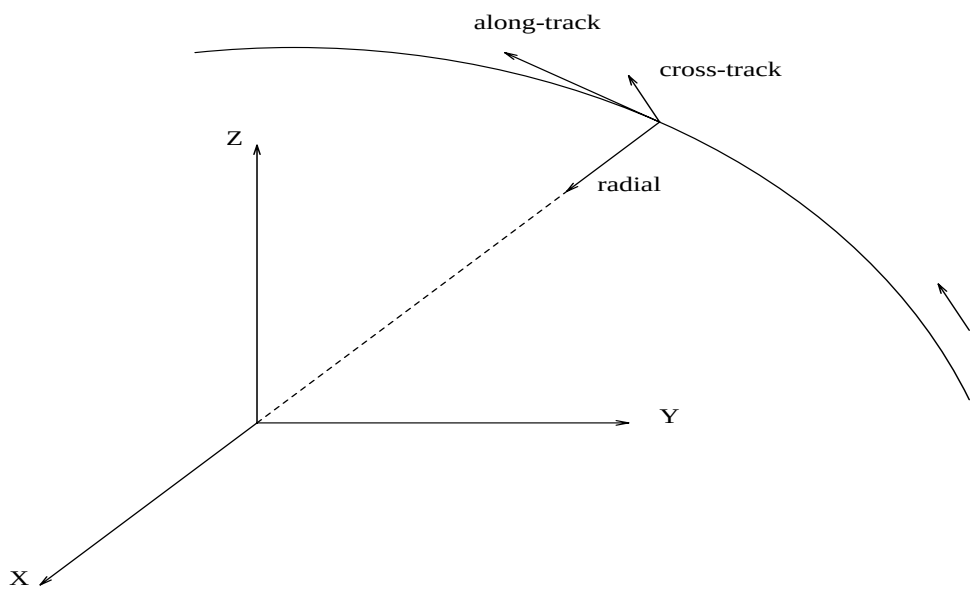

Figure 2.3: Satellite-centered coordinate system

Chapter 3

The Global Positioning System

The Global Positioning System (GPS) is a satellite-based system for positioning, navigation, and timing purposes developed and controlled by the United States Department of Defense (DoD). The system can be conveniently separated into three components, the space segment, the control segment and the user segment.

The space segment is composed of the orbiting satellites. The satellites have been divided according to their design into Block I (the prototypes), II and IIA. Currently there is only one Block I satellite still in operation. The Block II and IIA satellites have been distributed in the sky in such a way that four of them are in each of six orbital planes, to guarantee continuous global coverage. The satellites are in a nominally circular orbit (maximum eccentricity is about 0.01) with major semi-axis of about 26,560 km and inclination of about 55 degrees [*Langley*, 1991b]. Each satellite transmits a navigation signal composed of two carriers generated at 1575.42 MHz and 1227.60 MHz (referred to as L1 and L2 carriers, respectively), two binary pseudorandom noise (PRN) codes modulating the carriers at chipping rates of 10.23 MHz (the P, or precision, code) and 1.023 MHz (the C/A, or coarse/acquisition, code), and a navigation message formatted into frames of 1500 bits with a transmission rate of 50 bps. The C/A-code is modulated onto the L1 carrier, whereas the P-code is transmitted on both L1 and L2 [*Langley*, 1990].

The control segment is composed of a five ground-station tracking network, geographically spread in longitude around the world, belonging to the Operational Control System (OCS). One of them also acts as the Master Control Station (MCS). The MCS, based on the tracked data, calculates and predicts orbits and satellite clock errors. It can also maneuver the satellites and upload, along with 4 other sites, the ephemerides and clock correction to be broadcast by the satellites [*Langley*, 1991b].

The user segment is composed of all GPS receivers, and there is a great number of different makers and models in the market place (for a comprehensive list look up "GPS Receiver Survey" in the January 1995 issue of GPS World), from the handheld receivers for recreational purposes up to the most sophisticated geodetic ones. The latter are the ones we are interested in here. We shall refer to them as high performance GPS receivers due to their capacity of tracking all signal components and of recovering the full L2 carrier phase when they are operating under Anti-Spoofing (see Subsection 3.2.2).

This chapter contains a description of the GPS observation equations and of the errors and biases which affect the GPS observations. The correlations affecting the double difference observable are introduced. This is only a brief outline of GPS. Detailed information can be found in the several textbooks available such as *Wells at al.* [1987], *Ackroyd & Lorimer* [1990], *Hoffmann-Wellenhof et al.* [1992] and *Leick* [1995].

3.1 GPS observation equations

The basic measurement carried out by a GPS receiver is the signal's travel time from the GPS satellite to the receiver. This time, multiplied by the speed of light, yields the range between the satellite and the receiver antenna. Since this range has several errors and biases lumped into it, it is called a pseudorange [*Langley*, 1993]. The pseudorange is the basic observable for navigation. The observation equation of the

pseudorange can be written as [*Wells et al.*, 1987]:

$$p = \rho + c \cdot (dt - dT) + d_{trop} + d_{ion} + m_p + \epsilon_p, \tag{3.1}$$

where p represents the pseudorange observation, ρ the geometric satellite-receiver range, c the speed of light in a vacuum, dt the satellite clock offset from GPS Time, dT the receiver clock offset from GPS Time, d_{trop} the tropospheric delay, d_{ion} the ionospheric delay, m_p the error caused by code signal multipath, and ϵ_p random measurement errors.

For geodetic applications, a more precise observable is measured, the GPS carrier phase. The carrier phase measurement is obtained by differencing the incoming Doppler-shifted carrier signal from the satellite, and the signal's replica generated by the receiver. The carrier phase observation equation can be written as [*Wells et al.*, 1987]:

$$\Phi = \rho + c \cdot (dt - dT) + \lambda N + d_{trop} - d_{ion} + m_\Phi + \epsilon_\Phi, \tag{3.2}$$

where Φ is the carrier beat phase (in length units), λ is the wavelength, N the cycle ambiguity, m_Φ the error caused by phase signal multipath, and ϵ_Φ random measurement errors.

Equations (3.1) and (3.2) are directly comparable except for the (unknown) cycle ambiguity term that represents the indeterminate integer number of cycles between the satellite and the receiver when the receiver first locks onto the signal. At this time, the receiver assigns an arbitrary integer number to N [*Langley*, 1991a]. This number remains constant as long as no loss of phase lock occurs.

The research described by this dissertation has used as an observable the receiver-satellite carrier phase double difference. This observable is formed by differencing across two satellites as well as two receivers, and assumes exactly simultaneous measurements. This linear combination has the advantage of eliminating the receiver and

satellite clock offset and the Selective Availability δ-process (clock dither – see Subsection 3.2.2), and of reducing the effects caused by atmospheric and orbital biases [*Langley*, 1993]. The double difference observation equation is written as [*Wells et al.*, 1987]:

$$\nabla\Delta\Phi = \nabla\Delta\rho + \lambda \cdot \nabla\Delta N + \nabla\Delta d_{trop} - \nabla\Delta d_{ion} + \nabla\Delta m_{\Phi} + \nabla\Delta\epsilon_{\Phi}, \tag{3.3}$$

where $\nabla\Delta$ represents the double difference operator. We should point out that similar results are obtained whether using differenced or undifferenced carrier phase data, provided they are treated (weighted) properly.

The consequence of doubly differencing the carrier phases is that the observations become mathematically correlated. Let the double difference observations, for one epoch, be represented as:

$$\nabla\Delta\underline{\Phi} = \underline{R}\ \underline{\Phi}, \tag{3.4}$$

where $\underline{R}$ is a matrix with entries 0's, +1's and -1's and $\underline{\Phi}$ is the vector of undifferenced observations [*Santos*, 1990]. Applying the law of propagation of variances we arrive at the covariance matrix of the double difference observations:

$$\underline{C}_{\nabla\Delta\Phi} = \underline{R}\ \underline{C}_{\Phi}\ \underline{R}^{T}, \tag{3.5}$$

where $\underline{C}_{\Phi}$ is the covariance matrix of the vector $\underline{\Phi}$ which contains the undifferenced carrier phases at that epoch. The undifferenced phases are assumed to be uncorrelated. If the mathematical correlation is totally disregarded, $\underline{C}_{\nabla\Delta\Phi}$ equals an identity matrix (this is correct only if the physical correlation – see next paragraph, is also disregarded). If, in a network mode, the mathematical correlation of the double difference observations within each individual baselines is considered, the diagonal sub-matrices, one for each baseline, will have a block diagonal structure in $\underline{C}_{\nabla\Delta\Phi}$, and all off-diagonal sub-matrices will be equal to zero. If all mathematical correlations are

taken into account, there will be some non-zero elements in the off-diagonal submatrices, each representing correlations between baselines observing the same satellite. It goes without saying that matrix $\underline{C}_{\nabla\Delta\Phi}$ is scaled by the a priori variance factor of the double difference observations. The way we have gone about taking into account these correlations is by means of forming a matrix $\underline{R}$ which maps $\underline{\Phi}$ into $\nabla\Delta\underline{\Phi}$ at every observation epoch, and then evaluating eqn. (3.5). An efficient method for computing $\underline{C}_{\nabla\Delta\Phi}$ is described by *Beutler et al.* [1987].

Another type of correlation, the physical correlation, is a consequence of the common environments that envelope the observations making them spatially or temporally correlated. Physical correlation reflects the lack of knowledge on the environments, and may diminish as the modelling of the environments improves. *El-Rabbany* [1994] has investigated the effect of physical correlations on baseline determination. He concluded that physical correlation is inversely proportional to both sampling rate and baseline length. Disregarding these correlations results in over optimistic accuracy estimates for the adjusted parameters.

3.2 Errors and biases

GPS errors and biases may be classified into three categories: biases originating at the satellite (orbital biases, clock bias and Selective Availability), signal propagation biases (ionospheric and tropospheric delays) and biases and errors originating at the receiver (clock bias, receiver noise, multipath and antenna phase center variation). There are also geometrical effects coming from the satellite configuration geometry and the cycle ambiguity [*Kleusberg & Langley*, 1990]. The orbital bias, the one this research is most interested in, has already been explained in chapter 1.

3.2.1 Clock biases

Even though very accurate, the atomic clocks on board the satellites are not prefect, and tend to drift off the GPS time system, affecting the GPS measurements. The satellite clock bias can be reduced by using the corrections broadcast in the satellite navigation message or eliminated through differencing between receivers. As far as receiver clock bias is concerned, it can be treated as an unknown parameter or eliminated through differencing between satellites [*Kleusberg & Langley*, 1990].

3.2.2 Selective Availability and Anti-Spoofing

Selective Availability (SA) is the polite term the owners of GPS, the US military, used to describe the deliberate reduction of the C/A-code accuracy, which is the one used the most by non-authorized (civilian) users. The reason for its introduction is that, contrary to the original design, the accuracy of the C/A and P codes are nearly the same. With SA implemented, the nominal accuracy for horizontal and vertical positions is 100 m and 150 m, respectively, at a probability level of 95% [*Georgiadou & Doucet*, 1990].

Position accuracy is downgraded by SA in two ways. The first one, the so-called δ-process, is the dithering (manipulation) of the satellite clocks and affects all users. The second one, the so-called ϵ-process, is the addition of a slowly varying error into the broadcast ephemeris [*Georgiadou & Doucet*, 1990]. Two main effects of SA are the increase in noise in code and carrier phase measurement [*Kremer et al.*, 1990] and a bias in scale and orientation [*Talbot*, 1990; *Tolman et al.*, 1990]. The effects of SA can be significantly reduced by the use of Differential GPS (DGPS) corrections.

Anti-spoofing (A-S) means the denial of access to the P-code, which is replaced by a restricted Y-code [*Wells et al.*, 1987]. The objective of A-S is to prevent saboteurs to interfere (spoof) with the P-code by means of false signals. The consequences of A-S are a reduction in the accuracy of relative positioning based on code measurements

and in the effectiveness of rapid ambiguity resolution. A-S has been on since January 31 1994, on all Block II satellites, but has been recently on and off (turned off from April 19 to May 10, 1995, and turned off again on August 19, 1995). The status of A-S has been currently under debate. The way to overcome A-S is to use high performance receivers, capable of recovering the L2 carrier in the presence of A-S by means of squaring, code-aided squaring, cross-correlation or Z tracking techniques [*Ashjaee & Lorenz*, 1992]. An observed effect of anti-spoofing has been an increase in the scatter of baselines daily repeatability, as pointed out by J. F. Zumberge in the IGS Electronic Mail # 511.

3.2.3 Atmospheric effects

The atmosphere affects the GPS signals going through the ionosphere, and then through the troposphere.

The ionosphere comprises the uppermost part of the atmosphere where gases are ionized primarily by the sun's ultra-violet radiation. This phenomenon releases free electrons, and free electrons affect the propagation of GPS signals. The ionosphere causes a negative delay in the phase measurement (a phase advance) and a positive delay in the pseudorange measurement. The ionospheric delay is proportional to the number of free electrons along the signal's path or the total electron content (TEC). The TEC depends on time of the day, time of the year, solar cycle, and geographical location. The ionospheric delay, in length units, varies from 5 to 150 metres [*Klobuchar*, 1991].

The ionospheric delay can be dealt with in different ways. Since the ionosphere is frequency dependent, users of dual frequency receivers can eliminate the bulk of the effect by combining L1 and L2 carrier phase measurements into an ionosphere-free linear combination, known as L3 or Lc linear combination. This quasi-observable, in

units of length, is:

$$\Phi_{Lc} = \frac{f_{L1}^2 \Phi_{L1} - f_{L2}^2 \Phi_{L2}}{f_{L1}^2 - f_{L2}^2}, \tag{3.6}$$

where f_{L1} and f_{L2} are the frequencies of the L1 and L2 carrier phases. This linear combination should not be used for short baselines because it is noisier than single frequency observations, i.e., the standard deviation σ_{LC} is larger than either σ_{L1} or σ_{L2}. The 'short baseline' length depends on receiver noise and solar activity, being around 10 km during high solar activity (during the peak of a solar cycle) or around 30 km during low solar activity (at the minimum of a solar cycle) [*Komjathy*, 1995]. Users of single frequency receivers may use one of the many ionospheric models available, for instance, the Klobuchar ionospheric model or the IRI90 reference ionospheric model [*Komjathy et al.*, 1995].

By troposphere is usually meant the non-ionised part of the atmosphere (the correct designation should be "neutral atmosphere"). The tropospheric delay depends on the water vapour and dry air gas composition along the signal's path varying from around 2 metres at the zenith to 20 metres at 10 degrees elevation angle [*Wells et al.*, 1987]. This propagation delay is usually divided into a dry or hydrostatic and a wet component. Both of them can be described as the product of a delay at the zenith and a model of the elevation dependence of the propagation delay, known as a mapping function [*Mendes & Langley, 1994*]. This tropospheric delay can be predicted via theoretical models, calibrated via a water vapour radiometer (an expensive option) or estimated, along with the other parameters in the adjustment, as an offset or scale applied to an a priori estimate, or as a stochastic parameter [*van der Wal*, 1995].

3.2.4 Antenna and receiver errors

The most intriguing of all receiver errors is multipath. Multipath error occurs when the signal coming from a satellite arrives at the receiver's antenna following different paths as a result of reflections, principally those occurring near the receiver's antenna.

Code measurements are affected the most by multipath but the error multipath causes in carrier phase measurement can still be much larger than the receiver noise level. The best way to handle multipath is by avoiding it through a careful site selection, with no reflecting material in the antenna's vicinity [*Georgiadou & Kleusberg*, 1988].

Antenna phase centre variation depends on the direction of the incoming signal. The range error coming from this variation is different for L1 and L2 due to their usually different phase centres . This error is a function of antenna design and quality.

Finally, the measurement noise, which depends on the type of observable (and also on the receiver) used. *Kleusberg & Langley* [1990] stated that, by that time, measurement noise varied from a few metres, for C/A code, to a few millimeters, for carrier phase. Recent improvements in receiver technology have lowered this measurement noise. For example, the Ashtech Z-12 receivers have shown a C/A-code pseudorange noise at about the 4 cm level [*Wells et al.*, 1995].

3.2.5 Geometrical configuration of the satellites

The geometrical distribution of the satellites in the sky affects the accuracy of the GPS positions. It can be easily understood if we imagine two scenarios one in which all available satellites are bunched together in the sky, and the other in which they are well spaced. The accuracy resulting from the second situation will be much better. This happens because the design matrix is a function of the satellite sky distribution, affecting ultimately the solution and its covariance matrix. It has been shown that even with the full constellation there will be areas in the sky with no satellite coverage. The geometrical strength of the satellite configuration is measured by a number called the "dilution of precision" (DOP). The lower the DOP, the better the satellite geometry at the moment of measurements [*Santerre*, 1989; *Kleusberg & Langley*, 1990]. The geometrical strength of satellite configuration for relative positioning can be evaluated by means of the relative dilution of precision (RDOP) [*Goad*, 1988].

3.2.6 Ambiguity and cycle slips

The computation of the integer number corresponding to the initial cycle ambiguity represents the drawback of using carrier phase observations. For short baselines of up to around 30 km, depending on the behaviour of the ionosphere [*Komjathy, 1995*], a technique known as on-the-fly (OTF) ambiguity resolution [*Abidin*, 1992] has been developed. This technique incorporates the best of other techniques, namely the extrawidelaning [*Wubbena*, 1989], the ambiguity mapping function [*Remondi*, 1984; *Mader*, 1990] and the least squares approach [*Hatch*, 1990].

Ambiguity resolution becomes an even bigger problem the longer the baselines are. The linear combination of dual frequency GPS data into the wide lane (Lw), has shown to be very effective for over long baselines. This quasi-observable, in units of length, is:

$$\Phi_{Lw} = \frac{f_{L1}\Phi_{L1} - f_{L2}\Phi_{L2}}{f_{L1} - f_{L2}}. \tag{3.7}$$

The fact that the wide lane has a large wavelength, 86 cm, makes it well suited for the resolution of cycle ambiguities. Ambiguity resolution in long baselines is an iterative procedure in which a first solution is obtained with Lw. Subsequent solutions are then carried out using Lc or the narrow lane (Ln) linear combination. This quasi-observable, in units of length, is:

$$\Phi_{Ln} = \frac{f_{L1}\Phi_{L1} + f_{L2}\Phi_{L2}}{f_{L1} + f_{L2}}. \tag{3.8}$$

The problem is more critical for baselines of hundreds of kilometres. *Mervart et al.*, [1994] report that for the processing of the Epoch'92 campaign, they had to repeat the least-squares adjustment iteratively for both Lw and Ln, using an ionospheric model. Ionosphere is a major source of uncertainty in ambiguity resolution [*Wanninger*, 1993].

A problem closely related to ambiguity resolution is the occurrence of cycle slips. A cycle slip is an integer discontinuity in the phase measurement being observed by the GPS receiver. It causes the signal at the time of the discontinuity to shift by an

integer number of cycles. The possible causes for cycle slips are receiver dependent (low signal strength, dynamics of the antenna in kinematic surveying, internal signal processing) and observation dependent (obstructions, signal noise due to multipath or ionospheric activity and low satellite elevation) [*Lichteneger & Hoffmann-Wellenhof*, 1990].

Cycle slip detection and elimination, sometimes also referred to as data editing, is typically a pre-processing task. For dual frequency receivers, it can be done by using the different characteristics of the linear combinations between L1 and L2. Cycle slips in the undifferenced carrier phase can be detected using the ionospheric residual, $\delta\Phi$, time series [*Kleusberg et al.*, 1989]. This quasi-observable, in units of length, is:

$$\delta\Phi(t) = \Phi_{L2}(t) - \Phi_{L1}(t). \tag{3.9}$$

The ionospheric residual is usually a smooth quantity affected by the ionosphere only. Cycle slips would provoke sudden jumps in the function. That is what Figure 3.1 shows. The 6 prominent spikes were artificially introduced into the raw GPS data

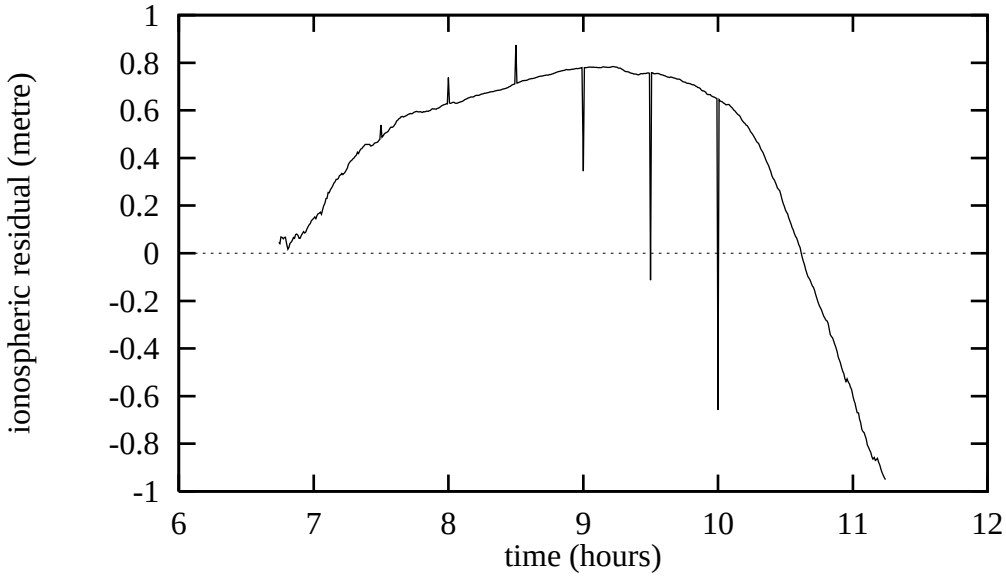

Figure 3.1: Cycle slips detected by the ionospheric residual

of satellite PRN 5, collected at station Algonquin, on January 2nd, 1994, with the

values shown in Table 3.1. Figure 3.2 displays the rate of change in the ionospheric

Table 3.1: Number of cycles added to L1 and L2 undifferenced carrier phases.

hour	L1	L2	hour	L1	L2
7:30	+1	+1	9:00	+1	-1
8:00	+2	+2	9:30	+2	-2
8:30	+3	+3	10:00	+3	-3

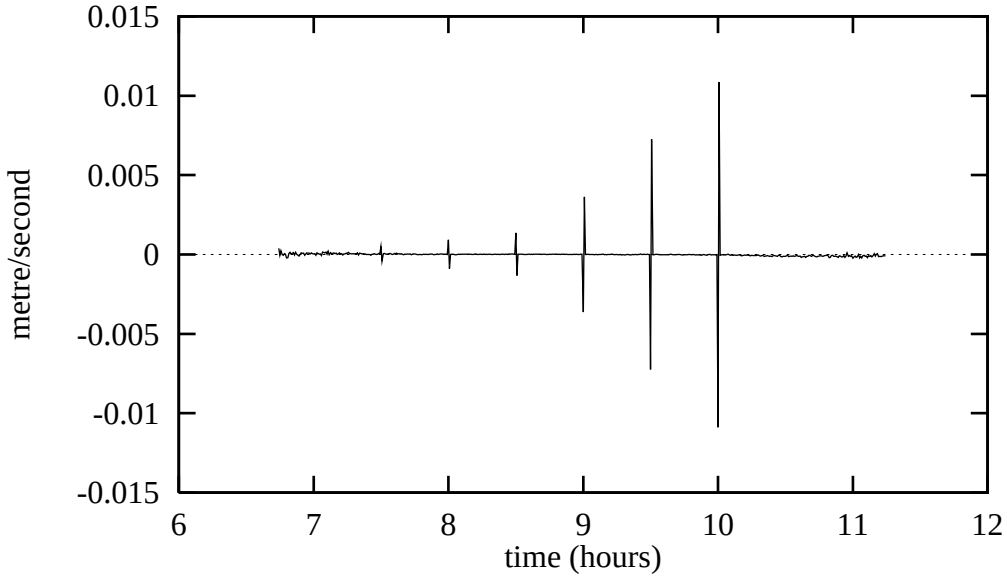

Figure 3.2: Rate of change of the ionospheric residual

residual for the same case study. The ionospheric residual can be used for cycle slip detection of undifferenced data in static real-time applications as follows. After a certain continuous number of observations are collected, they are fitted by a low-degree polynomial. A prediction to the next observation is then compared with the actual observation. If they differ by a value larger than a predefined threshold then potentially a cycle slip has just occurred and this observation is flagged as the end of the continuous observing interval.

For correcting the cycles slips which have occurred in dual frequency undifferenced

data, one has to compute the integer numbers quantifying the slips on both L1 and L2 carrier phases. These integers are then added to the collected phase measurements. They can be computed with the aid of a look-up table [*Lichteneger & Hoffmann-Wellenhof*, 1990] or using another linear combination. DIPOP [*Kleusberg et al.*, 1989] uses the wide lane linear combination. The estimates of the individual cycle slips are computed from these two linear combinations, the ionospheric residual and the wide lane combination.

If the dual frequency double difference is used as an observable, again linear combinations of L1 and L2 may be used. DIPOP uses the ionosphere-free and either the wide lane or the ionospheric residual linear combinations [*Komjathy*, 1995], subtracting from them a nominal range double difference. The detection and correction of cycle slips is somewhat similar to the undifferenced case. Straight line fitting is applied over five points in the ionosphere-free linear combination. If the difference between a predicted value based on this fit and the actual observation is larger than a preset threshold, it indicates a cycle slip. Figures 3.4 and 3.3 show actual cases of

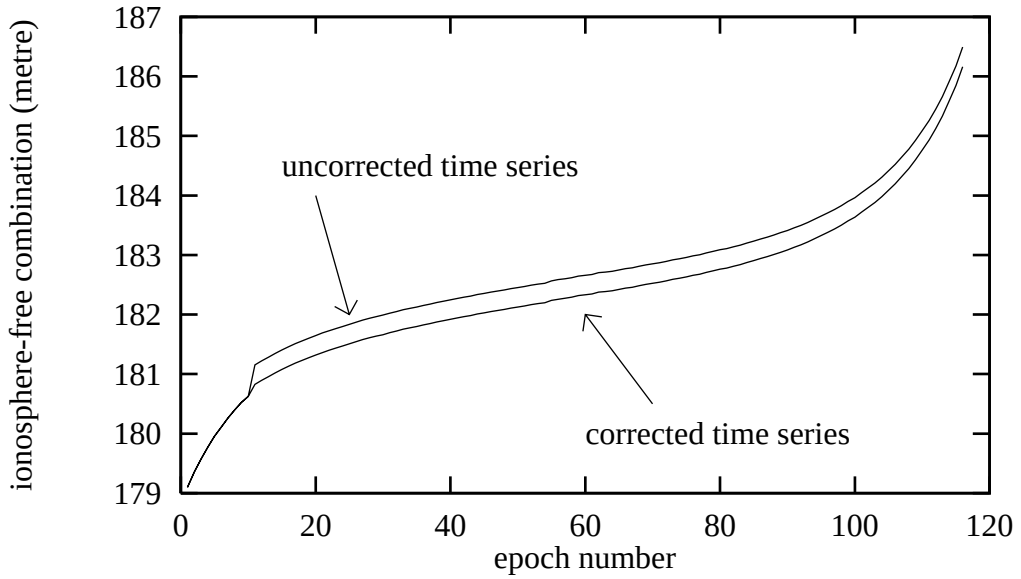

Figure 3.3: Cycle slip on the ionosphere-free linear combination double difference

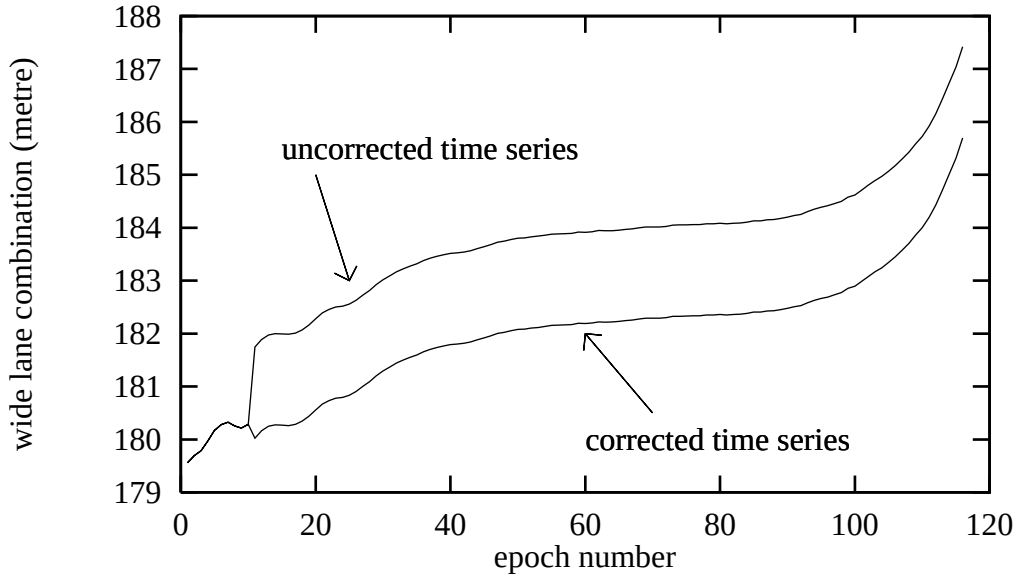

Figure 3.4: Cycle slip on the wide lane linear combination double difference

time series where the occurrence of cycle slip is evident, involving a particular satellite pair. The use of these linear combinations is well established and several authors have applied them for the purpose of cycle slip editing [e.g., *Blewitt*, 1990].

Other approaches which may also be applied, e.g., using the phase triple difference, shall not be presented here. One may refer to *Lichteneger & Hoffmann-Wellenhof* [1990] for a broad review on cycle slip editing.

We conclude by saying that the emphasis in data editing has been more and more on detection of all cycle slips. If they cannot be corrected at least they should be flagged so that a new ambiguity can be solved for. The problem is with undetected cycle slips, which may eventually degrade the solution. An example of that is presented in the penultimate chapter of this dissertation.

Chapter 4

Modelling and solving the equations of motion

4.1 Introduction to the problem

The orbit of a satellite is the solution of a second order differential equation system, known as the equations of motion, provided some initial or boundary conditions are satisfied. The equations of motion represented in an inertial geocentric coordinate system have the form:

$$\ddot{\underline{r}} = \frac{GM\underline{r}}{\| \underline{r} \|^3} + \ddot{\underline{p}}, \tag{4.1}$$

where $\ddot{\underline{r}}$ is the total acceleration vector of the satellite, GM is the earth's gravitational constant, $\underline{r}$ is the satellite geocentric position vector, and $\ddot{\underline{p}}$ represents the sum of the perturbing accelerations that act on the satellite. Equation (4.1) represents a kinematic formulation in which the mass of the satellite is not needed to describe its motion [*Vaníček*, 1973].

This system of second order differential equations can be integrated when conditions at an initial time t_0 are given. The initial conditions are a vector composed of

an initial position $[x, y, z]^T$ and velocity $[\dot{x}, \dot{y}, \dot{z}]^T$ of the satellite or its equivalent Keplerian elements ($a_0, e_0, i_0, \varpi_0, \Omega_0$, and one of the anomalies), at the initial epoch. The solution of the equations of motion yields a set of satellite positions and velocities, at any other time. In this dissertation, the vector composed of either $[x, y, z, \dot{x}, \dot{y}, \dot{z}]^T$ or ($a_0, e_0, i_0, \varpi_0, \Omega_0$ and one of the anomalies) is called the state vector.

The first term on the right-hand side of eqn. (4.1) describes the Keplerian motion of a satellite in a central field (i.e., under the influence of the central part of the gravitational field only), the orbit being a conic section. The second term represents the sum of the effects caused by the non-central part of the earth's gravitational field, the attraction of the moon, the sun, and other celestial bodies, the direct and indirect effects of the solar radiation pressure, the atmospheric drag effect, ocean and earth tides, relativistic effects, electromagnetic effects, thruster firings, out-gassing, etc. These perturbing accelerations cause a departure from the (elliptical) Keplerian orbit. If these perturbations were perfectly modelled, the integrated orbit would pinpoint the satellite position at any given time without error.

For the solution of the equations of motion an integration technique is required. The technique can be either analytical or numerical. The precision of the solution depends on the accuracy of the initial conditions, on how well the perturbing accelerations are modelled, and, up to a certain degree, on the integration technique chosen.

This chapter can be regarded as being composed of two parts. The first describes how the right-hand side of eqn. (4.1) is modelled; the second, the way we have gone about solving the equation. Most of the models and techniques described in this chapter have been implemented in our numerical integrator program, called PREDICT. This program is summarized in Appendix II.

4.2 Mathematical representation of the acceleration producing forces

4.2.1 Earth's gravitational field

The external potential W_g of the earth's gravitational field satisfies Laplace's differential equation [e.g., *Vaníček & Krakiwsky*, 1986]:

$$\nabla^2 W_g = 0. \tag{4.2}$$

The expansion of W_g into spherical harmonics, which constitute a general solution of eqn. (4.2), is the usual representation of W_g, and is given as [e.g., *Torge*, 1989]:

$$W_g = \frac{GM}{r}\left[1 + \sum_{n=2}^{\infty}\left(\frac{a_e}{r}\right)^n \sum_{m=0}^{n}\left(C_{nm}\cos m\lambda + S_{nm}\sin m\lambda\right)P_{nm}(\sin\beta)\right], \tag{4.3}$$

where the spherical coordinates r, β, λ represent, respectively, the geocentric distance to the satellite, the geocentric latitude and the geocentric longitude, a_e stands for the major semi-axis of the adopted ellipsoid, $P_{nm}(\sin\beta)$ are the associated Legendre functions, and C_{nm}, S_{nm} are geopotential coefficients of degree n and order m.

For the purpose of GPS satellite orbit computation, the upper limit for the first summation in eqn. (4.3) is truncated to a predefined degree and order, usually 8, because the effect on GPS orbits resulting from disregarding these coefficients is very small, being 0.2 m for a 5-day arc [*Santos*, 1994].

The coefficients C_{n0} in eqn. (4.3) are commonly replaced by $-J_n$. The coefficient J_2, known as the dynamic form factor, reflects the earth's equatorial ellipticity and is about three orders of magnitude larger than any other geopotential coefficient. The other coefficients depict the remaining irregularities of the earth's gravitational field. Disregarding J_2 results in a perturbation on GPS orbits of 3.5 km for a 6-hour arc and 110 km for a 5-day arc. The joint effect on GPS orbits coming from the other harmonics is equal to 100 m for a 6-hour arc and 3 km for 5-day arc [*Santos*, 1994].

It can be seen that eqn. (4.3) requires the satellite position expressed in spherical coordinates. The latter can be obtained from the satellite position vector $[x, y, z]^T$ by the following well known expressions:

$$
\begin{aligned}
r &= (x^2 + y^2 + z^2)^{1/2} \\
\beta &= \arcsin \frac{z}{r} \\
\lambda &= 2 \ \arctan \frac{y}{x + \sqrt{x^2 + y^2}}.
\end{aligned}
\tag{4.4}
$$

In general, the geopotential coefficients are furnished normalized, represented by $\overline{C}_{nm}$ and $\overline{S}_{nm}$. That is the case, for instance, of the GEMT3 geopotential model [*Lerch et al.*, 1992]. The relationship between the normalized and non-normalized geopotential coefficients is given by [*McCarthy et al.*, 1993]:

$$
\left.\begin{matrix} C_{nm} \\ S_{nm} \end{matrix}\right\} = \left[\frac{(n-m)!\,(2n+1)\,(2-\delta_{0m})}{(n+m)!}\right]^{1/2} \left\{\begin{matrix} \overline{C}_{nm} \\ \overline{S}_{nm}, \end{matrix}\right.
\tag{4.5}
$$

where the symbol δ_{0m} is the Kronecker delta:

$$
\delta_{0m} = \begin{cases} 1, & \text{for } m = 0 \\ 0, & \text{for } m \neq 0. \end{cases}
\tag{4.6}
$$

The geopotential coefficients are supplied in the CT-system. Hence, the satellite position vector has to be transformed from the adopted inertial coordinate system into the CT-system before applying eqns. (4.4).

To obtain the components of the gravitational accelerations $[\ddot{x}, \ddot{y}, \ddot{z}]^T$, the gradient of W_g has to be evaluated by means of the partial derivatives of eqn. (4.3) with respect to the Cartesian coordinates of the satellite. By applying the chain rule, we get:

$$
\begin{aligned}
\ddot{x} &= \frac{\partial W_g}{\partial x} = \frac{\partial W_g}{\partial r}\frac{\partial r}{\partial x} + \frac{\partial W_g}{\partial \beta}\frac{\partial \beta}{\partial x} + \frac{\partial W_g}{\partial \lambda}\frac{\partial \lambda}{\partial x} \\
\ddot{y} &= \frac{\partial W_g}{\partial y} = \frac{\partial W_g}{\partial r}\frac{\partial r}{\partial y} + \frac{\partial W_g}{\partial \beta}\frac{\partial \beta}{\partial y} + \frac{\partial W_g}{\partial \lambda}\frac{\partial \lambda}{\partial y}
\end{aligned}
\tag{4.7}
$$

$$\ddot{z} = \frac{\partial W_g}{\partial z} = \frac{\partial W_g}{\partial r}\frac{\partial r}{\partial z} + \frac{\partial W_g}{\partial \beta}\frac{\partial \beta}{\partial z} + \frac{\partial W_g}{\partial \lambda}\frac{\partial \lambda}{\partial z}.$$

The partial derivatives of W_g with respect to r, β and λ are:

$$\frac{\partial W_g}{\partial r} = -\frac{GM}{r^2}\left\{1 + \sum_{n=2}^{\infty}\left(\frac{a_e}{r}\right)^n \sum_{m=0}^{n}(n+1)\left[C_{nm}\cos m\lambda + S_{nm}\sin m\lambda\right]P_{nm}(\sin\beta)\right\}$$

$$\frac{\partial W_g}{\partial \lambda} = \frac{GM}{r}\sum_{n=2}^{\infty}\left(\frac{a_e}{r}\right)^n \sum_{m=0}^{n} m\left[S_{nm}\cos m\lambda - C_{nm}\sin m\lambda\right]P_{nm}(\sin\beta) \tag{4.8}$$

$$\frac{\partial W_g}{\partial \beta} = \frac{GM}{r}\sum_{n=2}^{\infty}\left(\frac{a_e}{r}\right)^n \sum_{m=0}^{n}\left[C_{nm}\cos m\lambda + S_{nm}\sin m\lambda\right]\frac{\partial}{\partial\beta}\left[P_{nm}(\sin\beta)\right],$$

where the derivative of the associated Legendre function with respect to β is [*McCarthy et al.*, 1993]:

$$\frac{\partial}{\partial\beta}[P_{nm}(\sin\beta)] = P_{nm+1}(\sin\beta) - m\tan\beta P_{nm}(\sin\beta). \tag{4.9}$$

The partial derivatives of the spherical coordinates with respect to the Cartesian coordinates are:

$$\begin{aligned}
\frac{\partial r}{\partial r_i} &= \frac{r_i}{r} \\
\frac{\partial \lambda}{\partial r_i} &= \frac{x}{y^2+x^2}\left(\frac{\partial y}{\partial r_i} - \frac{y}{x}\frac{\partial x}{\partial r_i}\right) \\
\frac{\partial \beta}{\partial r_i} &= \frac{1}{\sqrt{x^2+y^2}}\left(-\frac{zr_i}{r^2} + \frac{\partial z}{\partial r_i}\right),
\end{aligned} \tag{4.10}$$

where $r_i, i = 1, 2, 3$, stands for x, y and z.

The accelerations obtained by eqns. (4.7) are in the CT-system. They have to be transformed into the adopted inertial system before they can be used in the numerical integration.

4.2.2 Solar, lunar, and planetary gravitational perturbation

The gravitational perturbation induced by a third body, such as the sun, moon, or a planet, regarded as a point mass, can be represented as [*Rizos & Stolz*, 1985]:

$$\ddot{\underline{p}}_{tb} = GM_{tb}\left(\frac{\underline{r}_{tb} - \underline{r}}{\| \underline{r}_{tb} - \underline{r} \|^3} - \frac{\underline{r}_{tb}}{\| \underline{r}_{tb} \|^3}\right), \tag{4.11}$$

where M_{tb} is the mass of the third body, and $\underline{r}$ and $\underline{r}_{tb}$ are the geocentric position vectors of the satellite and the third body, respectively. These two vector quantities have to be expressed in the adopted inertial coordinate system for the perturbation to be used in eqn. (4.1). The effect of the perturbing force on GPS satellites coming from moon is, for a 6-hour arc and for a 5-day arc, respectively, 600 m and 7 km; the effect coming from the sun is, for the same arcs, 150 m and 3000 km [*Santos*, 1994]. The perturbation coming from planets is neglegible, and has been disregarded for our purpose.

4.2.3 Solar radiation pressure perturbation

The perturbation $\ddot{\underline{p}}_{srp}$ due to solar radiation pressure is the most complicated to model. This is due to the fact that the GPS satellites have a complex shape and that they are constructed of materials that have different reflectance, ranging from 0 (black) to 1 (white), and scattering, ranging from 0 (diffuse) to 1 (specular), characteristics, and thus respond differently to the incoming sunlight. There are thermal variations in the area of the satellite that is illuminated by the sun during the satellite's orbit around the earth. A complete solar radiation model has to take into account the various contributions stemming from the satellite main body, the solar panels, the antenna array and the rocket engine assembly [*Fliegel et al.*, 1985; *Delikaraoglou*, 1989; *Fliegel & Gallini*, 1989].

For the modelling of the solar radiation pressure perturbing acceleration, a satellite-centered coordinate system is considered using the fact that the antennas of the satellite are kept pointed towards the earth and the solar panel support beam is designed

to be perpendicular to the direction spacecraft-sun. The satellite-centered coordinate system is defined in such a way that its Z axis is positive along the antenna direction towards the center of mass of the earth, the Y axis is taken along the solar panel support beam, normal to the direction spacecraft-sun and the X axis completes this right-handed system. The sun is contained in the XZ plane. The Y axis is kept normal to the plane that contains spacecraft, sun and centre of mass of the earth. The solar panels are rotated around the Y axis in order to offer the maximum area to the sun.

The unit vectors which make the Cartesian triad of the above defined coordinate system are shown in Figure 4.1; also shown is $\underline{n}$, a unit vector pointing from the sun to the spacecraft. The unit vectors $\underline{e}_z$, $\underline{e}_x$ and $\underline{n}$ are always contained in the plane satellite-sun-earth.

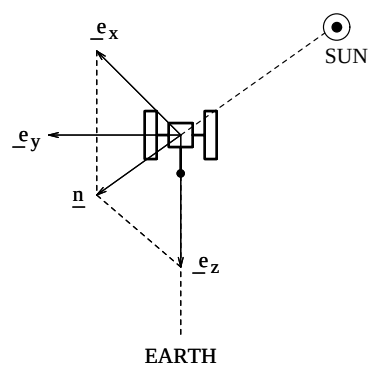

Figure 4.1: Satellite coordinate system

These unit vectors are described in the inertial Cartesian system as follows:

$$\underline{e}_z = -\frac{\underline{r}}{\| \underline{r} \|}$$

$$\underline{e}_y = \frac{\underline{e}_z \times \underline{n}}{\| \underline{e}_z \times \underline{n} \|}$$

$$\underline{e}_x = \frac{\underline{e}_y \times \underline{e}_z}{\| \underline{e}_y \times \underline{e}_z \|}$$

$$\underline{n} = \frac{\underline{r} - \underline{r}_s}{\| \underline{r} - \underline{r}_s \|}, \tag{4.12}$$

where $\underline{r}$ and $\underline{r}_s$ are the geocentric position vectors of the satellite and the sun, respectively. The vectors $\underline{e}_y$ and $\underline{e}_x$ are undefined when the angle θ, between vectors $\underline{e}_z$ and $\underline{n}$, is equal either to 0^0 or 180^0, i.e., when sun-satellite-earth are aligned.

The solar radiation pressure is usually divided into the direct solar radiation pressure $\ddot{\underline{p}}_{dir}$, and the radiation pressure in the Y direction, the so-called Y bias, $\ddot{\underline{p}}_y$. Hence:

$$\ddot{\underline{p}}_{srp} = \ddot{\underline{p}}_{dir} + \ddot{\underline{p}}_y. \tag{4.13}$$

Direct solar radiation pressure

The direct solar radiation pressure can be modelled in a first approximation by [*Feltens*, 1988]:

$$\ddot{\underline{p}}_{dir} = \nu P_s C_r \frac{a_{ES}^2}{\| \underline{r} - \underline{r}_s \|^2} \frac{A}{m} \underline{n}, \tag{4.14}$$

where ν is the eclipse factor (equal to zero when the satellite is in the earth's shadow and equal to one when it is in sunlight; ν is positive and smaller than one during its passage through the penumbra zone); P_s is the solar radiation pressure (which is the ratio of the intensity of radiation and the speed of light, expressed in N/m^2); C_r is the reflectivity factor which depends on the spacecraft reflectivity characteristics (unitless); A is the effective cross sectional area of the spacecraft affected by the solar radiation; a_{ES} is the major semi-axis of the earth's orbit around the sun (approximately equal to 1 Astronomical Unit - AU[1]); m is the mass of the satellite; and $\underline{r}$, $\underline{r}_s$ and $\underline{n}$ have been defined previously.

The model given by eqn. (4.14) describes the perturbing acceleration due to the solar radiation pressure on a spherical satellite [*Tapley*, 1989], being usually referred

[1] $1AU = 1.49597870 \times 10^{11} m$ [*Nautical Almanac Office*, 1983].

to as either the "cannonball model" [*Parrot*, 1989] or the "flat plate" model [*Delikaraoglou*, 1989], being the reflectivity factor C_r an adjustable parameter.

The usually unknown constants P_s, C_r and A/m are grouped into only one parameter known as the direct solar radiation pressure parameter, p_0 [*Beutler et al.*, 1986]. Hence, eqn. (4.14) can be rewritten as:

$$\ddot{\underline{p}}_{dir} = \nu \; p_0 \; \underline{n}, \tag{4.15}$$

with the additional assumption that $(a_{ES}^2 / \parallel \underline{r} - \underline{r}_s \parallel^2)$ is approximately equal to 1.

The mathematical model described by eqn. (4.15) has two sources of uncertainty. The first one is in the parameter p_0 and is due to variations in the solar pressure constant P_s, to the different reflectivity properties of the various materials from which the GPS satellites are constructed, and to the difficulty in determining the effective cross sectional area A. The second source of uncertainty stems from a proper definition of the earth's shadow and penumbra figuring in the computation of the eclipse factor ν [*Rizos & Stolz*, 1985]. The parameter p_0 is given an a priori value, and then estimated in the orbit improvement process.

Radiation pressure in the Y direction

The second component of the solar radiation pressure model takes into account the acceleration along the the direction of solar panel beam. The causes for this y-bias are, probably, connected to (a) nonlinearity of the solar panel beams with respect to the satellite body median plane, (b) misalignments of the solar sensors with respect to the z axis, and (c) the heat generated in the satellite's body is radiated preferentially from louvres on the $+y$ side of the Block I satellites [*Fleigel et al.*, 1992].

The effect of the y-direction radiation pressure can be modelled as [*Landau*, 1988]:

$$\ddot{\underline{p}}_y = \nu \; p_y \; \underline{e}_y, \tag{4.16}$$

where p_y is the y-bias parameter. The parameter p_y is given an a priori value, and is then estimated in the orbit improvement process.

The solar radiation model ROCK

The simplifying assumption made in the formulation of the solar radiation model seen before, namely,

- that the effective cross-sectional area A of the spacecraft illuminated by the sun is constant;
- that the reflectivity factor C_r is the same for all materials; and,
- that there is no shadowing effect of the antenna and the satellite body,

obviously do not depict exactly the reality. A more refined solar radiation model was developed for both the Block I (Navstar 1 to 11) and Block II (Navstar 13 to 21) GPS satellites and was coded into computer subroutines known as ROCK 4 [*Fliegel et al.*, 1985] and ROCK 42 [*Fliegel & Gallini*, 1989]. The force model represents the GPS satellites with 13 surfaces for Block I and 15 for Block II, each specified as being either a flat or a cylindrical surface with pre-assigned reflectivity and specularity. These subroutines are long and much of them are devoted to the antennas and the shadowing caused by them, even though this effect is only about 3% of the total solar pressure force [*Fliegel et al.*, 1992].

The input of the ROCK programs is the angle B between the sun and the $+Z$ axis. The outputs are the X and Z solar pressure force components (neglecting the Y bias). As an alternative to the long ROCK4 and ROCK42 subroutines, each output parameter can be represented as a short Fourier series, known as $T10$ formulas:

$$X = -4.55\sin(B) + 0.08\sin(2B + 0.9) - 0.06\cos(4B + 0.08) + 0.08 \quad (4.17)$$

$$Z = -4.54\cos(B) + 0.20\sin(2B - 0.3) - 0.03\sin(4B), \quad (4.18)$$

for Block I satellites, and as $T20$ formulas:

$$X = -8.96\sin(B) + 0.16\sin(3B) + 0.10\sin(5B) - 0.07\sin(7B) \quad (4.19)$$

$$Z = -8.43\cos(B) \quad (4.20)$$

for Block II satellites. These expressions use units of $10^{-5}N$, angle B in radians and include thermal radiation. They translate the ROCK 4 and ROCK 42 outputs with an error never exceeding 1.5% which occurs only during the eclipse seasons [*Fliegel et al.*, 1992]. Formulas $T20$ give also an adequate approximation for Block IIA satellites (from Navstar 22 on) which have about the same properties as Block II satellites.

The forces are then converted into accelerations after dividing them by the respective satellite masses. Nominal masses for some Block I satellites are shown in Table 4.1 [*Fliegel et al.*, 1992]. The nominal mass for a Block II satellite is 883.2 kilograms, whereas for a Block IIA satellite is 972.9 kilograms [*Fliegel*, 1993]. These masses are correct for late 1990. They will slightly change over time as the satellites are maneuvered and expend fuel, but for most practical purposes the above values will suffice [*Fliegel et al.*, 1992].

Table 4.1: Nominal mass of Block I GPS satellites.

SV number	PRN number	Nominal Mass (kg)
3	6	453.8
4	8	440.9
6	9	462.6
8	11	522.2
9	13	520.4
10	12	519.8
11	3	521.8

The solar radiation pressure results in an acceleration [*Lichten & Border*, 1987]:

$$\ddot{\underline{p}}_{srp} = \nu \left[\frac{a_{ES}^2}{\| \underline{r} - \underline{r}_s \|^2} (G_x a_x \underline{e}_x + G_z a_z \underline{e}_z) + G_y \underline{e}_y \right], \tag{4.21}$$

where G_x and G_z are solar pressure coefficient scaling factors, usually very close to 1 and estimated in the orbit improvement process, G_y is the Y bias, and a_x and a_z are the satellite-centered accelerations obtained via the ROCK models or T10 and T20 formulae.

The perturbations in GPS satellite motion caused by solar radiation pressure are significant. The effect of direct radiation is, for a 6-hour arc and a 5-day arc, respectively, equal to 40 m and 800 m; the effect of y-bias, for the same arcs, is equal to 2 m and 100 m [*Santos*, 1994].

The solar radiation models expressed by eqns. (4.15) and (4.16), and by eqn. (4.21) have been implemented. Tests have shown that, in practice, the difference between these two models is small, at the order of 3% of the total perturbing effect of the solar radiation pressure, provided the corresponding parameters in each model are estimated [*Santos*, 1994]. This result corroborates what had been pointed out by *Beutler* [1993b].

We conclude this subsection saying that an expanded solar radiation pressure model has been proposed and is presently under investigation by the Center for Orbit Determination in Europe (CODE) [*Beutler et al.*, 1994].

Computation of the Eclipse Factor

The knowledge of the eclipse factor ν is essential for the computation of $\ddot{\underline{p}}_{srp}$, specially during the two annual episodes when the satellite travels periodically through the earth's shadow, which are known as the eclipse seasons. Eclipse seasons are 30 to 40 days long, depending on the orbital plane. During each season, the satellite passes periodically through the umbra-penumbra region in less than 60 minutes.

The determination of ν can be carried out, e.g., as described by *McCarthy et al.* [1993] or by using a more refined approach, such as the one described by *Ash* [1972], which takes into account the non-abruptness of the satellite passage from sunlight to shadow (even though the span of time spent in the penumbra will be very brief).

The IERS Standards [*International Earth Rotation Service*, 1992] recommends the use of a model that takes into account both umbra and penumbra. The recommended earth's radius for such model is 6402 km.

Reflected solar radiation effect

Part of the solar radiation which reaches the earth is reflected back towards the satellite and causes an additional perturbing acceleration. This perturbation is directly proportional to the earth's *albedo*. The albedo is influenced by geographical and meteorological features which makes it too complicated to be described by a simple model that would realistically show the significant features of the phenomenon.

The modelling of this reflected solar radiation can be done by assuming that the effective reflecting surface is a disk with a unique reflective property. In a more rigorous approach [e.g., *McCarthy et al.*, 1993] the earth's surface is divided into surface elements. For each one of these cells, the albedo is modelled by a spherical harmonic expansion followed by the computation of the individual acceleration contributions. The latter are then summed up to approximate the actual surface integral.

The effect of reflected solar radiation on the orbit of GPS satellites is relatively small, being equal to 1.5 m for an arc of 2 days [*Santos*, 1994].

4.2.4 Solid earth and ocean tidal perturbation

The motion of the GPS satellites is also perturbed by the variations in the earth's gravitational potential which occurs as a consequence of the deformation of the solid earth and water provoked by the gravitational attraction of celestial bodies. This deformation is known as tidal deformation. The tidal deformation expresses itself by means of earth and ocean tides. The common approach is to take into account only the luni-solar contribution since the one due to the planets corresponds to only 0.005% of the former [*Vaníček & Krakiwsky*, 1986].

The effect of solid earth and ocean tidal perturbation on the orbit of GPS satellites is relatively small. The effect of the perturbation of the solid earth on the GPS satellite motion is equal to 1 m for a 5-day arc; the ocean tidal perturbation, equal to 0.5 m for a 5-day arc [*Santos*, 1994].

Solid earth tidal perturbation

The perturbation due to the solid earth tides can be directly modelled as variations in the normalized geopotential coefficients by means of any model having frequency dependent Love numbers, such as the Wahr model [*International Earth Rotation Service*, 1992].

A simplified expression for the perturbing acceleration vector due to the solid earth tides $\ddot{\underline{p}}_{se}$ is computed by first defining the tidal bulge potential (at the satellite altitude) W_s as [*Melchior*, 1983]:

$$W_s = \left(\frac{a_e}{\| \underline{r} \|} \right)^3 k_2 W_2, \tag{4.22}$$

where W_2 is the tidal potential given at the earth's surface. Taking the partial derivatives of the W_s with respect to the satellite geocentric position vector $\underline{r}$ [*Rizos & Stolz*, 1985]:

$$\ddot{\underline{p}}_{se} = \frac{3}{2} k_2 \frac{GM_{tb}}{\| \underline{r}_{tb} \|^3} \frac{a_e^5}{\| \underline{r} \|^4} \left[(1 - 5\cos^2 Z) \frac{\underline{r}}{\| \underline{r} \|} + 2\cos Z \frac{\underline{r}_{tb}}{\| \underline{r}_{tb} \|} \right], \tag{4.23}$$

where M_{tb} is the mass of third body, $\underline{r}_{tb}$ is third body geocentric position, Z is the angle between $\underline{r}_{tb}$ and the satellite geocentric position vector $\underline{r}$ and k_2 is the second degree Love number.

Ocean tidal perturbation

The perturbation due to the ocean tides can also be directly modelled as periodic variations in the normalized geopotential coefficients [*International Earth Rotation Service*, 1992]. This perturbation is more difficult to model, since it is a function of coastline geometry, etc. A global ocean tidal model has to be used, such as that of *Schwiderski* [1983].

4.2.5 Relativistic perturbation

The motion of the satellite as shown in eqn. (4.1) is described by Newtonian physics and as such neglects the relativistic effects. The earth's gravitational field provokes a relativistic perturbation $\ddot{\underline{p}}_r$ on the orbital motion of the satellites. This perturbation can be modelled as [*Zhu & Groten*, 1988; *International Earth Rotation Service*, 1992]:

$$\ddot{\underline{p}}_r = -\frac{GM}{c^2 \parallel \underline{r} \parallel^3} \left[\left(4\frac{GM}{\parallel \underline{r} \parallel} - \parallel \dot{\underline{r}} \parallel^2 \right) \underline{r} + 4\,(\underline{r} \cdot \dot{\underline{r}})\, \dot{\underline{r}} \right] \tag{4.24}$$

where $\underline{r}$ and $\dot{\underline{r}}$ are geocentric position and velocity vectors of the satellite, respectively, and c represents the velocity of light. The error in the orbital motion of GPS satellites caused by disregarding the relativistic perturbation is equal to 1.5 m for a 5-day arc [*Santos*, 1994].

4.2.6 Other perturbations

Some perturbations are usually disregarded when dealing with GPS satellites. They are briefly described as follows.

Atmospheric drag

Any near-earth orbiting satellite undergoes a drag due to its interaction with the particles of the atmosphere. This drag-like force depends on the atmospheric density which is a function of the satellite height. At the height of the GPS satellites, the atmospheric density is assumed to be zero and hence so is the perturbation due to atmospheric drag [*Milani et al.*, 1987].

Electromagnetic effect

This effect is of a similar nature to the atmospheric drag. It is a consequence of the interaction between the satellite electrical charge, acquired due to collisions with electrons and ions while passing through the ionosphere, with the geomagnetic field.

At the altitude of GPS satellites the current knowledge about the plasma properties, particularly on its density and temperature, is still limited. A complication is that these quantities depend on geometrical parameters (latitude, solar hour and declination of the sun) and on the level of solar and geomagnetic activity [*Milani et al.*, 1987]. The perturbation caused by electromagnetic effects on GPS orbits has been disregarded.

Satellite maneuvering

From time to time, the GPS control segment needs to carry out orbital maneuvers in order to maintain a certain satellite configuration. This is done by activating the satellite thrusters. These maneuvers change the orbital motion and appear as sudden changes in the orbit itself. If that happens, a solution would be to set up new initial conditions after the maneuver is over.

Smaller satellite movements, related to the attitude control of the satellites, are called "momentum dumps". The satellites are stabilized by means of reaction wheels which operate with nominally zero momentum. Secular disturbing torques eventually saturate the momentum storage capacity. It is then compensated (emptied) through external torques created by an autonomous activation of the satellite thrusters. In our approach, momentum dumps are taken care of within the estimation of the solar radiation pressure parameters. They may constitute a good reason for stochastic modelling of the solar radiation pressure [*Beutler*, 1993]. Changes in the yaw attitude of the satellite during eclipse are also absorbed by the solar radiation pressure parameters. We conclude by saying that a model for the changes in the yaw attitude during eclipses has been presented by *Wu et al.* [1993].

4.2.7 Force model accuracy level

We would like to conclude this section by trying to gauge the accuracy of the implemented force model. Our force model is constituted of the attraction due to earth's gravitational field, up to degree and order 8, luni-solar gravitational perturbation, with moon and sun regarded as point masses, direct and y-bias solar radiation pressure perturbation, solid earth tidal perturbation and relativistic perturbation. We believe that this force model of a GPS satellite is below the metre level for arcs of up to about 5 days because only after then the joint effect of the neglected perturbations are at the metre level. Therefore, for our purpose of real-time orbit improvement, the force model implemented is more than enough to guarantee below metre accuracy of orbits.

4.3 Solution of the equations of motion

The equations of motion of a satellite can be solved either analytically or by numerical integration. The analytical solution of the equations of motion is an iterative process. It starts by taking into account only the earth's gravitational perturbation. This first approximation is then used for a second-order solution, which is then used for higher order solutions [*Kovalevsky*, 1989]. The analytical integration of the equations of motion is very useful if one wants to gain insight into the behaviour of the orbit under perturbations. It has major drawbacks, however, such as the need for complex algebraic derivations and evaluations of many trigonometric functions. Besides, the solutions obtained are always approximate (Keplerian, first-order, ..., nth-order perturbation) [*Beutler et al.*, 1984]. An additional disadvantage is the difficulty with the inclusion of non-gravitational forces such as the solar radiation pressure because of the earth's shadowing on the satellite which causes the acceleration discontinuities [*Kovalevsky*, 1989]. For high precision orbit determination, the numerical approach is required.

The numerical integration of the equations of motion as formulated by eqn. (4.1) can be directly carried out by Cowell's method. Other suitable methods for the numerical integration of orbits found in the literature are Encke's and the variation of parameters methods, but they require a slightly different formulation of the equations of motion [*Brouwer and Clemence*, 1961; *Conte*, 1962; *Herrick*, 1972].

In Cowell's method, the equations of motion are directly integrated in Cartesian coordinates based on a state vector for an initial epoch, yielding the Cartesian coordinates of the perturbed body at any subsequent epoch. Cowell's method presents the advantage of a simple formulation for the equations of motion. On the other hand, since it takes no advantage of the elliptical nature of the motion, a shorter step size is required, which may result in a larger round-off error; the overall accuracy may suffer as a result. In general, the smaller the number of integration steps, the more attenuated are the effects of round-off error. In spite of this drawback, Cowell's method has found much acceptance and has been used in several contemporary software packages. A description of the formulation we have made use of in our implementation follows.

4.3.1 Methods for numerical integration

There are several methods for the numerical solution of differential equations. They can be divided in single-step and multi-step. The former is a method in which each step uses only values obtained in a single step, i.e., in the preceding step. The latter, on the other hand, uses values that come from more than one preceding step. An example of a single-step procedure is the Runge-Kutta method [*Batin*, 1987]; examples of multi-step methods are the predictor-correctors described below. In orbit integration, predictor-corrector methods are usually preferred instead of single-step methods because fewer evaluations of the right-hand side of the equations of motion are necessary, which speeds up the whole numerical integration process.

The equations of motion of GPS satellites are second-order differential equations,

with an initial value problem of the form [*Kreyszig*, 1988]:

$$\ddot{\underline{r}} = \underline{f}(t, \underline{r}), \quad \underline{r}(t_0) = \underline{r}_0, \quad \dot{\underline{r}}(t_0) = \dot{\underline{r}}_0, \tag{4.25}$$

where $\ddot{\underline{r}}$, $\dot{\underline{r}}$ and $\underline{r}$ represent, respectively, the acceleration, velocity and position vectors, and t the time. Equation (4.25) shows that the satellite positions are obtainable by either direct integration of eqn. (4.1) or by doubly-integrating it, i.e., by a two step integration in which the satellite velocities are integrated from the accelerations, and then the positions are integrated from the velocities. Both alternatives have been studied and implemented, and are summarized as follows.

4.3.2 Methods for first-order differential equations

A multi-step method, known as Adams-Moulton, of nth order [*Velez & Maury*, 1970], is composed of a predictor:

$$\dot{\underline{r}}^p(t) = \dot{\underline{r}}(t-h) + h \sum_{i=0}^{n-1} \xi_i^p \; \ddot{\underline{r}}[t-(1+i)h], \tag{4.26}$$

and a corrector, which corresponds to the actual new value:

$$\dot{\underline{r}}^c(t) = \dot{\underline{r}}(t-h) + h \sum_{i=0}^{n-1} \xi_i^c \; \ddot{\underline{r}}[t-ih]. \tag{4.27}$$

where h is the step size given by $h = t_i - t_{i-1}$, $i = 1, 2, 3, \ldots$, and

$$f\,[t, \dot{\underline{r}}^p(t)] = \ddot{\underline{r}}(t).$$

The value of the coefficients ξ^p and ξ^c depend on the order of the predictor-corrector. The predictor-corrector is not self starting. A common approach is to compute the starter values $\ddot{\underline{r}}(t-2h)$, $\ddot{\underline{r}}(t-3h)$, $\ddot{\underline{r}}(t-4h)$, etc; by the Runge-Kutta algorithm [*Morsund & Duris*, 1967] or by Taylor series. The Adams-Moulton method is applied iteratively as follows:

1. The starter values of $\ddot{\underline{r}}(t-h)$, $\ddot{\underline{r}}(t-2h)$, ..., $\ddot{\underline{r}}(t-nh)$ are known.

2. Compute the predicted value $\dot{\underline{r}}^0(t)$, for the 0th iteration, using eqn. (4.26).

3. Evaluate $f[t, \ddot{\underline{r}}^p(t)]$.

4. Compute the corrected value $\dot{\underline{r}}^{k=1}(t)$, for the first iteration, using eqn. (4.27).

5. Iterate on k until

$$| \dot{\underline{r}}^k(t) - \dot{\underline{r}}^{k-1}(t) | < \epsilon,$$

for a prescribed ϵ .

This algorithm is complete only if it is specified what to do in case of non-convergence. The options would be to quit the iteration after a certain number of steps or to use a self-adjusted step size.

When applied for the solution of the equations of motion for the determination of position, the Adams-Moulton method has to be applied twice in the following order. First, compute the predicted velocity; then, compute predicted position; evaluate acceleration with the predicted position; compute corrected velocity; and, finally, compute corrected position (using the corrected velocity). The method iterates as described before.

4.3.3 Methods for second-order differential equations

In the same manner as for the solution of a first-order differential equation, a predictor-corrector can be applied with advantage over the single-step methods. We mention here the multi-step method based on the Störmer predictor and Cowell corrector [*Velez & Maury*, 1970], also known as Gauss summation or the Gauss-Jackson method, which has the general form:

$$\underline{r}^p(t) = 2\underline{r}(t-h) - \underline{r}(t-2h) + h^2 \sum_{i=0}^{n-1} \xi_i^p \; \ddot{\underline{r}}[t-(1+i)h], \tag{4.28}$$

for the predictor, and:

$$\underline{r}^c(t) = 2\underline{r}(t-h) - \underline{r}(t-2h) + h^2 \sum_{i=0}^{n-1} \xi_i^c \; \ddot{\underline{r}}[t-ih], \tag{4.29}$$

for the corrector.

The coefficients ξ^p and ξ^c assume values which depend on the order of the integrator. The implementation of the Störmer-Cowell predictor-corrector method follows the same iterative algorithm as described for the Adams-Moulton method. The application of the Störmer-Cowell method yields only the positions of the satellite. If the velocity of the satellite is also of interest, the Adams-Moulton method has to be used at the same time. The coefficients required by Adams-Moulton and the Störmer-Cowell methods can be computed by following the algorithm described by *Velez & Maury* [1970].

A question may be posed here on which one of these predictor-corrector methods, the Adams-Moulton or the Störmer-Cowell, yields the best solution of the equations of motion of the GPS satellites. To answer this question, we tested both of them in the same situation. We integrated the equations of motion taking into account only the radial gravitational field, and then compared the result with a pure Keplerian solution, for a 30 day period, using different integration step sizes. One of the results is shown in Figure 4.2 using the Störmer-Cowell method with a step size of 7.5 minutes. This Figure shows the the difference between the Keplerian orbit and the orbit resulting from the numerical integration. A similar result was obtained using the Adams-Mouton method. Besides the conclusion that both methods yield generally the same results, another is that they are indeed very stable.

In GPS orbit determination, the integration step size is usually chosen to be between 7 and 15 minutes. For our purpose of real-time orbit improvement, we used a step size equal to the interval with which the GPS observations were collected (2 minutes) in most of our tests. But in some tests, we also used 15 minutes. The tests of the real-time orbit improvement approach are described in Chapter 6.

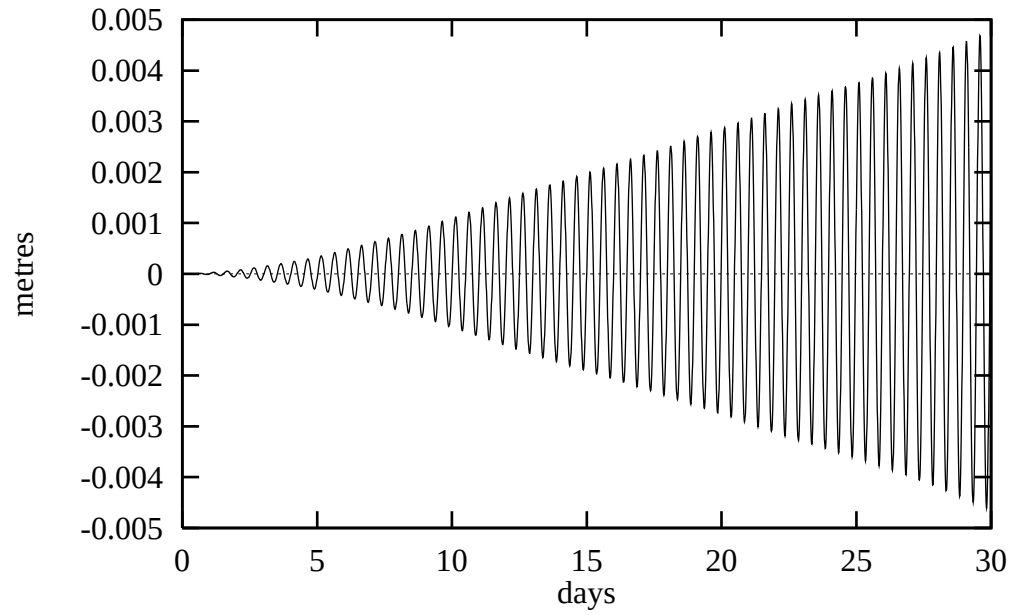

Figure 4.2: Störmer-Cowell; X-coordinate error

4.3.4 Multi-step starting procedures

An important characteristic of the multi-step methods, such as the Adams-Moulton and Störmer-Cowell, is that they are not self starting. To get started they require the previous knowledge of n values of $\ddot{\underline{r}}(t_0 - ih)$, for $i = (1, n)$, where t_0 is the initial time and n is the order of the integrator. These starting values have to be obtained by some independent method, for example, by using Taylor's algorithm or one of the Runge-Kutta methods. One has to make sure that the starting values are as accurate as necessary for the overall required accuracy.

The starting algorithm we have made use of is given by *Velez & Maury* [1970], as:

$$\dot{\underline{r}}(t_0 + Kh) = \dot{\underline{r}}(t_0) + h \sum_{i=0}^{n-1} \xi_i^L \; \ddot{\underline{r}}\,[t_0 + (5-i)h]\,, \tag{4.30}$$

for a first-order differential equation ($L = 1$), and:

$$\underline{r}(t_0 + Kh) = \underline{r}(t_0) + Kh\dot{\underline{r}}(t_0) + h^2 \sum_{i=0}^{n-1} \xi_i^L \; \ddot{\underline{r}}\,[t_0 + (5-i)h]\,, \tag{4.31}$$

for a second-order differential equation ($L = 2$), where n is the order of the integration, ξ^L represents coefficients, t_0 the initial epoch and $K = (1, k)$, $k = n - 1$.

The same authors suggest that the given initial values $\underline{\dot{r}}(t_0)$ and $\underline{r}(t_0)$ be located in the center of the required starting values, provided k is even, in order to reduce the number of required iterations of eqns. (4.30) and (4.31). In this case, $K = (-k/2, k/2)$, $K \neq 0$.

We conclude this section by saying that in previous research at UNB, *Parrot* [1989] and *Chen* [1991] have relied on the Störmer-Cowell method for the solution of the equations of motion. In addition to the Störmer-Cowell method we have implemented the Adams-Moulton method, allowing us to compute both position and velocity vectors of a satellite. For the tests described in Chapter 6, we made use of the Adams-Moulton method for the numerical integration of velocity and the Störmer-Cowell method for the numerical integration of position. As far as the starting procedure is concerned, we have the options of using eqns. (4.30) and (4.31) depending on the choice of the numerical integrator.

Chapter 5

Real-time GPS orbit improvement

This chapter contains the description of our primary contribution, namely, our model for real-time orbit improvement for the GPS satellites. Its first section contains an overview of the principles of orbit improvement and the traditional approaches, the short-arc and the long-arc, followed by a description of the least-squares solution. The second section presents the real-time method for orbit improvement and the problems inherent in it. The chapter ends with a section in which some considerations of a real-time orbit service are given, such as the components of the service, nature of data link and what type of message would be broadcast to users.

5.1 Principles of orbit improvement

By the term 'orbit improvement' we understand the procedure by which the initial state vector and dynamical parameters of a satellite are estimated using observations on this satellite collected by stations whose coordinates are known, or which are to be estimated together with the satellite initial state vector and dynamical parameters.

For the formulation of the GPS orbit improvement two sets of equations are formed:

$$\underline{f}(\underline{R}, \underline{r}, \underline{y}) - \underline{\ell} = 0, \quad \underline{C}_\ell, \underline{C}_R, \underline{C}_y, \tag{5.1}$$

$$\underline{g}(\underline{r}, \underline{s}, \underline{p}) = 0, \quad \underline{C}_s, \underline{C}_p, \tag{5.2}$$

where $\underline{R}$ represents the vector of station coordinates, $\underline{r}$ the vector of satellite positions, $\underline{y}$ the vector of nuisance parameters, $\underline{\ell}$ the vector of observations, $\underline{s}$ the initial state vector and $\underline{p}$ the vector of initial dynamical parameters (only solar radiation parameters in the case of GPS satellites). The covariance matrices are represented by $\underline{C}_\ell$, $\underline{C}_R$, $\underline{C}_s$, $\underline{C}_p$ and $\underline{C}_y$. Equation (5.1) partly represents a pure geometric model whereas (5.2) is an explicit solution of the equations of motion as a function of the initial conditions. The inconsistency in eqn. (5.1) requires a reformulation of the model with the consequent introduction of the residual vector $\underline{v}$, which accounts for the differences between the set of estimates of $\underline{\ell}$ from the original set of $\underline{\ell}$ [*Vaníček and Krakiwsky*, 1986]. Their linearization yields the GPS observation equation:

$$\underline{A}_R\underline{\delta}_R + \underline{A}_r\underline{B}_1^*\underline{\delta}_s + \underline{A}_r\underline{B}_2^*\underline{\delta}_p + \underline{A}_y\underline{\delta}_y + \underline{w} = \underline{v}, \tag{5.3}$$

where $\underline{A}$ represents the first design matrices, $\underline{\delta}$ the vectors of corrections to the estimated parameters and $\underline{w}$ the misclosure vector. The partial derivatives dwelling in $\underline{A}_R, \underline{A}_r$ and $\underline{A}_y$ are described in Appendix III. It is important to point out for later developments that the misclosure vector is given by:

$$\underline{w} = \underline{f}(\underline{R}^o, \underline{y}^o, \underline{s}^o, \underline{p}^o). \tag{5.4}$$

where the superscript '0' signify initial (approximate) values.

Some words on the computation of matrices $\underline{B}_1^*$ and $\underline{B}_2^*$ now follow. These Jacobian matrices contain the *variational partials* which are the partial derivatives of a satellite position, in the inertial system, with respect to the initial state vector $\underline{s}$ and the vector of initial dynamical parameters $\underline{p}$ for this satellite. These matrices are regarded as components of a matrix $\underline{B}^*$:

$$\underline{B}^* = \begin{bmatrix} \underline{B}_1^* & \underline{B}_2^* \end{bmatrix} = \begin{bmatrix} \dfrac{\partial \underline{r}}{\partial \underline{s}} & \dfrac{\partial \underline{r}}{\partial \underline{p}} \end{bmatrix}. \tag{5.5}$$

The partial derivatives in matrix $\underline{B}^*$ are the solution of a system of second-order differential equations known as *variational equations*. The entries $\partial\underline{r}/\partial\underline{s}$ and $\partial\underline{r}/\partial\underline{p}$

can be obtained by double integration of $\partial\ddot{\underline{r}}/\partial\underline{s}$ and $\partial\ddot{\underline{r}}/\partial\underline{p}$, respectively. Therefore, the matrix:

$$\underline{F}^* = \left[\frac{\partial\ddot{\underline{r}}}{\partial\underline{s}} \; \frac{\partial\ddot{\underline{r}}}{\partial\underline{p}}\right] \tag{5.6}$$

is the entity to be integrated for the solution of $\underline{B}^*$. The variational partials have the same relationship to the variational equations as the satellite position vector does to the equations of motion [*McCarthy et al.*, 1993]. The equations of motion of a GPS satellite are written in the form:

$$\ddot{\underline{r}} = \underline{f}(\underline{r}, \ddot{\underline{p}}_{srp}), \tag{5.7}$$

meaning that the acceleration $\ddot{\underline{r}}$, at a epoch t, is computed by a force model that needs the satellite position $\underline{r}$ and the solar radiation pressure acceleration $\ddot{\underline{p}}_{srp}$, at a epoch t, to be evaluated. By taking the total derivatives with respect to the initial state vector $\underline{s}$ and the initial dynamical parameters $\underline{p}$, both related to the initial epoch t_0, we arrive at the variational equations, for the initial state vector:

$$\frac{\partial\ddot{\underline{r}}}{\partial\underline{s}} = \frac{\partial\underline{f}}{\partial\underline{r}} \frac{\partial\underline{r}}{\partial\underline{s}}, \tag{5.8}$$

and, for the dynamical parameters:

$$\frac{\partial\ddot{\underline{r}}}{\partial\underline{p}} = \frac{\partial\underline{f}}{\partial\underline{r}} \frac{\partial\underline{r}}{\partial\underline{p}} + \frac{\partial\underline{f}}{\partial\underline{p}}, \tag{5.9}$$

which is similar to the form presented by *Chen* [1991]. Equations (5.8) and (5.9) can be grouped and represented in a matrix form as:

$$\underline{F} = \underline{W}\;\underline{B}^* + \underline{K}. \tag{5.10}$$

The variational equations are formed in the inertial system. The variational partials contained in $\underline{B}^*$ are obtained by numerical integration using the same methods as described in Chapter 4. The integration is commonly carried out simultaneously with the solution of the equations of motion in order to save computer time. The

partials have then to be transformed to the CT-system, which is the one in which the observation equation is formed.

Instead of computing all variational partials contained in $\underline{B}^*$ by numerical integration, which consumes a great deal of computational time, we have adopted a hybrid solution, in which case the Keplerian part of $\underline{B}^*$ is solved analytically and the solar radiation pressure part of $\underline{F}$ is numerically integrated. In this approach, matrix $\underline{B}^*$ is spelled out as:

$$\underline{B}^* = \left[\begin{array}{cc} \underline{B}_1^* & \underline{B}_2^* \end{array} \right] = \left[\frac{\partial \underline{r}}{\partial \underline{\kappa}} \; \frac{\partial \underline{r}}{\partial \underline{p}} \right], \tag{5.11}$$

where $\underline{\kappa}$ is the initial Keplerian elements vector, $\underline{p}$ the initial solar radiation parameters vector and $\underline{r}$ the satellite position vector. The only difference between eqns. (5.5) and (5.11) is that in the latter, $\underline{B}_1^*$ is now an explicit function of the Keplerian elements vector $\underline{\kappa}$.

The submatrix which depends on the Keplerian elements (the first six columns of $\underline{B}^*$ in eqn. (5.11)) is computed analytically following *Langley et al.* [1984] and *Parrot* [1989] (see Appendix III). The submatrix which contains the solar radiation pressure parameters (remaining columns) is computed by numerically integrating:

$$\frac{\partial \ddot{r}_i}{\partial p_k} = A_{ij} \frac{\partial r_j}{\partial p_k} + \frac{\partial \ddot{p}_i}{\partial p_k}, \tag{5.12}$$

where $r_{i,j} = 1,2,3$ are the Cartesian components of $\underline{r}$, p_k is equal to either (p_0, p_y), for $k = 1,2$, or (G_x, G_y, G_z), for $k = 1,2,3$, at t_0, $\ddot{p}_i$ represents the x, y, z components of the solar radiation pressure contribution, cf. eqns. (4.13) and (4.21), and $\underline{A}$ is the part of matrix $\underline{W}$ containing only the radial field contribution:

$$\underline{A} = -\frac{GM}{r^3} \left(\frac{\underline{I} - 3 \; \underline{r} \; \underline{r}^T}{r^2} \right), \tag{5.13}$$

with $\underline{I}$ being a unit matrix of dimension 3 and r is the norm of $\underline{r}$. The initial conditions for the solution of eqns. (5.12) are:

$$\frac{\partial r_j}{\partial p_k} = 0. \tag{5.14}$$

The orbit improvement is carried out by first predicting an orbit using an a priori initial state vector and solar radiation parameters. This predicted orbit is then improved (adjusted) using the GPS observations. This process yields a least-squares correction vector to the initial state vector and values for the solar radiation pressure parameters. The improved state vector and solar radiation pressure parameter values are then used to predict a new (improved) orbit, i.e., the up-to-date ephemerides for the GPS satellites.

An example of the effect of orbit improvement can be visualized from Figures 5.1 and 5.2. Figure 5.1 shows the radial, along-track and cross-track components of the difference between the predicted orbit of satellite PRN 25, as computed by program PREDICT (see Appendix II), and a reference orbit for the same satellite obtained from the (final) IGS orbits. The initial conditions used for the prediction were taken from the reference orbit. It can be seen that after a day, a difference of up to 30 meters is encountered. Figure 5.2 shows the radial, along-track and cross-track components of the difference between the predicted orbit of satellite PRN 25, using initial conditions improved with respect to the reference orbit (used as "pseudo-observations"), and the reference orbit itself. The peak-to-peak difference is now below the 2 centimeter level. Let us point out that the improvement shown was the best solution among the several satellites used, and do not represent a typical one.

5.1.1 Least-squares solution

To obtain the least-squares solution for the process of orbit improvement let us first denote:

$$\underline{A}_x = [\underline{A}_R, \underline{A}_r \underline{B}_1^*, \underline{A}_r \underline{B}_2^*], \tag{5.15}$$

and:

$$\underline{\delta}_x = [\underline{\delta}_R, \underline{\delta}_s, \underline{\delta}_p]^T. \tag{5.16}$$

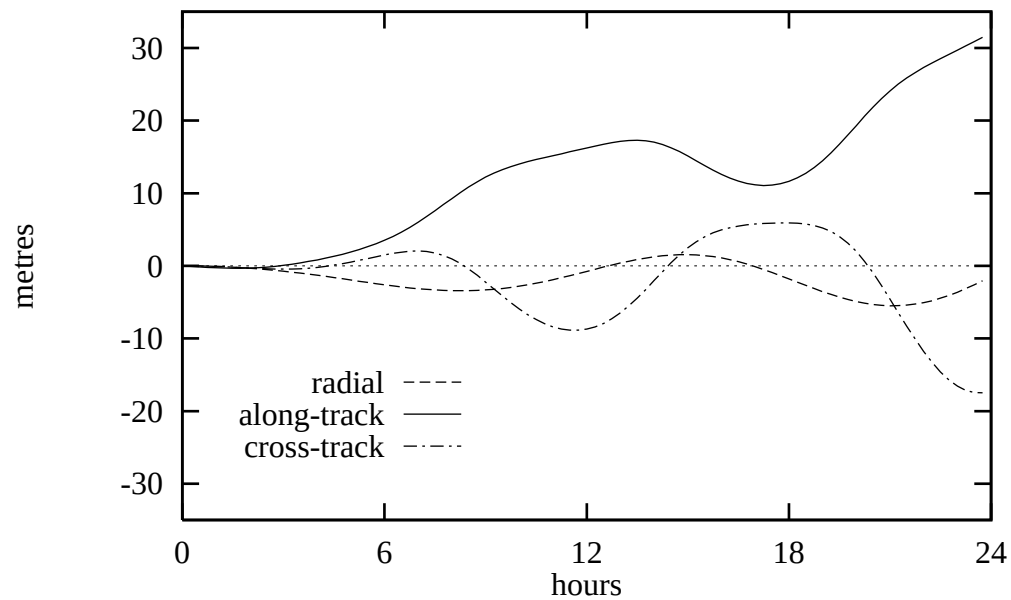

Figure 5.1: Difference between predicted orbit and reference orbit

The weighted parametric model is then given by:

$$\underline{A}_x\underline{\delta}_x + \underline{A}_y\underline{\delta}_y + \underline{w} = \underline{v}, \quad \underline{C}_\ell, \underline{C}_x, \underline{C}_y, \tag{5.17}$$

where $\underline{C}_x$ and $\underline{C}_y$ represent respectively the a priori covariance matrix for the unknown parameters grouped in $\underline{\delta}_x$ and unknown nuisance parameters, and $\underline{C}_\ell$ the covariance matrix for the observations, regarded as uncorrelated between different epochs.

By minimizing the quadratic norm of $\underline{v}$ [*Vaníček & Krakiwisky*, 1986] we arrive at the system of normal equations

$$\begin{bmatrix} \underline{C}_\ell^{-1} & -\underline{I} & \underline{0} & \underline{0} \\ -\underline{I} & \underline{0} & \underline{A}_x & \underline{A}_y \\ \underline{0} & \underline{A}_x^T & \underline{C}_x^{-1} & \underline{0} \\ \underline{0} & \underline{A}_y^T & \underline{0} & \underline{C}_y^{-1} \end{bmatrix} \begin{bmatrix} \hat{\underline{v}} \\ \hat{\underline{k}} \\ \hat{\underline{\delta}}_x \\ \hat{\underline{\delta}}_y \end{bmatrix} = \begin{bmatrix} \underline{0} \\ \underline{w} \\ \underline{0} \\ \underline{0} \end{bmatrix},$$

where $\underline{k}$ is the so-called Lagrange correlates vector.

First, we want to get a solution $\hat{\underline{\delta}}_x$ as a function of the observations only accumulated during the first (j) epochs. For that, we apply the rules of parameter elimination

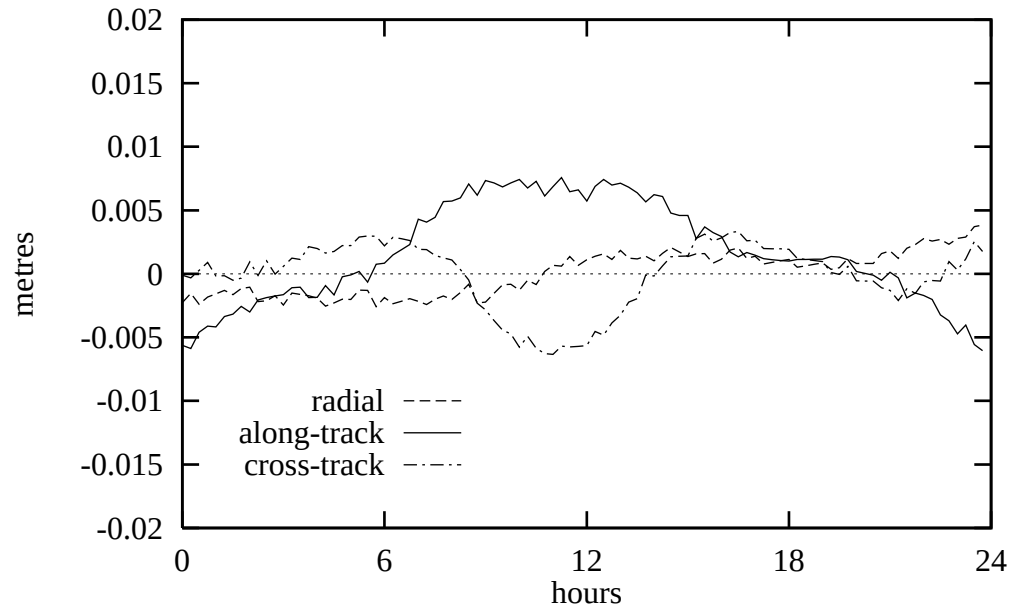

Figure 5.2: Difference between improved orbit and reference orbit

by partitioning [*Vaníček & Krakiwisky*, 1986] and eliminate $\underline{\hat{v}}$, $\underline{\hat{k}}$ and $\underline{\hat{\delta}}_y$, obtaining:

$$\underline{\hat{\delta}}_x^{(j)} = \left[\underline{N}_{xx}^{(j)} - \underline{N}_{yx}^{(j)^T} \underline{N}_{yy}^{(j)^{-1}} \underline{N}_{yx}^{(j)}\right]^{-1} \left[\underline{u}_x^{(j)} - \underline{N}_{yx}^{(j)^T} \underline{N}_{yy}^{(j)^{-1}} \underline{u}_y^{(j)}\right], \tag{5.18}$$

which is an expression for a simultaneous (batch) solution, where:

$$\underline{N}_{xx}^{(j)} = \sum_{i=1}^{j} \underline{A}_{x_i}^T \underline{C}_{\ell_i}^{-1} \underline{A}_{x_i} + \underline{C}_x^{-1}, \tag{5.19}$$

$$\underline{N}_{yx}^{(j)} = \sum_{i=1}^{j} \underline{A}_{y_i}^T \underline{C}_{\ell_i}^{-1} \underline{A}_{x_i}, \tag{5.20}$$

$$\underline{N}_{yy}^{(j)} = \sum_{i=1}^{j} \underline{A}_{y_i}^T \underline{C}_{\ell_i}^{-1} \underline{A}_{y_i} + \underline{C}_y^{-1}, \tag{5.21}$$

$$\underline{u}_x^{(j)} = \sum_{i=1}^{j} \underline{A}_{x_i}^T \underline{C}_{\ell_i}^{-1} \underline{w}_i, \tag{5.22}$$

$$\underline{u}_y^{(j)} = \sum_{i=1}^{j} \underline{A}_{y_i}^T \underline{C}_{\ell_i}^{-1} \underline{w}_i. \tag{5.23}$$

It may be advantageous to compute the solution vector $\underline{\hat{\delta}}$ at every epoch, or after a certain numbers of epochs, in a stepwise fashion. The solution obtained in this way is identical to the simultaneous solution only if the effect of previous steps on the

solution vector and its covariance matrix is properly transmitted to the next step. An advantageous characteristic of the stepwise procedure is that we can get the proper solution (output) after each observation set is added, allowing a continuous check on the effect of the added observations. To obtain the increment vector $\Delta\underline{\hat{\delta}}_x$ which shows the change $\underline{\hat{\delta}}_x$ undergoes from epoch $(j-1)$ to epoch (j) we denote:

$$\Delta\underline{\hat{\delta}}_x = \underline{\hat{\delta}}_x^{(j)} - \underline{\hat{\delta}}_x^{(j-1)}. \tag{5.24}$$

For a solution $\underline{\hat{\delta}}_x$ expressed as a function of the nuisance parameters $\underline{\hat{\delta}}_y$, they have to be evaluated first. To do that, we go back to the system of normal equations, and eliminate $\underline{\hat{v}}$, $\underline{\hat{k}}$ and $\underline{\hat{\delta}}_x$ by partitioning. This yields the nuisance parameters vector valid for epoch j:

$$\underline{\hat{\delta}}_y^{(j)} = [\underline{N}_{yy}^{(j)} - \underline{N}_{yx}^{(j)}\underline{N}_{xx}^{(j)^{-1}}\underline{N}_{yx}^{(j)^T}]^{-1}[\underline{u}_y^{(j)} - \underline{N}_{yx}^{(j)}\underline{N}_{xx}^{(j)^{-1}}\underline{u}_x^{(j)}]. \tag{5.25}$$

The increment vector $\Delta\underline{\hat{\delta}}_x$ is then given as:

$$\Delta\underline{\hat{\delta}}_x = (\underline{N}_{xx} + \underline{C}_{\hat{x}}^{(j-1)^{-1}})^{-1}(\underline{u}_x - \underline{N}_{yx}^T\underline{\hat{\delta}}_y^{(j)} - \underline{N}_{xx}\underline{\hat{\delta}}_x^{(j-1)}), \tag{5.26}$$

where:

$$\underline{N}_{xx} = \underline{A}_x^T\underline{C}_\ell^{-1}\underline{A}_x, \tag{5.27}$$

$$\underline{N}_{yx} = \underline{A}_y^T\underline{C}_\ell^{-1}\underline{A}_x, \tag{5.28}$$

$$\underline{u}_x = \underline{A}_x^T\underline{C}_\ell^{-1}\underline{w}. \tag{5.29}$$

The solution vector is then:

$$\underline{\hat{\delta}}_x^{(j)} = \underline{\hat{\delta}}_x^{(j-1)} + \Delta\underline{\hat{\delta}}_x. \tag{5.30}$$

The a posteriori covariance matrix of the solution for epoch (j) is given by:

$$\underline{C}_{\hat{x}}^{(j)} = \underline{C}_{\hat{x}}^{(j-1)} + \Delta\underline{C}_{\hat{x}}, \tag{5.31}$$

where:

$$\underline{C}_{\hat{x}}^{(j-1)} = [\underline{N}_{xx}^{(j-1)} - \underline{N}_{yx}^{(j-1)^T}\underline{N}_{yy}^{(j-1)^{-1}}\underline{N}_{yx}^{(j-1)}]^{-1}, \tag{5.32}$$

and:

$$\Delta \underline{C}_{\hat{x}} = [\underline{N}_{xx} - \underline{N}_{yx}^T \underline{N}_{yy}^{-1} \underline{N}_{yx}]^{-1}. \tag{5.33}$$

Accordingly, we have:

$$\underline{C}_{\hat{y}}^{(j)} = \underline{C}_{\hat{y}}^{(j-1)} + (\underline{N}_{yy}^{-1} + \underline{N}_{yy}^{-1} \underline{N}_{yx} \Delta \underline{C}_{\hat{x}} \underline{N}_{yx}^T \underline{N}_{yy}^{-1})^{-1}. \tag{5.34}$$

5.1.2 Traditional approach for GPS orbit improvement

In the context of this dissertation, by "baseline observing session", or simply "session", is meant the time span over which GPS signals are received continuously and simultaneously by receivers that occupy both ends of a baseline [*Vaníček et al.*, 1985]. We further define "observation window" as the time span which encompasses simultaneously observed sessions, and "orbital session" as the arc length over which the same set of initial conditions are improved [*Parrot*, 1989]. Intrinsic to the concept of orbital session comes two strategies for orbital estimation, namely, the short-arc [*Parrot*, 1989] and the long-arc [*Chen*, 1991] approaches.

Table 5.1 summarizes the characteristics of the short and long-arc approaches. The major distinction between them is the arc length definition of the orbital session. The other characteristics reflecting nothing else but a consequence of the arc-length definition.

Table 5.1: Typical characteristics of short-arc and long-arc approaches.

	short-arc	long-arc
orbital session	less than 6 hours	greater than 6 hours
force model	less complex	more complex
initial state vector	Keplerian elements	Keplerian elements plus solar radiation pressure parameters

The arc-length definition has further consequences in the case of multi-day observation of a network. Figure 5.3 depicts an example for a network observing for

6 hours in n consecutive days. The arrows represent orbital sessions. The long arrow indicates one long-arc orbital session which spans all observation windows: only one set of initial conditions per satellite plus the station coordinates of the network (plus some nuisance parameters) are estimated. The short arrows indicate three short-arc orbital sessions: there will be three sets of initial conditions per satellite to be improved, plus the station coordinates (at the beginning of the first observation window). The long-arc approach yields a continuous orbit representation over all observation windows, being also computationally more efficient due to the smaller number of orbital parameters to be estimated.

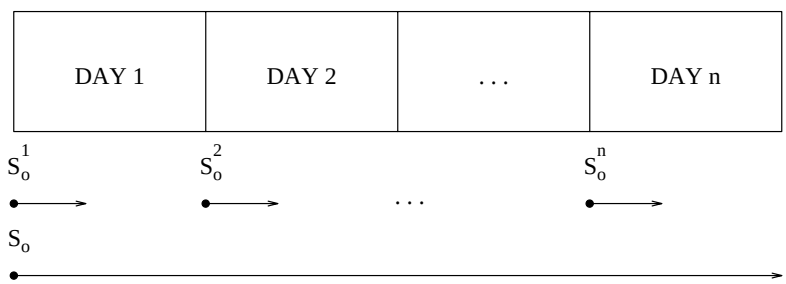

Figure 5.3: Long-arc and short-arc strategies

In the traditional approach, the solution vector $\hat{\underline{\delta}}_x$ is computed by eqn. (5.18). A priori orbital arcs are used to form the design matrix and the misclosure vector. The normal equations are accumulated independently, whether the observations are acquired baseline by baseline or in a network mode. The traditional approach can also be carried out sequentially, but the estimated initial conditions are related to the whole orbital arc, at least, one day long.

After the adjustment, the improved initial conditions can be used to generate new orbital arcs in another iteration over the orbital session. The above described characteristics define what we call the "traditional" approach for orbit improvement (iteration over orbital session) as opposed to the "real-time" (iteration over observations), which is described in the next section.

5.2 Real-time orbit improvement

The major goal of the research described in this dissertation was to investigate the possibility of real-time high-accuracy GPS orbit determination, i.e., the possibility of obtaining at any time the best possible estimate of orbit, based on all observations collected up to that time [*Santos*, 1992]. The algorithm for real-time orbit improvement is detailed in the following subsections. The test of the algorithm and discussion of the results are described in the next chapter.

5.2.1 The real-time algorithm

Let us start detailing the mechanics of the real-time orbit improvement approach by defining the observation sampling step Δt as the difference between two consecutive observation epochs t_i and t_{i+1}. Therefore:

$$t_i = i\ \Delta t, \tag{5.35}$$

where i is an integer number. Let us define the orbital arc $\Delta\tau$, over which the orbit improvement takes place, as the difference between epochs τ_j and τ_{j+1}, the initial and final epoch of the orbit improvement, respectively. Therefore:

$$\tau_j = j\ \Delta\tau, \tag{5.36}$$

where j is an integer number. The observation sampling step Δt and the orbital arc $\Delta\tau$ are related by the integer update step k:

$$\Delta\tau = k\ \Delta t. \tag{5.37}$$

The update step k defines the frequency in which the orbit improvement takes place: if k is equal to 1, then $\Delta\tau$ is equal to Δt, and we are in the realm of the real-time orbit improvement; if k is a big value that makes $\Delta\tau$ encompasses the whole observation window, we are in the realm of the traditional approach.

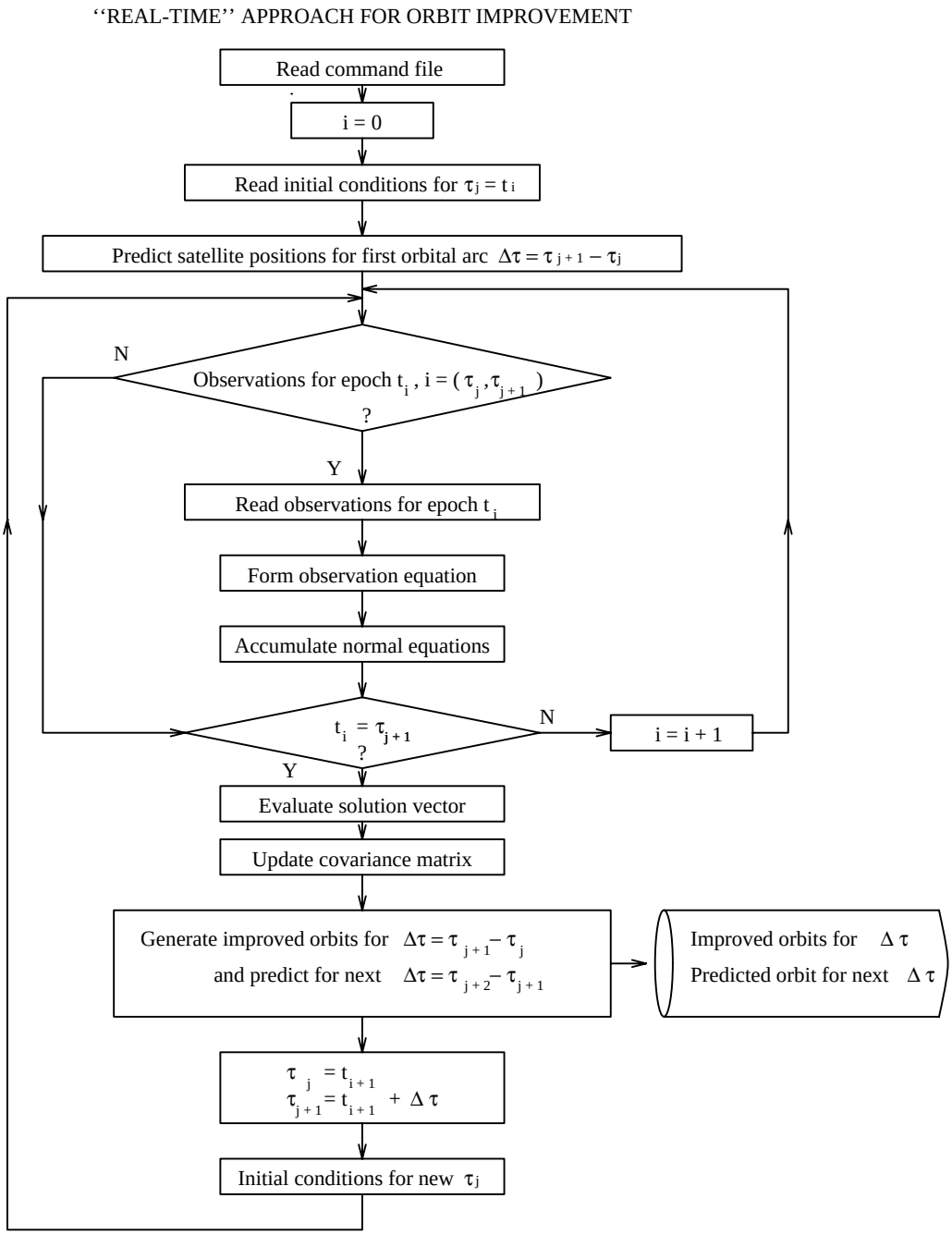

Figure 5.4: Real-time orbit improvement flow-chart

The proposed real-time approach for GPS orbit improvement is diagrammatically portrayed by Figure 5.4 and explained as follows. First, a command file containing, among other pieces of information, the a priori weights for the parameters is read. The initial conditions at epoch τ_j, coinciding with the first observation epoch t_i, where i is equal to 0, are also read. The process then starts with an orbit prediction over the first orbital arc $\Delta\tau = (\tau_j, \tau_{j+1})$. Whenever observations for a generic epoch t_i within the arc defined by (τ_j, τ_{j+1}) arrive from the network, they are used to form the observation equations. The "read" in the flowchart means the observations are free from cycle slips. The observation equations are then accumulated into the normal equations. The observation epoch t_i is tested to see whether it corresponds to the end of the orbital arc $\Delta\tau$, i.e., whether it is equal to τ_{j+1}. If the update step k is equal to 1, this test is always affirmative. Whenever the test is affirmative, the solution vector, composed of station coordinates and initial conditions, is computed. The covariance matrices are updated. This guarantees that the solution is based on all observations collected up to this time. The adjusted (improved) initial conditions are then used to generate improved orbits for the current orbital arc $\Delta\tau^{(j)} = (\tau_j, \tau_{j+1})$, as well as predicted orbits for the next orbital arc $\Delta\tau^{(j+1)} = (\tau_{j+1}, \tau_{j+2})$. Both the improved orbits and the predicted obits are the output of this jth iteration. The predicted orbits are also to be used for the next iteration. The orbital arc for the next iteration is then defined by taking the predicted orbits at τ_{j+1} as its initial conditions. The epochs τ_j and τ_{j+1} are then shifted forward by $\Delta\tau$. Provided there is no satellite maneuvering this process can continue ad infinitum.

The real-time approach is based on iteration over observations, i.e., at every new observation, or group of observations, the initial conditions are estimated, which, in turn are used to generate a new set of orbits to be used in the adjustment. This can be better understood by going back to eqn. (5.4) and concentrating on the vector of initial conditions $\underline{s}$. The misclosure vector (as well as the design matrix) is a function of the expansion points $\underline{s}^o$, i.e., formed making use of the approximate position vector

of a satellite which is the rigorous solution of the equations of motion, corresponding to the best estimate of the initial conditions. For the first orbital segment (represented by superscript) $\Delta\tau^1$, the misclosure vector is

$$\underline{w}^1 = \underline{f}(\underline{R}^o,\ \underline{y}^o,\ \underline{s}^o). \tag{5.38}$$

For the second orbital segment we have

$$\underline{w}^2 = \underline{f}(\underline{R}^o,\ \underline{y}^o,\ \hat{\underline{s}}^1), \tag{5.39}$$

where $\hat{\underline{s}}^1$ represents the best estimate of the value of $\underline{s}$, meaning that the orbits used in $\Delta\tau^2$ are generated as a function of $\underline{s}^1$, and so on. Every new orbital arc j uses the initial conditions estimated for the previous arc $(j-1)$ and all the preceeding observations

$$\underline{w}^j = \underline{f}(\underline{R}^o,\ \underline{y}^o,\ \hat{\underline{s}}^{j-1}). \tag{5.40}$$

The definition of the length of the orbital arc depends on the frequency with which one needs to have improved orbits. For example, it may be equal to 15 minutes to agree with the National Geodetic Survey (NGS) precise orbits format orbit interval [*Remondi*, 1989]. In this case, for a sampling rate of 120 seconds an orbital segment would encompass 7 or 8 observations records.

5.2.2 The screening of observations

In Chapter 4 we wrote about the linear combinations of L1 and L2 that can be used to detect and correct cycle slips. At the same time it was said that a cycle slip may simply be flagged and treated as a new ambiguity to be solved in the adjustment process. Both alternatives are valid but we think that it is better to fix the observation from the cycle slip in order to make the observation flow uninterrupted: if a cycle slip can be fixed, then fix it. This can be done by simply continuously adding the integer number of cycles corresponding to the cycle slip to all the new observations.

With the quality of today's geodetic receivers, cycle slips will not be so common. A real-time orbit service, such as the one discussed in the next section should rely on an automatic cycle slip correction program.

5.3 A real-time orbit service

A service of real-time orbit distribution may very well become part of an active control system or be within a wide-area differential GPS system. Such a service would be composed of a fiducial or control network occupied by high performance GPS receivers and by a master center. These two components would be linked by a reliable communication system that guarantees continuous flow of information. A communication system would also be needed for the dissemination of the ephemerides to multiple users, the passive component of the system.

5.3.1 Monitor stations

The unmanned monitor stations have the duty of continuously tracking the GPS satellites and relaying the pertinent information to the master center via a communication link. The GPS receivers occupying the network would be part of the monitor stations. The monitor stations would comprise not only the receiver but also a computer, environmental sensors (if any) and output communication components (e.g., modem and telephone line, ethernet links, radio access, etc). As the receivers will be operating 24 hours a day, logistical problems such as power supply have to be taken care of.

5.3.2 Master Center

The Master Center would have the following duties: (a) to control the operation of the monitor stations; (b) to process the GPS data and related information obtained from

the monitor stations; and (c) to disseminate the orbit to the users via a communication link. The processing of the GPS data and related information involves the screening of the GPS data for cycle slips, forming the double differences, and carrying out the stepwise orbit improvement. The output of the latter, the up to date best initial state vector, is used for generating the real-time orbits, the quantities of interest to be transmitted to the users.

5.3.3 The transmitted information

The real-time orbit improvement yields as output the improved orbit for a specific orbital arc, at epoch τ_j, and the predicted orbit for the next orbital arc. These orbits consist of the Cartesian coordinates of the satellites, referred to their center-of-mass, in the Geodetic Reference System 1980 (GRS 80), realized by the set of station coordinates of the network used to gather the observations, such as one of the ITRFs. This is the basic information to be transmitted by the orbit service.

The orbits may be transmitted in different ways. For example, within a message consisting of the satellite state vectors in Cartesian coordinates. The constituents of this message would be the improved orbits plus a certain number of predicted orbits, in order to allow the user to interpolate the satellite's positions within a central interval. In another way of transmission, the orbits would be a broadcast-type ephemerides, consisting of the improved orbit, in Keplerian elements, plus corrections to these Keplerian elements computed using the predicted orbit. These corrections would be used by the user to predict the orbits according to the observation sampling rate used, as if they were the broadcast ephemerides contained in the satellite navigation messages. The message type 17 of the RTCM DGPS message format [*RTCM Special Committee # 104*, 1994] can be used to accommodate the Keplerian message. In order to allow a lower warming up time for the user's receiver, the Master Center would transmit the message with an interval equal to 1 or 2 minutes. A historical record with all transmitted orbits would also be made available from the orbit service.

Chapter 6

Test of the algorithm and discussion of results

This chapter describes the tests on the orbits generated by the real-time algorithm. It starts with the definition of what type of tests can be made for this purpose followed by a brief explanation of the software implementation. The real-time orbit improvement tests used GPS data collected by a network composed of eight IGS stations located in Canada and the U.S. The characteristics of this network are described. The GPS processing was carried out under controlled conditions. We tested the generated orbits to assess their accuracy and precision. To get closer to a real life situation, artificial cycle slips were introduced into the real data. Also, the effect of using predicted Earth Orientation Parameters (EOP) was studied.

6.1 Assessing orbit precision and accuracy

A key question we have to face is how to assess the quality of the orbits generated using the real-time algorithm. Different ways of assessing the quality of a orbit have been used in several analyses [*Lichten & Border*, 1987; *Lichten & Bertiger*, 1989; *Rothacher*, 1992; see also the IGS Electronic Reports], and can be divided into the

categories:

1. comparison of overlapping arcs;

2. comparison with an independently-generated orbit; and,

3. analysis of their effect in geodetic positioning.

A good way to assess the orbit precision is by comparing overlapping arcs. Two comparisons can be made here. The first, usually referred to as "orbit repeatability", compares two overlapping orbits improved independently of each other. The second, referred to as "extrapolation", compares an extrapolated arc, i.e., an orbit predicted beyond its improved arc, with another improved orbit. Figure 6.1 shows diagrammatically the idea behind orbit repeatability and extrapolation.

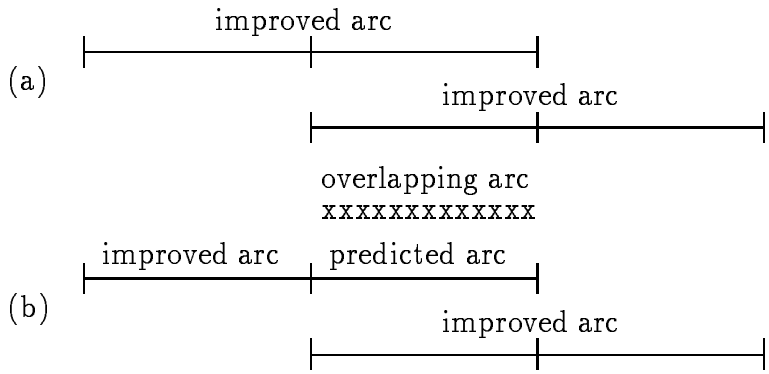

Figure 6.1: Comparing overlapping arcs: (a) orbit repeatability; (b) extrapolation

A simple way to qualitatively assess the orbit accuracy is by comparing it with an external (independently-generated) solution. A problem here comes from the fact that this external solution may have used slightly different models and could be attached to a different reference frame due to a different station coordinate set definition.

The final test is an analysis of the effect of the orbits in geodetic positioning. This is done by constraining them during the processing of baselines, and then analysing the short term baseline component repeatability, or by comparing the baseline vectors components with VLBI or SLR, provided both compared quantities are in the same coordinate frame, otherwise a similarity transformation should be applied to make both coordinate frames compatible for the comparison. This test is a practical realization of the rule of thumb (see Chapter 1). We must be aware of the fact that the final baseline solutions may be affected by errors which are independent of orbit. Therefore, this type of test may indicate other error sources.

The results of the tests will be presented in the next sections. For the comparison of overlapping arcs, we have used arcs which have been independently improved. For the comparison with an external orbit solution, we have used the IGS orbit as such. These two comparisons are performed by simply differencing the orbit under scrutiny with the one used as reference. The result shall be referred to as "orbital residuals". The orbital residuals are presented graphically for some particular satellites denoting a typical solution, and in tables presenting the best case, the worst case, and the average case. The orbital residuals are given as rms of the radial, along-track and cross-track components (see Chapter 2), and as the 3-dimensional rms ($3drms$). The rms (about the mean) is given by:

$$rms = \sqrt{\frac{1}{n}\sum_{i=1}^{n}(\delta_i - \overline{\delta})^2}, \tag{6.1}$$

where δ is the difference between the two orbits being compared (orbital residuals), $\overline{\delta}$ the average value, and n the number of samples.

The 3drms is defined (according to IGS Electronic Mail # 37) as:

$$3drms = \sqrt{X_{rms}^2 + Y_{rms}^2 + Z_{rms}^2}, \tag{6.2}$$

where X_{rms}, Y_{rms} and Z_{rms} are the rms (about the mean) of the orbital residuals along the Cartesian axes.

6.2 Software implementation

The implementation of the real-time algorithm has led us to a great effort in software implementation. The first one was the development of an orbital integrator, which we have called program PREDICT. This program turned out to be a major support work for our research. It is briefly described in Appendix I.

The second software implementation was in transforming DIPOP version 2.1 [*Vaníček et al.*, 1985; *Kleusberg et al.*, 1989] from "session oriented" (i.e., processing one baseline at a time) into "network oriented" (i.e., capable of handling observations that come into the adjustment from different baselines at the same time). This fact allowed us to take into account the mathematical correlation between baselines, as described in Chapter 3. Another very important modification was in the capability of orbit improvement. This network-oriented DIPOP incorporates several other modifications that have been made recently in support of other on-going research at UNB, such as the option to choose from a variety of tropospheric delays models, the estimation of tropospheric delay correction parameters and taking into account the different antenna heights for L1 and L2 phase centers [*Mendes & Langley*, 1994; *van der Wal*, 1995; *Komjathy*, 1995]. It should be mentioned that we have also used some subroutines from the previous research of *Parrot* [1989] and *Chen* [1991].

The third and final software implementation effort was in giving a step-wise characteristic for the weighted least-squares adjustment of the network-oriented DIPOP in order to process one orbital arc at a time, and to propagate the initial conditions for the beginning of the new orbital arc. The trickiest point resided in guaranteeing that all coordinate system transformations are related to the new initial time of reference. This implementation follows the real-time flowchart presented in Chapter 5.

6.3 Data set description

Two types of data were needed for the tests: GPS data and orbit data. The GPS data was used in the orbit improvement and in the test of the effect of the orbits in geodetic positioning; the orbit data was used in a direct comparison with our generated orbits.

The GPS data used for the tests described in this chapter were collected by eight stations, listed in Table 6.1, located in Canada and in the U.S. These stations are part of the global network of the IGS. Figure 6.2 portrays their geographical distribution. The GPS data spans a period of 4 days, GPS days 002, 003, 004 and 005 of the GPS week 730, corresponding to January 2nd (Sunday) to 5th (Wednesday), 1994. The data files were obtained via anonymous ftp from the Scripps institute of Oceanography (SIO) GARNER archives. Each file corresponds to a particular day and station. They contain data that have had outliers removed and are free of cycle slips. We made sure this was the case by running the data through program PREDD, of the DIPOP package. The conclusion: the data was really cycle slip free. The data is in RINEX format [*Gurtner*, 1994].

We have formed two networks. The first, encompassing all eight stations, was used for testing the real-time orbit improvement. We shall refer to this network as the "8-station network". The baselines formed are ALGO-STJO, ALGO-PIE1, GOLD-PIE1, PIE1-RCM5, GOLD-DRAO, FAIR-DRAO and YELL-DRAO. The second, used for testing the baseline component repeatability, is composed of four stations centered on GOLD, and has been called the "star-shape network". The baselines formed are GOLD-ALGO, GOLD-PIE1 and GOLD-DRAO. The criteria for selecting the baselines were: first, maximum number of double-differences; second, shortest baseline length. Due to the regional extent of the 8-station network, the GPS satellites have not been observed continuously by all stations throughout the period. We shall refer to this lack of simultaneous observations for a particular satellite as a data gap or lack of coverage.

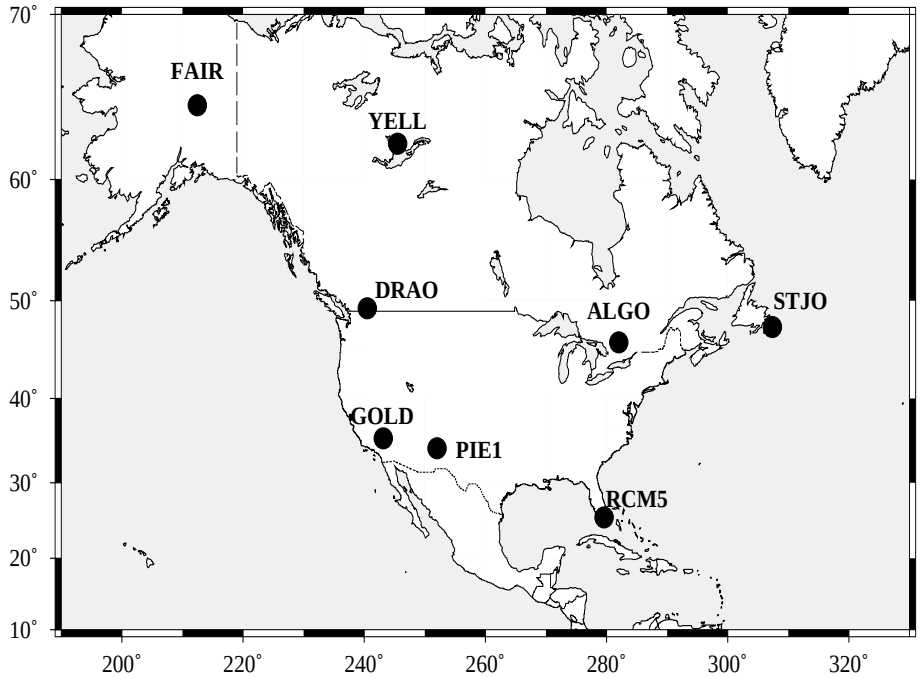

Figure 6.2: North-American network (based on IGS stations).

We have used the International Earth Rotation Service Terrestrial Reference Frame of 1992 (ITRF92) attached to epoch 1994.0 for the definition of the station coordinates, as given by IGS Electronic Mail # 421 and # 430. The IGS processing centers started using this set of coordinates since GPS week 730, according to IGS Electronic Mail # 433 and # 437. We have also followed the same definition of fiducial stations [*Kouba*, 1993]. Table 6.2 lists the coordinate set indicating which stations were used as fiducial for the processing of the 8-station network. For the star-shape network, only GOLD was used as a fiducial station. The geometric distances between all baselines used for both networks are listed in Table 6.3. The antenna heights as well as the information on what receivers were used during the days in question came from the file "localtie.tab", also obtained from the SIO GARNER archives. This information is compiled in Table 6.4.

Table 6.1: IGS stations used in our analysis.

IGS code	Location	SIO code
ALGO	Algonquin	ALGO
DRAO	Penticton	DRAO
FAIR	Fairbanks	FAIR
GOLD	Goldstone	DS10
PIE1	Pie Town	PIE1
RCM5	Richmond	RCM5
STJO	Saint John's	STJO
YELL	Yellowknife	YELL

Table 6.2: IGS station coordinates in the ITRF92 (epoch 1994.0) (F= fiducial stations).

Station	Coordinates (metre)		
	X	Y	Z
ALGO (F)	918129.578	-4346071.246	4561977.828
DRAO	-2059164.616	-3621108.398	4814432.403
FAIR (F)	-2281621.346	-1453595.783	5756961.940
GOLD (F)	-2353614.103	-4641385.429	3676976.476
PIE1	-1640916.725	-5014781.174	3575447.128
RCM5	961334.780	-5674074.150	2740535.131
STJO	2612631.303	-3426807.011	4686757.751
YELL (F)	-1224452.415	-2689216.088	5633638.270

Table 6.3: Baseline lengths, based on ITRF92 (1994.0) input coordinates.

Baseline	Distance (metre)
Algonquin-St.John's	1931826.301
Algonquin-Pie Town	2822965.422
Fairbanks-Penticton	2374017.662
Goldstone-Algonquin	3402167.628
Goldstone-Pie Town	810968.645
Goldstone-Penticton	1556107.871
Pie Town-Richmond	2811308.977
Yellowknife-Penticton	1495414.989

Table 6.4: Receivers and antenna heights.

Station	Receiver used	Antenna Height (metre)
ALGO	Rogue SNR-8	0.1140
DRAO	Rogue SNR-8	0.1180
FAIR	Rogue SNR-8	0.1160
GOLD	Rogue SNR-8	0.0000
PIE1	TurboRogue SNR 8000	0.0610
RCM5	TurboRogue SNR 8000	0.0000
STJO	MiniRogue SNR-8C	0.1620
YELL	MiniRogue SNR-8C	0.1170

The (final) IGS orbits used as reference for the tests were also obtained from the SIO GARNER archives. These IGS orbits, usually referred to as IGS product (along with EOP), are the result of a combination of all orbits computed by the IGS Analysis Centers. The motivation behind this orbit combination is to obtain a more reliable orbit by combining the individual products according to their internal consistency, which approaches the 20 cm level rms per coordinate. The combined orbit should be as precise as the best individual orbit. Two methods of orbit combination have been investigated by the IGS, one based on a weighted average and the other using orbit dynamics. It has been shown that both methods agree at the 5 cm rms in position and allow baseline repeatability at or below the 3 ppb level [*Beutler et al.*, 1993]. The IGS has made use of the weighted average method for the computation of its orbit product since it became operational [*Beutler*, 1995].

The SP3 orbit format [*Remondi*, 1989] has been adopted by the IGS for orbit dissemination. Each file contains the satellite positions for a period of 23 hours and 45 minutes, spaced by 15 minutes. A certain discontinuity between consecutive days at the day boundary is expected. A typical value would be of the order of 10 to 30 cm. This value could be a little bit worse for eclipsing satellites [*Beutler, 1995*].

6.4 Testing the real-time orbits

The tests carried out have as a main objective the assessment of precision and accuracy of the real-time orbits. In this section, 'real-time' orbits means that we use an update step k equal to 1, which makes the orbital arc for the improvement $\Delta\tau$ equal to the observation sampling rate Δt (cf. Chapter 5). The first step in the testing process was to carry out the real-time orbit improvement based on the 8-station network. This processing started with a batch adjustment for day 002, intended to generate a good set of initial conditions for the real-time improvement, followed by the real-time algorithm, as described in Chapter 5, for days 003 (49355), 004 (49356) and 005 (49357). The number between parentheses is the Modified Julian Date. The step size used for the numerical integration is 2 minutes coinciding with the observation sampling rate.

It should be pointed out that the test was carried out under in a controlled manner. The data were freed from cycle slips, and estimated EOP, extracted from IERS Bulletin B, have been used. In a real life situation, cycle slips could pass undetected and predicted EOP would have to be used. We will come back to this later.

The processing strategy applied is summarized below:

- Fiducial stations weighted according to the ITRF92 positions standard deviations (around 5 mm); floating stations weighted at 10 metres.
- Satellites used: all available.
- Carrier phase measurement noise: 12 millimetres.
- Troposphere wet zenith delay model: Saastamoinen [*Saastamoinen*, 1973].
- Troposphere dry zenith delay model: Saastamoinen [*Saastamoinen*, 1973].
- Troposphere wet mapping function: Ifadis [*Ifadis*, 1986].

- Troposphere dry mapping function: Ifadis [*Ifadis*, 1986].
- A priori standard deviation for tropospheric zenith delay correction: 20 cm.
- Elevation cut-off angle: 15 degrees.
- Data sampling interval: 120 seconds.
- Solution type: ionosphere-free linear combination of phase double difference.
- Carrier phase cycle ambiguities: estimated as real-valued parameters;
- Adopted models: GEM-T3 geopotential model up to degree and order 8 with C_{21} and S_{21} consistent with the mean pole (as defined by the *IERS* [1992]); gravitational effect of sun and moon regarded as point masses; T10 and T20 solar radiation pressure formulae and y-bias radiation, with penumbral effect included; solid earth tides with Love number equal to 0.29; relativistic effect.

A decision had to be made in terms of the a priori weights to be applied to the station coordinates. We decided to use realistic weights for the fiducial networks and allow them, along with the floating stations, to converge towards their actual location. As the time passes by, the weight matrix elements would grow larger and larger and the only motion of the station coordinates would be due to crustal motions. In our case these motions would be very small because all stations are within the same tectonic plate. Another way would be to constrain the fiducial stations with heavier weights and apply the ITRF92 station velocities.

6.4.1 Effect on geodetic positioning

To assess the effect of the real-time orbits on geodetic positioning, we simulated a user of the orbit service occupying the star-shape network and processing the incoming GPS data with the same interval as the real-time orbits, i.e., 2 minutes. The data used

span 3 days. The stations to be estimated were assigned low weights so that they could learn from the observations and converge around the correct value. Station GOLD was assigned an a priori standard deviation of 5 mm. The results of this processing can be seen by Figures 6.3 and 6.4.

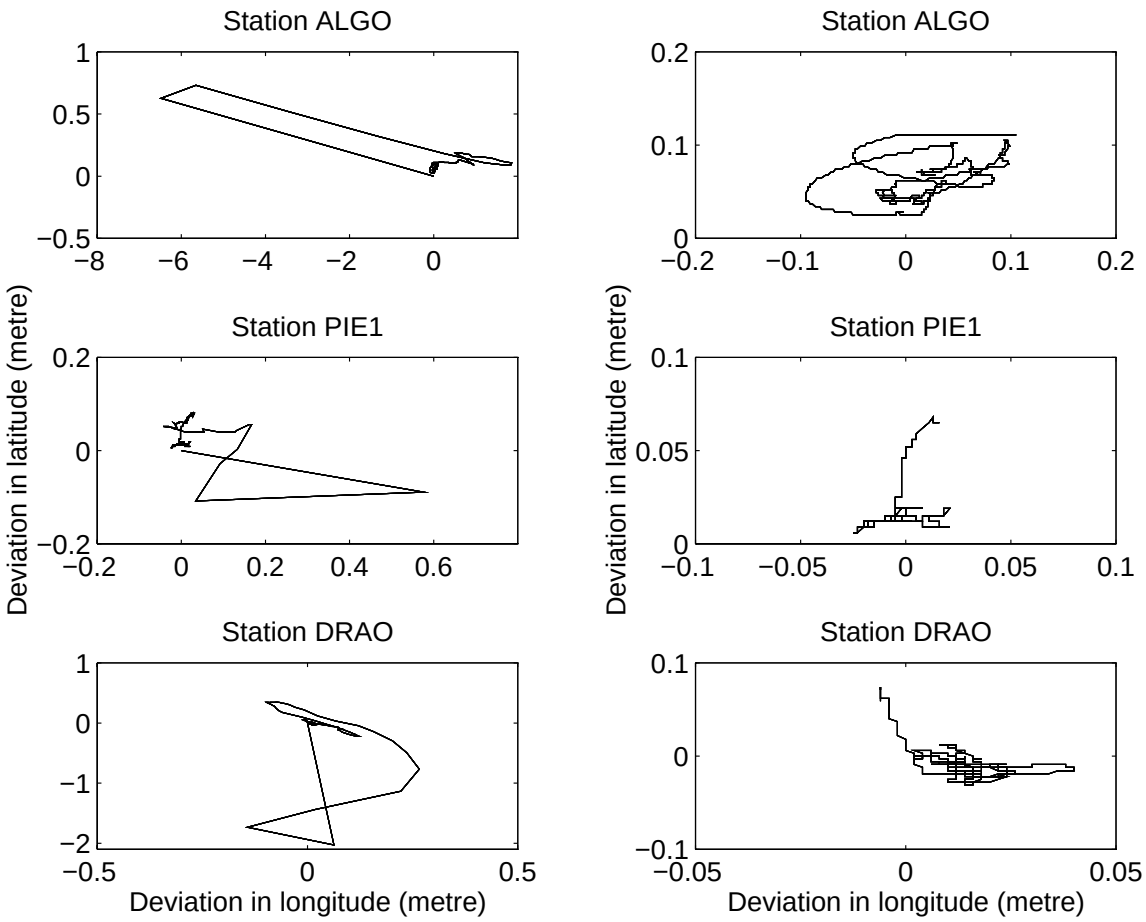

Figure 6.3: Deviation of latitude and longitude with respect to ITRF92

Figure 6.3 shows the deviation of latitude and longitude with respect to the ITRF92 coordinates for every solution. The left-hand side of the figure shows all solutions since the first one, whereas on the right-hand side, the first 5 hours have been withdrawn. The intention is to show that the use of the real-time orbits can yield positions at the order of 0.05 ppm after 5 hours of processing. This result lumps

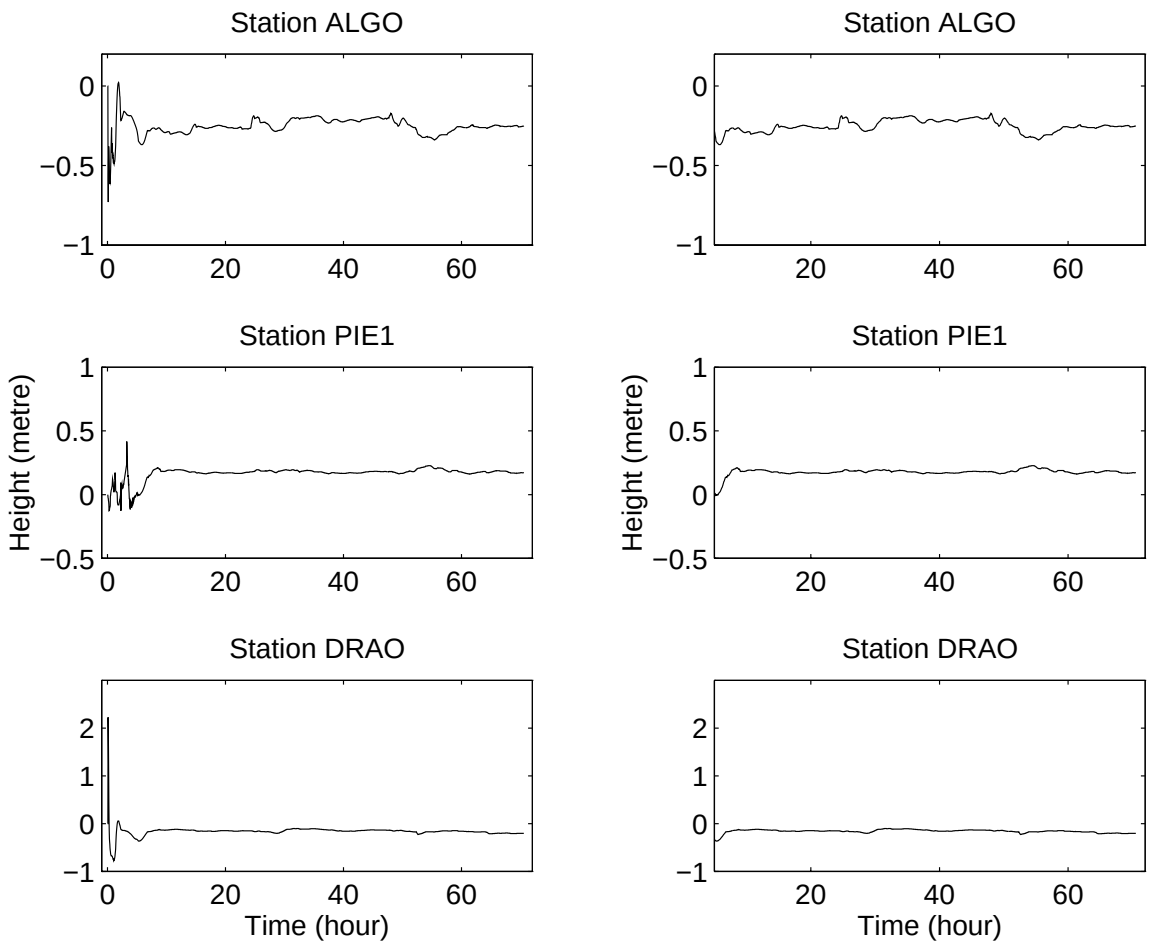

Figure 6.4: Deviation of height with respect to ITRF92

all errors coming from mismodellings of all kinds together. It seems intriguing to notice that the solutions somehow converge northward of the ITRF92 latitude. Figure 6.4 portrays the deviation of height with respect to the heights in the ITRF92. Again the plots on right-hand side omit the first 5 hours. One tropospheric delay correction was estimated every two minutes.

A similiar processing test was carried out for the baseline between ALGO and STJO, using ALGO as reference, and estimating STJO. The result is depicted by Figure 6.5. Again after 5 hours, the results are within 0.05 ppm of the ITRF92 coordinates in latitude and longitude.

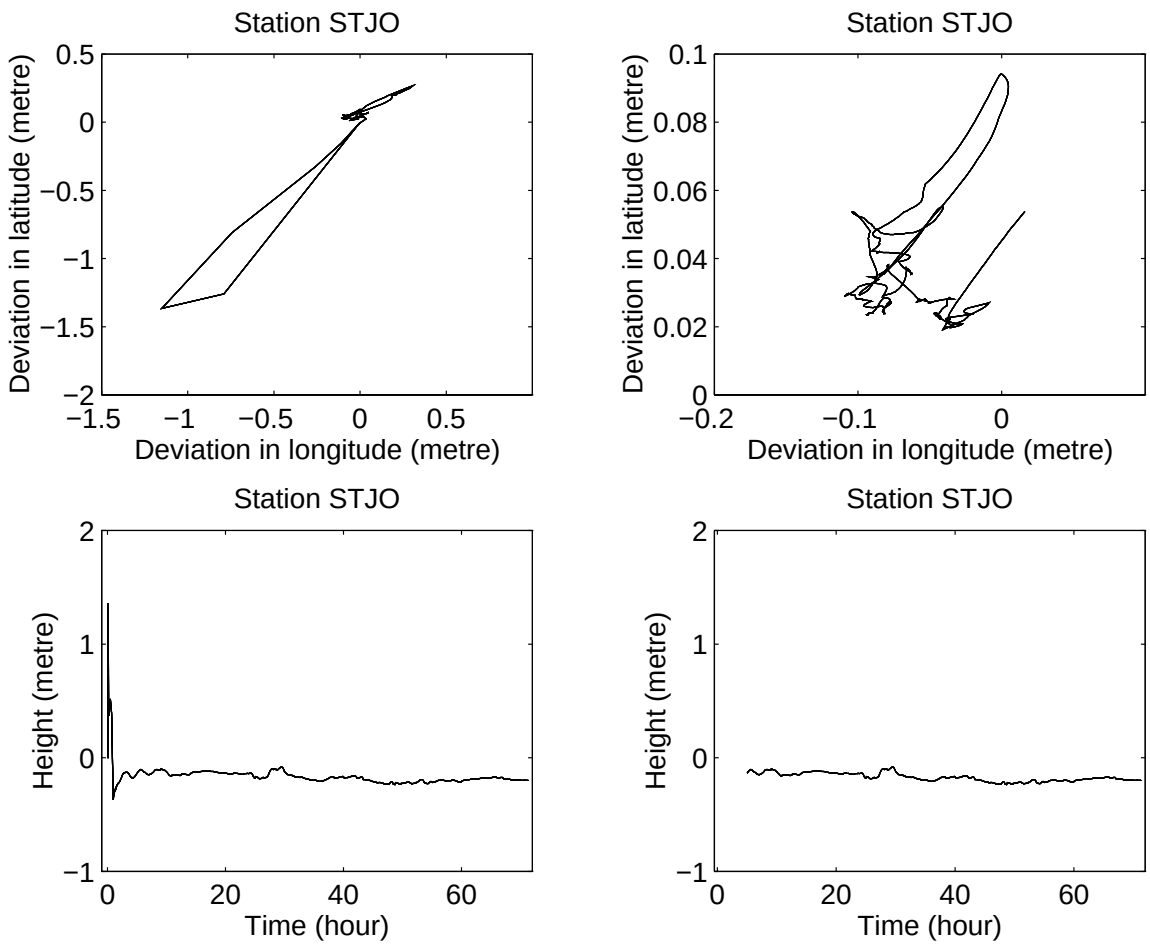

Figure 6.5: Deviation of baseline components with respect to ITRF92

Another test was made as follows. The real-time orbits were separated into 3 distinct files, each corresponding to a different day. Both the star-shape network and the baseline ALGO-STJO were then processed three times, once for each day, each being a solution independent from the others. We then computed the average relative error in the baseline taking the baseline derived from the ITRF92 coordinates as reference. The same processing was repeated but this time using the broadcast ephemerides. The intention was to get a feeling of how much solutions using the real-time and the broadcast orbits differ from each other. Figure 6.6 illustrates this comparison. The symbol "RT" indicates the results using the real-time orbits; the

symbol "BR" the results using the broadcast orbits. The average relative error in the baseline using the real-time orbits is at the 0.02 ppm level whereas using the broadcast ephemerides, it is at the 0.1 ppm level. From the point of view of the users of the orbit service, these are the results that really matter: the use of the real-time orbits allow position determinatiom at the 0.02-0.05 ppm level.

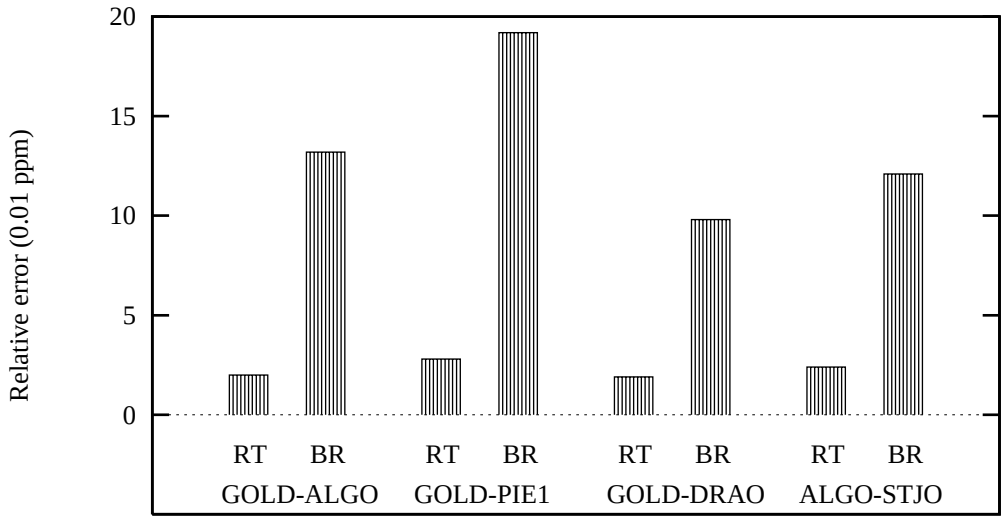

Figure 6.6: Relative error in baseline length

6.4.2 Comparison with IGS orbits

Results coming from the comparison of the real-time with the IGS orbits are presented in this subsection. This comparison was originally intended to give us an idea of the external consistency of the improved orbits, being the IGS orbits used as a benchmark. But the orbital residuals in this comparison may be biased by the differences between the strategies used to generate the orbits being compared: the IGS orbits are combined orbits of several global orbital solutions, i.e., generated based on a global network, whereas our orbits are regional, i.e.,they come from a regional network. In the case of regional orbits, the orbit trajectories tend to adjust themselves to the data, distorting

somewhat the part of the orbit with no data coverage. Our interest is with the actually improved part of our solution. The arcs outside the data coverage region are of no interest.

As said before, the comparison carried out is a simple subtraction between our solution and the IGS orbit. Figure 6.7 shows the orbital residuals for satellite PNR 3. Table 6.5 shows a summary of the statistics of the comparison with the IGS orbits

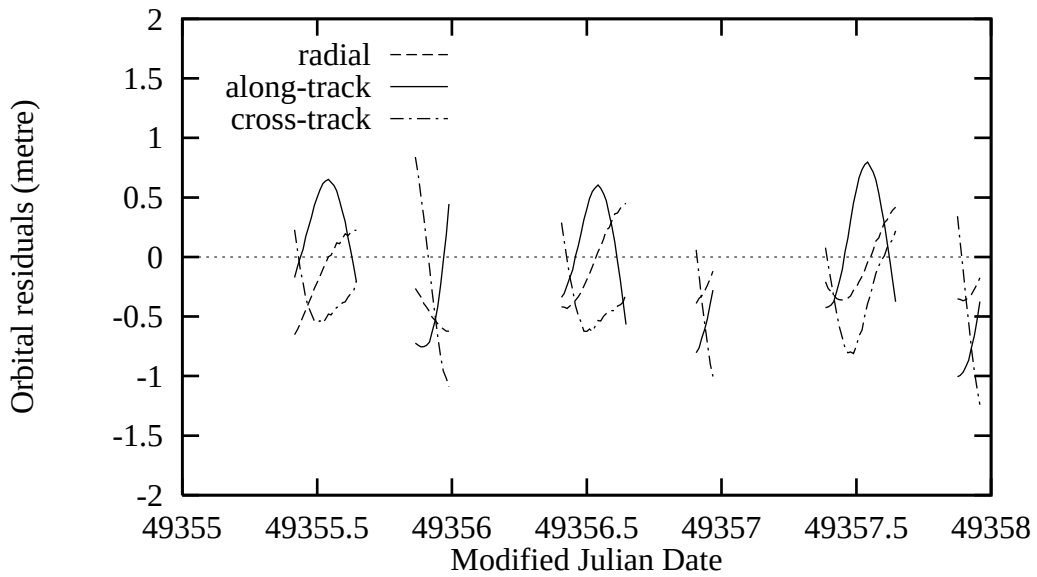

Figure 6.7: Orbital residuals with respect to IGS – PRN 3

comprising the part with GPS data coverage for each satellite. Satellite PRN 4, an eclipsing satellite, has been the most difficult to model. This problem has also been pointed out by some of the IGS Analysis Centers (e.g., IGS Report # 715). It shows the largest residuals with respect to the IGS.

In terms of peak-to-peak variation, the improved orbits show a consistency with respect to the IGS orbits below the 2.0 metre level. The worst peak to peak variation was of 5 metres with satellite PRN 4 and the best below one metre with satellite PRN 26. On average, the real-time orbits are at or below the 1 metre 3drms level.

Table 6.5: Comparison with IGS (values in metres).

$\Delta\tau$ = 2 minutes	radial	along track	cross track	3drms
best solution	0.71	0.98	0.90	0.91
average	0.78	1.22	0.98	1.15
worst solution	0.91	1.54	1.01	1.41

6.5 Other tests

Additional tests carried out are described below.

6.5.1 Relative error in baseline length

In the previous section, an update step k equal to 1 was used, and the real-time orbits were tested. Theoretically the same results should be obtained if using an update step greater than 1, i.e., if batches were used, because all observations are taken into account by the weight matrices. We have generated improved orbits using orbital arcs of 1 hour, 3 hours, 6 hours, 12 hours and 24 hours, applying the same processing strategies described before (with the difference that the fiducial station coordinates were heavier weighted). We went through the testing on the effect of these orbits in geodetic positioning. Even though the results were not exactly the same, they all remained at around the 0.05 ppm level as obtained with the real-time orbits. The reason for the small differences is attributed to the tropospheric delay estimation because a different number of tropospheric delay corrections were estimated during the various processing tests.

We shall mention in this section, just for the sake of completness, that we also compared these orbits with the IGS orbits, encoutering similar results as those when the real-time orbits were used. Again we point out that the direct comparison with the IGS orbits also indicates the different characteristics of the global and regional orbits.

6.5.2 Orbit repeatability

Another test made was on the orbit repeatability. Orbit repeatability is obtained by means of overlapping two consecutive orbits improved independently of each other. This comparison is intended to give us an idea of the internal consistency of the improved orbits. Orbital arcs of 48 hours were generated and the 24 hours-arc overlapping was compared. Table 6.6 summarizes this comparison. The average values of

Table 6.6: Orbit repeatability (values in metres).

$\Delta\tau$ = 24 hours	radial	along track	cross track	3drms
best solution	0.26	0.71	0.24	0.71
average	0.26	0.76	0.29	0.73
worst solution	1.54	3.68	2.13	3.28

these comparisons are shown. Figure 6.8 illustrates the fact that the orbits of most satellites reached sub-meter level precision. Again satellite PRN 4 has been the one with the worst repeatability.

The results coming from testing on orbit repeatability seems to corroborate our assumption, made in Chapter 4, that the force model adopted is accurate below the metre level. The metre level seems to be a limit for orbit determination when using regional networks, as pointed out before by *Lichten & Bertiger* [1989] and *Rothacher* [1992].

6.5.3 Effect of cycle slips and predicted EOP

In an attempt to analyse the effect that undetected cycle slips would have in orbit determination, we performed the following test. We first purposefully introduced an artificial cycle slip into the actual double difference observations involving a particular satellite. Acting this way we knew both when the cycle slip happened and its value, allowing us to have a control on the test. Then we carried out an orbit improvement

using an orbital arc of 24 hours, using the data containing the artificial cycle slip, and used the improved initial conditions of this satellite to generate a 24 hours improved orbital arc. This arc was then compared with the IGS product, and the orbital residuals were expressed in terms of 3drms. This 3drms was then compared with the 3drms of the corresponding 24 hour arc which was generated using the original data which we believe has no cycle slips. The difference between these two 3drms values was expressed in percentage terms representing the increase that the cycle slip provoked in the orbit 3drms. We repeated the same procedure for different satellites. At the end, we averaged out the set of percentage numbers representing the increase in orbit 3drms.

The cycle slip was introduced in the double difference observations via program CYCLE of the DIPOP package, created by K. Doucet in 1989. This program is intended to free the double differences from cycle slips. We used the program in the opposite way. The cycle slips were applied in the middle of the first data coverage interval for a particular satellite. The effect of the cycle slip in the orbital solution of the satellites that had eventually formed double differences with it were ignored.

We have chosen 6 combinations of cycle slips in L1 and L2. These cycle slips provoke a great variety of discontinuities in the ionosphere-free linear combination, ranging from 0 cm (case with no cycle slip) to 259.1 cm. Table 6.7 shows the nominal value of the discontinuities (cm) in the ionosphere-free linear combination Lc caused by the studied values of cycle slips in L1 (δN_1) and in L2 (δN_2). The complete table can be found in *Héroux & Kleusberg* [1989].

Table 6.7: Nominal discontinuities (cm) in Lc caused by cycle slips.

discontinuity	δN_1	δN_2	discontinuity	δN_1	δN_2
10.7	+1	+1	86.2	+1	-1
21.4	+2	+2	172.4	+2	-2
32.0	+3	+3	259.1	+3	-3

Figure 6.9 summarizes this study of the effect of undetected cycle slips on orbit determination. This figure should be interpreted as follows: if a satellite has its 3drms equal to 1 metre, an undetected cycle slip corresponding to 86.2 cm in Lc would increase its 3drms by 14%.

It should be pointed out that the cycle slips we introduced were kept unchanged throughout the processing. In a real-life situation other cycle slips could have happened and somehow ameliorated (or deteriorated) the effect. Another thing to say is that the cycle slips that may possibly pass undetected are the ones at or below the 2 cycle level, which corresponds to a typical noise level of the ionosphere. Cycle slips above this level have been studied for the sake of completeness.

We have also studied the possible impact of using predicted values of earth orientation parameters (EOP) as given by the IERS Bulletin A, for a 7-day period, instead of the estimated values of EOP as given by Bulletin B. For this purpose we processed a 24 hour orbital segment using predicted EOP. We then generated an improved orbit covering the 24 hours segment. The orbits were compared with their counterparts generated as a function of the estimated EOP. The results of this study show an average increase of 0.24 metres in 3drms for the improved orbits. We conclude by saying that, for an orbit service, the availability of accurate EOP seems essential.

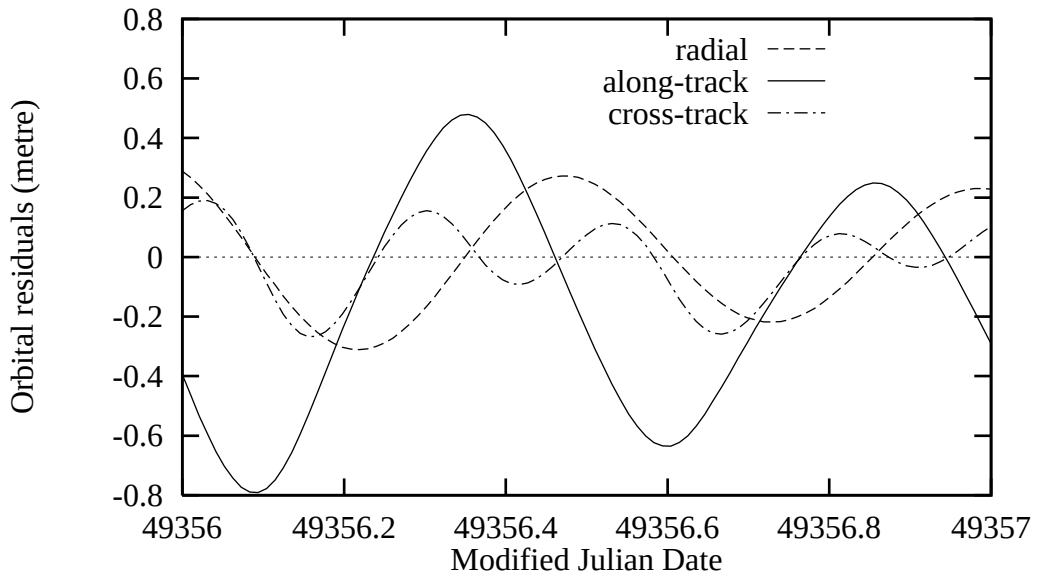

Figure 6.8: Orbit repeatability for PRN 26

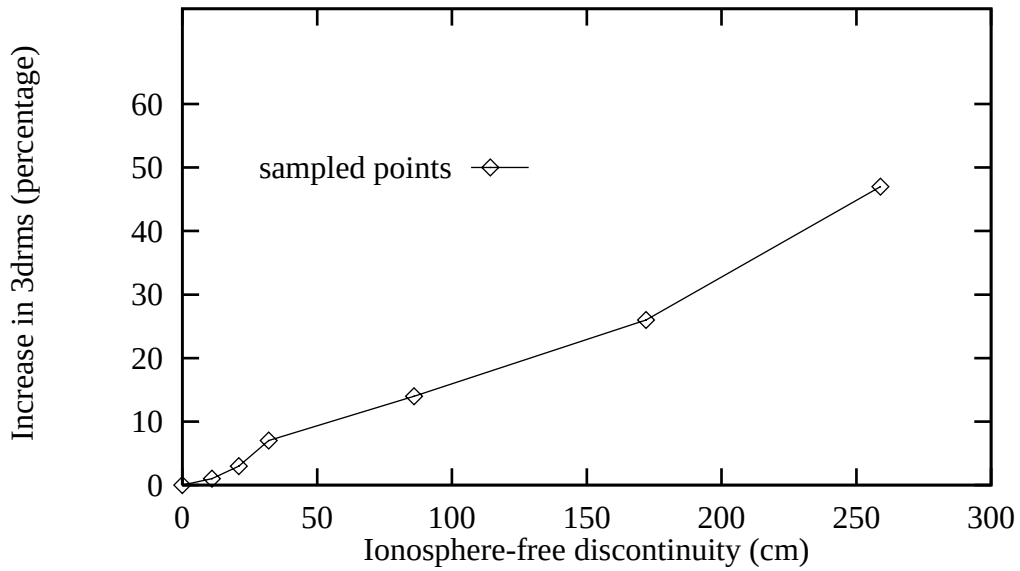

Figure 6.9: Percentage increase in orbit 3drms caused by cycle slips.

Chapter 7

Conclusions and recommendations

7.1 Summary and conclusions

In this dissertation we have set forth a new algorithm intended to make available high-accuracy orbits for GPS users in real-time. We have called the approach the real-time orbit improvement. The approach is based on a unit, called the update step, which defines the length of the orbital arc over which the improvement takes place. The initial conditions improved in one orbital arc are used for generating the orbits covering the arc over which the improvement took place, and the next one, where they are used as a priori orbits for the new improvement. In this way, the last improved orbit provides the initial conditions for the new orbit improvement. These moving initial conditions is what we have called the multiple expansion point.

The two type of orbits continuously generated, the improved and predicted ones, may have different lengths depending on the length of the orbital arc used, as defined by the update step k.

These orbits may be distributed by an orbit service. The major characteristics of such a service have been described. In the context of an orbit service, we have called the transmitted orbits as "real-time" orbits.

The algorithm was implemented based on UNB's DIPOP software. A major modification was the implementation of fully rigorous network adjustment, i.e., to process all simultaneous observations, taking into account the mathematical correlation between baselines. The orbit generation is carried out by our orbit integrator, called program PREDICT. The models used for the software mostly follow the ones recommended by the IERS.

We have tested the real-time orbits as well as the generated orbits using 5 different orbital arcs, 1 hour, 3 hours, 6 hours, 12 hours and 24 hours, in many different ways, by assessing their internal and external consistency and their effect in geodetic positioning. For these tests, we have used a regional network for the orbit improvement.

Based on these tests we conclude that the approach is capable of generating improved orbits at or below the 1 metre level 3drms. Also, the use of these orbits can yield baselines with relative error varying from 0.05 to 0.02 ppm, over baselines of hundreds of kilometres. This represents an improvement of 1 order of magnitude over the broadcast orbits, the only ones presently available for real-time applications.

The GPS data used was cycle-slip free. Therefore, a simulation of the effect of undetected cycle slips on orbit determination was done. Also studied was the effect of using predicted EOP instead of post-fitted ones.

7.2 Recommendations for future work

Recommendations for future work are:

- the models used in this investigation may be further refined. The effect of ocean tidal loading on station coordinates should be implemented. As far as the satellite force model is concern, it can be improved by modelling the perturbation caused by ocean tides. In addition, the solar radiation pressure model can be improved by incorporating a better model for the yaw attitude of the eclipsing satellites and by accommodating momentum dumps;

- this investigation used a numerical integrator with a fixed step size. The use of a shorter step size during eclipse seasons seems advantageous. An option allowing for a variable step size should be implemented;

- in this investigation we have used a regional network for the orbit improvement and orbit generation. The processing should be repeated using a global network. A globally consistent orbit should be obtained in this case;

- in this investigation the effect of network configuration on orbit determination was overlooked. An example of the need for such a study is to know beforehand what would happen if one receiver in the network temporarily stops operating;

- in this investigation we have used very long baselines for testing the effect of the generated orbits in geodetic positioning. The same type of test should be made using shorter baselines;

- in this investigation we have used GPS data that are cycle slips free. In a real world situation this might not be the case. The implementation of a totally automatic cycle slip procedure for this real-time static application should be carried out;

- in this investigation the ambiguities have not been fixed to integer numbers. This is typically a time consuming and iterative procedure for very long baselines, carried out in post-processing mode. A real-time ambiguity resolution algorithm for very long baselines is yet to be developed;

- in this investigation data not affected by A-S was used. The effect of A-S on orbit determination should be studied.

References

[1] Abbot, R. I., Y. Bock, C. C. Counselman II and R. W. King (1986). "GPS orbit determination." *Proceedings of the Fourth International Geodetic Symposium on Satellite Positioning*, Austin, Tex., U.S.A., April 28 – May 2, Vol. 1, pp. 271–275.

[2] Abidin, H. Z. (1992). *Computational and Geometrical Aspects of on-the-Fly Ambiguity Resolution*, Ph. D. dissertation, Department of Geodesy and Geomatics Engineering Technical Report No. 164, University of New Brunswick, Fredericton, N.B., Canada, 290 pp.

[3] Ackroyd, N. and R. Lorimer (1990). *Global navigation: a GPS user's guide*, Lloyd's of London Press, London.

[4] Aoki, S., B. Guinot. G. H. Kaplan, H. Kinoshita, D. D. McCarthy and P. K. Seidelmann (1982). "The new definition of Universal Time." *Astronomy and Astrophysics*, Vol. 105, pp. 359–361.

[5] Ash, M. E. (1972). "Determination of earth satellite orbits." Technical Note 1972-5, Massachusetts Institute of Technology, Cambridge, Mass.

[6] Ashjaee, J., and R. Lorenz (1992). "Precision GPS surveying after Y-code." *Proceedings of Fifth International Technical Meeting of the Satellite Division of The Institute of Navigation*, Albuquerque, N. Mex., U.S.A., September 16-18, pp. 657-659.

[7] Ashkenazi, V., C. Hill, T. Moore and S. Whalley (1990). "Orbit determination for GPS satellites." *Global Positioning System: an overview*, Y. Bock and N. Leppard (Ed.), IAG Symposium No. 102, Edinburgh, Scotland, August 7-8, 1989, Springer-Verlag, Berlin, pp. 187–194.

[8] Ashkenazi, V., C. J. Hill and W. Y. Ochieng (1993). "Wide-area differential GPS: a performance study." *Navigation: Journal of The Institute of Navigation*, Vol. 40, No. 3, pp. 297–319.

[9] Batin, R. H. (1987). *An introduction to the mathematics and methods of Astrodynamics*, American Institute of Aeronautics and Astronautics, New York, NY, U.S.A.

[10] Bauersima, I. (1983)."NAVSTAR/Global positioning System (GPS) III: Erdvermessung durch radiointerferometriche satellitenbeobachtungen." Miteilungen der satellitenbeobachtungstation Zimmerwald Nr. 12, Drucherei der Universität Bern, Bern, Switzerland.

[11] Beutler, G., D. A. Davidson, R. B. Langley, R. Santerre, P. Vaníček and D. E. Wells (1984). "Some theoretical and practical aspects of geodetic positioning using carrier phase difference observations of GPS satellites." Department of Surveying Engineering Technical Report No. 109, University of New Brunswick, Fredericton, N.B., Canada.

[12] Beutler, G., W. Gurtner, I. Bauersima and R. B. Langley (1985). "Modelling and estimating the orbits of GPS satellites." *Proceedings of the First International Symposium on Precise Positioning with the Global Positioning System*, Rockville, Md., U.S.A., April 15-19, pp. 99–111.

[13] Beutler, G., W. Gurtner, M. Rothacher, T. Schildknecht, I. Bauersima (1986). "Determination of GPS orbits using double difference carrier phase observations from regional networks." *Bulletin Géodésique*, Vol. 60, pp. 205–220.

[14] Beutler, G., I. Bauersima, W. Gurtner and M. Rothacher (1987). "Correlations between simultaneous GPS double difference carrier phase observations in the multistation mode: implementation considerations and first experiences." *Manuscripta Geodaetica*, Vol. 12, pp. 40–44.

[15] Beutler, G., I. Bauersima, W. Gurtner, M. Rothacher and T. Schildknecht (1988). "Static positioning with the Global Positioning System (GPS): the state of the art." *Lecture Notes in Earth Science*, Vol. 19, E. Groten and R. Strauß(Eds.), Springer-Verlag, Berlin, pp. 363–380.

[16] Beutler, G. (1991). "Himmelsmechanik I." Mitteilungen der satellitenbeobachtungsstation Zimmerwald Nr. 25, University of Berne, Berne, Switzerland.

[17] Beutler, G., J. Kouba and T. Springer (1993). "Combining the orbits of the IGS Processing Centers." *Proceedings of the IGS Analysis Center Workshop*, J. Kouba (Ed.), Natural Resources Canada, Ottawa, Canada, October 12-14, pp. 20–56.

[18] Beutler, G. (1993a) "The 1992 IGS test campaign, Epoch'92, and the IGS pilot service: an overview." *Proceedings of the 1993 IGS Workshop*, G. Beutler and

E. Brockmann (Ed.), University of Berne, Berne, Switzerland, March 25-26, pp. 3–9.

[19] Beutler, G. (1993b). Personal communication. Astronomical Institute of the University of Berne, Berne, Switzerland.

[20] Beutler, G., E. Brockmann, W. Gurtner, L. Mervart, M. Rothacher and A. Verdun (1994). "Extended orbit modeling techniques at the CODE Processing Center of the International GPS Service for Geodynamics (IGS): theory and initial results." *Manuscripta Geodaetica*, Vol. 19, pp. 367–386.

[21] Beutler, G., R. Weber, U. Hugentobler, M. Rothacher and A. Verdun (1995). "GPS satellite orbits." Lecture Notes of the International School GPS for Geodesy, Delft, The Netherlands, March 26 – April 1, 1995, Netherlands Geodetic Commission.

[22] Beutler, G. (1995). Personal communication. Astronomical Institute of the University of Berne, Berne, Switzerland.

[23] Blewitt, G. (1990). "An automatic editing algorithm for GPS data." *Geophysical Research Letters*, Vol. 17, No. 3, pp. 199–202.

[24] Brown, A. (1989). "Extended differential GPS." *Navigation: Journal of The Institute of Navigation*, Vol. 36, No. 3, pp. 265–285.

[25] Brouwer, D. and G. M. Clemence (1961). *Methods of Celestial Mechanics*, Academic Press, New York.

[26] Chen, D.-S. (1991). *A Long Arc Orbit Approach to GPS Satellite Orbit Improvement.* M. Sc. E. thesis, Department of surveying Engineering Technical Report No. 154, University of New Brunswick, Fredericton, N.B., Canada, 216 pp.

[27] Conte, S. D. (1962). "The computation of Satellite Orbit Trajectories." *Advances in Computers*, Vol. 3, pp. 2–76, Academic Press, New York.

[28] Davidson, J.M., C. L. Thornton, C. J. Vegos, L. E. Young and T. P. Yunck (1985). "The March 1985 demonstration of the fiducial network concept for geodesy: a preliminary report." *Proceedings of the First International Symposium on Precise Positioning with the Global Positioning System*, Rockville, Md., U.S.A., April 15-19, Vol. 2, pp. 603–611.

[29] Delikaraoglou, D., R. R. Steeves and N. Beck (1986). "Development of a Canadian Active Control System using GPS." *Proceedings of the Fourth International Geodetic Symposium on Satellite Positioning*, Austin, Tex., U.S.A., April 28 – May 2, Vol. 2, pp. 1189–1203.

[30] Delikaraoglou, D. (1989). "On Principles, methods and recent advances in studies towards a GPS-based control system for Geodesy and Geodynamics." NASA Technical Memorandum 100716, Greenbelt, Md., U.S.A.

[31] Eanes, R., J. Schutz and B. Tapley (1983). "Earth and ocean tide effects on Lageos and Starlette." *Proceedings of the Ninth International Symposium on Earth Tides*, J. T. Kuno (Ed.), New York, N.Y., U.S.A., August 17-22, 1981, E. Sckeizerbart'sche Verlagabuchhandlung, Stuttgart, Germany, pp. 239-250.

[32] El-Rabbany, A. E. (1994). *The Effect of Physical Correlations on the Ambiguity Resolution and Accuracy Estimation in GPS Differential Positioning.* Ph. D. dissertation, Department of Geodesy and Geomatics Engineering Technical Report No. 170, University of New Brunswick, Fredericton, N.B., Canada, 161 pp.

[33] Escobal, P. R. (1976). *Methods of Orbit Determination*, John Wiley & Sons, New York, New York.

[34] Feltens, J. (1988). "Several aspects of solar radiation pressure." *Lecture Notes in Earth Science*, Vol. 19, E. Groten and R. Strauß(Eds.), Springer-Verlag, Berlin, pp. 487–502.

[35] Fliegel, H. F., W. A. Fees, W. C. Lanton and N. W. Rhodus (1985). "The GPS radiation force model." *Proceedings of the First International Symposium on Precise Positioning with the Global Positioning System*, Rockville, Md., U.S.A., April 15-19, Vol. 1, pp. 113–119.

[36] Fliegel, H. F. and T. E. Gallini (1989). "Radiation Pressure models for Block II GPS satellites." *Proceedings of the Fifth International Geodetic Symposium on Satellite Positioning*, Las Cruces, N. Mex., U.S.A., March 13-17, pp. 789–798.

[37] Fliegel, H. F., T. E. Gallini and E. R. Swift (1992). "Global positioning system radiation force model for geodetic applications." *Journal of Geophysical Research*, Vol. 97, No. B1, pp. 559–568.

[38] Fliegel, H. (1993). Personal communication, The Aerospace Corporation, El Segundo, Calif, U.S.A., July.

[39] Fortes, L. P. S. (1993). "Brazilian network for continuous monitoring of the Global Positioning System – RBMC." *Permanent Satellite Tracking Networks for Geodesy and Geodynamics*, G.L. Mader (Ed.), IAG Symposium No. 109, Vienna, Austria, August 11-24, 1991, Springer-Verlag, Berlin, pp. 95–101.

[40] Georgiadou, Y. and A. Kleusberg (1988). "On carrier phase multipath effects in relative GPS positioning." *Manuscripta Geodaetica*, Vol. 13, pp. 172–179.

[41] Georgiadou, Y. and K. D. Doucet (1990). "The issue of selective availability." *GPS World*, Vol. 1, No. 5, pp 53–56.

[42] Goad, C. C. (1988). "Investigation of an alternate method of processing global positioning survey data collected in kinematic mode." *Lecture Notes in Earth Science*, Vol. 19, E. Groten and R. Strauß(Eds.), Springer-Verlag, Berlin, pp. 93–106.

[43] Gurtner, W. (1994). "RINEX: the receiver-independent exchange format." *GPS World*, Vol. 5, No. 7, pp. 48–52.

[44] Hamming, R. W. (1962). *Numerical Methods for Scientists and Engineers*, McGraw-Hill Book Company, New York.

[45] Hatch, R. (1990). "Instantaneous ambiguity resolution." *Kinematic and Inertial Systems Symposium*, K.-P. Schwarz and G. Lachapelle (Eds.), IAG Simposium No. 107, Banff, Canada, September 10-13, Springer-Verlag, Berlin, pp. 299–308.

[46] Héroux, P., A. Kleusberg (1989). "GPS precise relative positioning and ionosphere in auroral regions." *Proceedings of the Fifth International Geodetic Symposium on Satellite Positioning*, March 13-17, Vol. 1, Las Cruces, N. Mex., U.S.A., pp. 475–486.

[47] Herrick, S. (1972). *Astrodynamics*, Volume 2, Van Nostrand Reinhold, New York.

[48] Hofmann-Wellenhof, B., H. Lichtenegger and J. Collins (1992). *Global Positioning System, Theory and Practice*, Springer-Verlag, Berlin.

[49] Hughes, J. A., C. A. Smith and G. H. Kaplan (Eds.) (1991). *IAU Proceedings of 127th Colloquium of the IAU, Reference Systems*, US Naval Observatory, Washinghton, D.C., U.S.A.

[50] Ifadis, I. I. (1986). "The atmospheric delay of radio waves: modeling the elevation angle depedence on a global scale." Technical Report 38L, Chalmers university of Technology, Götemberg, Sweden.

[51] International Earth Rotation Service (1992). *IERS Standards*, International Earth Rotation Service (IERS) Technical Note 13, D. D. McCarthy (Ed.), Central Bureau of IERS, Paris, France.

[52] Kee, C., B. W. Parkinson and P. Axelrad (1991). "Wide area differential GPS." *Navigation: Journal of The Institute of Navigation*, Vol. 38, No. 2, pp. 123–145.

[53] King, R. W., E. G. Masters, C. Rizos, A. Stolz and J. Collins (1985). *Surveying with GPS*, Monograph No. 9, School of Surveying, The University of New South Wales, Kensington, N.S.W., Australia.

[54] Kleusberg, A., Y. Georgiadou, F. van den Heuvel and P. Héroux (1989). "Single and dual frequency GPS data preprocessing with DIPOP 2.1." Department of Surveying Engineering Technical Memorandum TM-21, University of New Brunswick, Fredericton, N.B., Canada.

[55] Kleusberg, A. and R. B. Langley (1990). "The limitations of GPS." *GPS World*, Vol. 1, No. 2, pp. 50–52.

[56] Klobuchar, J. (1990). "Ionospheric effects on GPS." *GPS World*, Vol. 2, No. 4, pp. 48–51.

[57] Komjathy, A. (1995). Personal communication. Department of Geodesy and Geomatics Engineering, University of New Brunswick, Fredericton, N.B., Canada.

[58] Komjathy, A., R. B. Langley and F. Vejražka (1995). "A comparison of predicted and measured ionospheric range error correction." *EOS Trans. AGU*, Spring Meeting Supplement, Vol. 76, No. 17, p. S87.

[59] Kouba, J. (Ed.) (1993). *Proceedings of the IGS Analysis Center Workshop*, Natural Resources Canada, Ottawa, Canada, October 12–14.

[60] Kovalevsky, J. (1989). "Lectures in Celestial Mechanics." Theory of Satellite Geodesy and Gravity field, *Lecture Notes in Earth Science*, Vol. 25, F. Sansò and R. Rummel (Eds.), Springer-Verlag, Berlin, pp. 69–114.

[61] Krakiwsky, E. J. and D.E. Wells (1971). "Coordinate systems in geodesy." Department of Surveying Engineering Lecture Notes No. 16, University of New Brunswick, Fredericton, N.B., Canada.

[62] Kremer, G. T., R. M. Kalafus, P. V. W. Loomis and J. C. Reynolds (1990). "The effect of Selective Availability on differential GPS corrections." *Navigation: Journal of The Institute of Navigation*, Vol. 37, No. 1, pp. 39–64.

[63] Kreyszig, E. (1988). *Advanced Engineering Mathematics*, 6th edition, John Wiley & sons, New York.

[64] Landau, H. (1988). "Zur Nutzung des Global Positioning System in Geodäsie und Geodynamik: Modellbildung, Software-Entwicklung und Analyse." Studiengang Vermessungswesen, Universität der Bundeswehr München, Munich, Germany.

[65] Langley, R. B., G. Beutler, D. Delikaraoglou, B. Nickerson, R. Santerre, P. Vaníček and D. E. Wells (1984). "Studies in the application of the Global Positioning System to differential positioning." Department of Surveying Engineering Technical Report No. 108, University of New Brunswick, Fredericton, N.B., Canada.

[66] Langley, R. B. (1990). "Why is the GPS signal so complex?" *GPS World*, Vol. 1, No. 3, pp. 56–59.

[67] Langley, R. B. (1991a). "The GPS receiver: an introduction." *GPS World*, Vol. 2, No. 1, pp. 50–53.

[68] Langley, R. B. (1991b). "The orbits of GPS satellites." *GPS World*, Vol. 2, No. 3, pp. 50–53.

[69] Langley, R. B. (1991c). "The mathematics of GPS." *GPS World*, Vol. 2, No. 7, pp. 54–50.

[70] Langley, R. B. (1993a). "The GPS observables." *GPS World*, Vol. 4, No. 4, pp. 52–59.

[71] Lapucha, D. and M. Huff (1993). "Multisite real-time DGPS system using satellite data link: operational results." *Navigation: Journal of The Institute of Navigation*, Vol. 40, No. 3, pp. 283–296.

[72] Leick, A. (1995). *GPS satellite surveying*, 2nd. Edition, John Wiley & Sons, New York.

[73] Lerch, F., R. Nerem, B. Putney, T. Felstentreger, B., Sanches, S. Klosko, G. Patel, R. Williamson, D. Chinn, J. Chan, K. Rachlin, N. Chandler, J. McCarthy, J. Marshall, S. Luthcke, D. Pavlis, J. Robbins, S. Kapoor and E. Pavlis (1992). "The GEM-T3 gravitational model." NASA Technical Memorandum 104555, NASA/Goddard Space Flight Center, Greenbelt, Md., U.S.A.

[74] Lichten, S. M. and J. S. Border (1987). "Strategies for High-Precision Global Positioning System Orbit Determination." *Journal of Geophysical Research*, Vol. 92, No. B12, pp. 12751–12762.

[75] Lichten, S. M. and W. I. Bertiger (1989). "Demonstration of sub-meter GPS orbit determination and 1.5 parts in 10^8 three-dimensional baseline accuracy." *Bulletin Géodésique*, Vol. 63, pp. 167–189.

[76] Lichten, S. M. (1990). "High accuracy Global Positioning System orbit determination: progress and prospects." *Global Positioning System: an overview*, Y.Bock and N. Leppard (Ed.), IAG Symposium No. 102, Edinburgh, Scotland, August 7-8, 1989, Springer-Verlag, Berlin, pp. 146–164.

[77] Lichteneger, H. and B. Hoffmann-Wellenhof (1990). "GPS-data preprocessing for cycle slip detection." *Global Positioning System: an overview*, Y.Bock and N. Leppard (Ed.), IAG Symposium No. 102, Edinburgh, Scotland, August 7-8, 1989, Springer-Verlag, Berlin, pp. 57–68.

[78] Mader, G. L. (1990). "Rapid static and kinematic Global Positioning system using the ambiguity function technique." *Journal of Geophysical Research*, Vol. 97, No. B3, pp. 3271–3283.

[79] McCarthy, J. J., S. Rowton, D. Moore, D. E. Pavlis, S. B. Luthcke and L. S. Tsaoussi (1993). "GEODYN II, Systems Description." Volume 1, NASA, Greenbelt, Md., U.S.A.

[80] Melbourne, W. G., S. S. Fisher, R. E. Neilan, T. P. Yunck, B. Engen, Ch. Reigber and S. Tatevjan (1993). "The first GPS IERS and Geodynamics experiment – 1991." *Permanent Satellite Tracking Networks for Geodesy and Geodynamics*, G. L. Mader (Ed.), IAG Symposium No. 109, Vienna, Austria, August 11-24, 1991, Spring-Verlag, Berlin, pp. 65–80.

[81] Mendes, V. B. and R. B. Langley (1994). "A comprehensive analysis of mapping functions used in modeling tropospheric propagation delay in space geodetic data." *Proceedings of KIS94, International Symposium on Kinematic Systems in Geodesy, Geodynamics and Navigation*, Banff, Canada, August 30 - September 2 , pp. 87-98

[82] Mervart, L., G. Beutler, M. Rothacher and U. Wild (1994). "Ambiguity resolution strategies using the results of the International GPS Geodynamics Service (IGS)." *Bulletin Géodésique*, Vol. 68, No. 1, pp. 29–38.

[83] Milani, H., A. M. Nobili and P. Farinella (1987). *Non-gravitational perturbations and satellite Geodesy*, Adam Hilger, Bristol, England.

[84] Moritz, H. and I. J. Mueller (1988). *Earth rotation, theory and observation*, Ungar, New York.

[85] Morsund, D. G. and C. S. Duris (1967). *Elementary Theory and Application of Numerical Analysis*, Mcgraw-Hill Book Company, New York.

[86] Mueller, I. I. (1969). *Spherical and Practical Astronomy as Applied to Geodesy*, Ungar, New York.

[87] Mueller, I. I. and G. Beutler (1992). "The International GPS Service for Geodynamics – development and current structure." *Proceedings of the Sixth International Symposium on Satellite Positioning*, Columbus, Ohio, U.S.A., March 17-20, pp. 823–835.

[88] Mueller, I. I. (1993). "Planning an international service using the Global Positioning System (GPS) for geodynamic applications." *Permanent Satellite Tracking Networks for Geodesy and Geodynamics*, G. L. Mader (Ed.), IAG Symposium No. 109, Vienna, Austria, August 11-24, 1991, Spring-Verlag, Berlin, pp. 1–22.

[89] Mueller, T. (1994). "Wide-area differential GPS." *GPS World*, Vol. 5, No. 6, pp. 36–44.

[90] Nautical Almanac Office (1994). *The Astronomical Almanac for the year 1995*, U.S. Government Printing Office, Washington, D.C., U.S.A.

[91] Parrot, D. (1989). *Short-Arc Orbit Improvement for GPS Satellites.* M. Sc. E. thesis, Department of Surveying Engineering Technical Report No. 143, University of New Brunswick, Fredericton, N.B., Canada, 192 pp.

[92] RTCM Special Committee # 104 (1994). "RTCM recommended standards for differential NAVSTAR GPS service." Radio Technical Commission for Maritime Services (RTCM) paper 194-93/SC 104-STD, Washington, D.C., U.S.A.

[93] Remondi, B. (1984). *Using the Global Positioning System (GPS) Phase Observable for Relative Geodesy: Modelling, Processing and Results*, Ph.D. Dissertation, Center for Space Research, University of Texas at Austin, Austin, Tex., U.S.A.

[94] Remondi, B. (1989). "Extending the National Geodetic Survey standards GPS orbit formats." NOAA Technical Report NOS 133 NGS 46, Rockville, Md., U.S.A.

[95] Remondi, B. W. and B. Hoffmann-Wellenhof (1990). "GPS broadcast orbits versus precise orbits: a comparison study." *Global Positioning System: an overview*, Y.Bock and N. Leppard (Ed.), IAG Symposium No. 102, Edinburgh, Scotland, August 7-8, 1989, Springer-Verlag, Berlin, pp. 203–217, 360 pp.

[96] Rizos, C. and A. Stolz (1985). "Force modelling for GPS satellite orbits." *Proceedings of the First International Symposium on Precise Positioning with the Global Positioning System*, Rockville, Md., U.S.A., April 15-19, Vol. 1, pp. 87–96.

[97] Rothacher, M. (1992). "Orbits of satellite systems in space geodesy." Ph. D. Thesis, Astronomical Institute of the University of Berne, Published by the Swiss Geodetic Commission, Berne, Switzerland, 243 pp.

[98] Saastamoinen, J. (1973). "Contributions to the theory of atmospheric refreaction." In three parts. *Bulletin Géodésique*, No. 105, pp. 279–298; No. 106, pp. 383–397; No. 107, pp. 13–34

[99] Santerre, R. (1989). *GPS Satellite Sky Distribution: Impact on the Propagation of Some Important Errors in Precise Relative positioning.* Ph.D. dissertation, Department of Surveying Engineering Technical Report No. 145, University of New Brunswick, Fredericton, N.B., Canada, 220 pp.

[100] Santos, M. C. (1990). *NAVSTAR/GPS: Aspectos Teóricos e Aplicações Geofísicas*, Special Publication No. 7, National Observatory, Rio de Janeiro, RJ, Brazil.

[101] Santos, M. C. (1992). "Real-time GPS orbit improvement." Ph.D. Thesis Proposal, Department of Geodesy and Geomatics Engineering, University of New Brunswick, Fredericton, N.B., Canada.

[102] Santos, M. C. (1994). "Analysis of errors in GPS orbit determination." Graduate Seminar, Department of Geodesy and Geomatics Engineering, University of New Brunswick, Fredericton, N.B., Canada.

[103] Schenewerk, M. S., G. L. Mader, M. Chin, W. Kass, R. Dulaney, J. R. Mackay and R. H. Foote (1990). "Status of CIGNET and orbit determination at the National Geodetic Survey." *Proceedings of the Second International Symposium on Precise Positioning with the Global Positioning System*, Ottawa, Canada, September 3-7, pp. 179–189.

[104] Seidelmann, P. K. (Ed.) (1992). *Explanatory Supplement to the Astronomical Almanac*, Nautical Almanac Office, U. S. Naval Observatory, University Science Books, California, U.S.A.

[105] Schutz B. E., C. S. Ho, P. A. M. Abusali and B. D. Tapley (1990). "Casa Uno GPS orbit and baseline experiments." *Geophysical Research Letters*, Vol. 17, No. 5, pp. 643–646.

[106] Schwiderski, E. (1983). "Atlas of ocean tidal charts and maps, part I: the semidiurnal principal lunar tide M_2." *Marine Geodesy*, Vol. 6, pp. 219–256.

[107] Swift, E. R. (1993). "GPS orbit/clock estimation based on smoothed pseudorange data from a ten-station global network." *Permanent Satellite Tracking Networks for Geodesy and Geodynamics*, G. L. Mader (Ed.), IAG Symposium No. 109, Vienna, Austria, August 11-24, 1991, Spring-Verlag, Berlin, pp. 151–160.

[108] Tapley, (1989). "Principles of orbit determination." Theory of Satellite Geodesy and Gravity field, *Lecture Notes in Earth Science*, Vol. 25, F. Sansò and R. Rummel (Eds.), Springer-Verlag, Berlin, pp. 235–260.

[109] Talbot, N. C. (1990). "Selective availability influences on static differential GPS surveying." *CISM Journal*, Vol. 44, No. 2, pp. 131–140.

[110] Tolman, B. W., J. R. Clynch, D. S. Coco and M. P. Leach (1990). "The effects of selective availability on differential GPS positioning." *Proceedings of the Second International Symposium on Precise Positioning with the Global Positioning System*, Ottawa, Canada, September 3-7, pp. 34–49.

[111] Torge, W. (1989). *Gravimetry*, de Gruyter, Berlin.

[112] Torge, W. (1991). *Geodesy*, de Gruyter, Berlin.

[113] van der Wal, A. D. (1995). "Evaluation of Strategies for Estimating Residual Neutral-atmosphere Propagation Delay in High Precision Global Positioning System Data Analysis." Department of Geodesy and Geomatics Engineering M. Sc. E. thesis (in preparation), University of New Brunswick, Fredericton, N.B., Canada.

[114] Vaníček, P. (1973). "Gravimetric satellite Geodesy." Department of Surveying Engineering Lecture Notes No. 32, University of New Brunswick, Fredericton, N.B., Canada.

[115] Vaníček, P., G. Beutler, A. Kleusberg, R. B. Langley, R. Santerre and D. E. Wells (1985). "DIPOP Differential positioning package for the Global Positioning System." Department of Surveying Engineering Technical Report No. 115, University of New Brunswick, Fredericton, N.B., Canada.

[116] Vaníček, P. and E. J. Krakiwsky (1986). *Geodesy, the concepts*, 2nd. Ed., North-Holland, Amsterdam.

[117] Velez, C. E. and J. L. Maury (1970). "Derivation of Newtonian-type integration coefficients and some applications to orbit calculations." NASA Technical Note TN D-5958, Goddard Space Flight Center, Md., U.S.A.

[118] Wanninger, L. (1993). "Effects of severe ionospheric conditions on GPS data processing." *Permanent Satellite Tracking Networks for Geodesy and Geodynamics*, G. L. Mader (Ed.), IAG Symposium No. 109, Vienna, Austria, August 11-24, 1991, Spring-Verlag, Berlin, pp. 141–150.

[119] Ware, R. H., C. Rocken, K. J. Hurst and G. H. Rosborough (1986). "Determination of the OVRO-Mojave baseline during the spring 1985 GPS test." *Proceedings of the Fourth International Geodetic Symposium on Satellite Positioning*, Austin, Tex., U.S.A., April 28 – May 2, Vol. 2, pp. 1089–1101.

[120] Wells, D. E., N. Beck, D. Delikaraoglou, A. Kleusberg, E. Krakiwsky, G. Lachapelle, R. Langley, M. Nakiboglu, K. Schwarz, H. Tranquilla, P. Vaníček (1987). *Guide to GPS Positioning*, Canadian GPS Associates, Fredericton, N.B., Canada.

[121] Wells, D. E., R. B. Langley, A. Komjathy and D. Dodd (1995). "Acceptance tests on Ashtech Z-12 receivers." Final Report prepared by the Department of Geodesy and Geomatics Engineering, University of New Brunswick, Fredericton, N.B., Canada, for Public Works and Government Services Canada, Moncton, N.B., Canada, February.

[122] Williams, B. G. (1986). "GPS orbit determination results from the march 1985 field test." *Proceedings of the Fourth International Geodetic Symposium on Satellite Positioning*, Austin, Tex., U.S.A., April 28 – May 2, Vol. 1, pp. 289–302.

[123] Wu, S. C., W. G. Melbourne and T. P. Yunck (1988). "Impact of tracking network variation on GPS orbit determination." AIAA 26th Aerospace Scienc Meeting.

[124] Wu, J.T., S. C. Wu, G. A. Hajj, W. I. Bertiger and S. M. Lichten (1993). "Effects of antenna orientation on GPS carrier phase." *Manuscripta Geodaetica*, Vol. 18, pp. 91–98.

[125] Wubbena, G. (1989). "The GPS adjustment software package GEONAP – concepts and models." *Proceedings of the Fifth International Geodetic Symposium on Satellite Positioning*, March 13-17, Las Cruces, N. Mex., U.S.A., Vol. 1, pp. 452–461.

[126] Zhu, S. Y. and E. Groten (1988). "Relativistic effects in GPS." *Lecture Notes in Earth Science*, Vol. 19, E. Groten and R. Strauß(Eds.), Springer-Verlag, Berlin, pp. 41–46.

[127] Zieliński, J. B (1989). "GPS baseline error caused by the orbit uncertainty." *Manuscripta Geodaetica*, Vol. 14, No. 2, pp. 117–124.

Appendix I

Transformation between Keplerian elements and the OR-system

This appendix contains a description of the transformations between Keplerian elements and the orbital (OR) system. It is a complement to Chapter 2.

I.1 Keplerian elements to the OR-system

If the Keplerian elements of a satellite are given, its position and velocity in the OR-system can be obtained at any time by [*Wells et al.*, 1987]:

$$\underline{r}^{OR} = \frac{a\,(1-e^2)}{(1+e\cos f)} \begin{bmatrix} \cos f \\ \sin f \\ 0 \end{bmatrix} = \begin{bmatrix} a\ \cos E - a\ e \\ a\ \sqrt{1-e^2}\ \sin E \\ 0 \end{bmatrix}, \tag{I.1}$$

$$\underline{\dot{r}}^{OR} = \frac{n\ a}{(1-e\ \cos E)} \begin{bmatrix} -\sin E \\ \sqrt{1-e^2}\ \cos E \\ 0 \end{bmatrix}, \tag{I.2}$$

with n being the mean motion:

$$n = \sqrt{\frac{GM}{a^3}}, \tag{I.3}$$

and GM the geocentric gravitational constant.

I.2 OR-system to Keplerian elements

The inverse transformation, i.e., the transformation from Cartesian coordinates $\underline{r}^{OR}$ and $\dot{\underline{r}}^{OR}$ at a time t into (osculating) Keplerian elements is given as follows [*Beutler*, 1991]. To begin with, the angular momentum of a satellite, represented by the constant vector $\underline{h}$, normal to the orbital plane, is defined as:

$$\underline{h} = \underline{r} \times \dot{\underline{r}}. \tag{I.4}$$

This vector can be expressed, treating h, i and Ω as: polar coordinates as

$$\underline{h} = \begin{bmatrix} h \ \sin i \ \sin\Omega \\ -h \ \sin i \ \cos\Omega \\ h \ \cos i \end{bmatrix}, \tag{I.5}$$

where $h = \| \underline{h} \|$. The Keplerian elements Ω and i follow directly from equation I.5:

$$\Omega = \arctan\left(\frac{h_1}{-h_2}\right), \tag{I.6}$$

$$i = \arccos\frac{h_3}{h}. \tag{I.7}$$

where $h = [h_1, h_2, h_3]^T$. The major semi-axis a is computed from the "angular-momentum integral" [*Vaníček & Krakiwsky*, 1986]:

$$\frac{1}{a} = \frac{2}{r} - \frac{\dot{r}^2}{GM}, \tag{I.8}$$

where $\dot{r} = \| \dot{\underline{r}} \|$. The eccentricity e follows as:

$$e = \sqrt{1 - \frac{p}{a}}, \tag{I.9}$$

where $p = h^2/GM$. The argument of perigee is given by:

$$\varpi = arctan\frac{q_2}{q_1} - f, \tag{I.10}$$

where:

$$\underline{q} = \underline{R_1}(i)\ \underline{R_3}(\Omega)\ \underline{r}, \tag{I.11}$$

in which $\underline{q}$ is an auxiliary coordinate system, with axes q_1 along the nodal line, q_2 along the angular momentum vector and q_3 completes a right-handed system. The true anomaly is:

$$f = \arctan \frac{(p/r) - 1}{\frac{\sqrt{\frac{p}{GM}}}{r}\ (\underline{r} \cdot \dot{\underline{r}})}. \tag{I.12}$$

where $r = \| \underline{r} \|$. Finally, the time of perigee passing T_o can be computed, starting from Kepler's equation realizing that:

$$M = (E - e\ \sin E) = n\ (t - T_o), \tag{I.13}$$

$$T_o = t - \frac{(E - e\ \sin E)}{n}, \tag{I.14}$$

where:

$$\tan \frac{E}{2} = \sqrt{\frac{1-e}{1+e}}\ \tan \frac{f}{2}. \tag{I.15}$$

In the above equations E is the eccentric anomaly and n is the mean motion.

Appendix II

Program PREDICT

This appendix describes the numerical integrator developed. It has been called program PREDICT. Its flowchart is depicted by Figure II.1.

The purposes of this program are:

1. to generate ephemerides for GPS satellites; and,
2. to improve GPS satellite initial conditions vis-á-vis a reference orbit.

The purposes of the program are accomplished as a function of the user's choice in terms of models. The models are as described in Chapter 4. The implemented ones are listed on item 2 below. The user can choose among:

1. source of initial conditions (given or interpolated from an orbital file);
2. force model (geopotential model and maximum degree and order, luni-solar contribution, 3 different solar radiation pressure models, solid earth tides and relativistic effects);
3. numerical integration techniques (Adams-Moulton and/or Stormer-Cowell);
4. a priori standard deviation for orbital parameters;

5. input reference orbit in either broadcast (RINEX), NGS SP1 or PREDICT formats; and,

6. output in either NGS SP1 or PREDICT format.

The inertial coordinate system adopted is the True Right Ascension system at the initial epoch.

PROGRAM "PREDICT"

(An orbital integrator for GPS satellites)

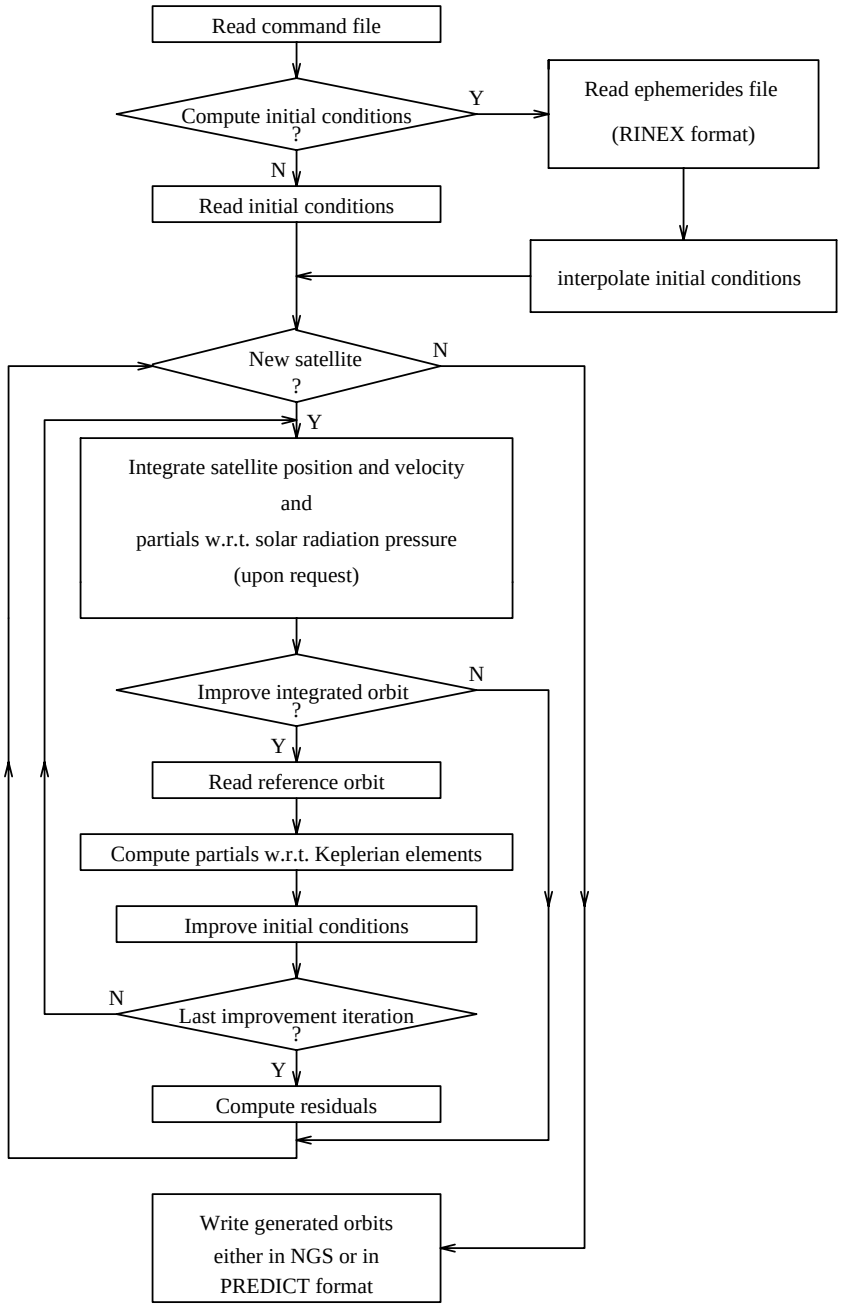

Figure II.1: Program PREDICT flowchart

Appendix III

Partial derivatives

This appendix contains the partial derivatives of the GPS carrier phase double difference observation with respect to the estimated parameters, namely, station coordinates, orbital parameters, tropospheric delay parameters and carrier phase ambiguity. For that purpose, let us first rewrite the equation of the GPS carrier phase double difference observation, without the time argument, replacing the double difference operators by the superscripts i and j and by the subscripts k and ℓ, representing, respectively, receivers and satellites. The equation reads:

$$\Phi_{ij}^{k\ell} = \rho_{ij}^{k\ell} + d_{trop_{ij}}^{k\ell} - d_{ion_{ij}}^{k\ell} + \lambda N_{ij}^{k\ell} + \epsilon_{ij}^{k\ell}, \tag{III.1}$$

where $\Phi_{ij}^{k\ell}$ represents the double difference observation in unit of length, and:

$$\begin{aligned} \rho_{ij}^{k\ell} &= \rho_{ij}^{k} - \rho_{ij}^{\ell}, \\ \rho_{ij}^{k} &= \rho_{i}^{k} - \rho_{j}^{k}, \\ \rho_{i}^{k} &= \| \underline{R}_i - \underline{r}^k \|, \end{aligned} \tag{III.2}$$

with ρ_i^k representing the geometric distance between receiver i, at the time of signal reception, and satellite k, at the time of signal transmission, with both station and

satellite coordinates defined in the CT-system. Vectors $\underline{R}$ and $\underline{r}$ represent the geocentric position vectors of the receiver and of the satellite, respectively. The other elements in the equation III.1 are as previously defined.

III.1 Station coordinates

The partial derivatives with respect to the station coordinates are straightforward. They are valid for either $L1$ and $L2$ or for any of their linear combinations. They read:

$$\frac{\partial \Phi_{ij}^{k\ell}}{\partial \underline{R}_i} = -\underline{e}_i^k + \underline{e}_i^\ell \tag{III.3}$$

$$\frac{\partial \Phi_{ij}^{k\ell}}{\partial \underline{R}_j} = \underline{e}_j^k - \underline{e}_j^\ell, \tag{III.4}$$

where $\underline{e}$ is the receiver-satellite unit vector.

III.2 Orbital parameters

The partial derivatives with respect to the satellite initial state vector and initial dynamical parameters, grouped in $\underline{s}$, are also valid for either $L1$ and $L2$ or any other linear combination. They are given as:

$$\frac{\partial \Phi_{ij}^{k\ell}}{\partial \underline{s}^1} = \frac{\partial \Phi_{ij}^{k\ell}}{\partial \underline{r}^1} \cdot \frac{\partial \underline{r}^1}{\partial \underline{s}}, \tag{III.5}$$

where the superscript 1 replaces k or ℓ. The components of vector $\underline{r}$ are represented in the inertial system.

The first part of the right-hand side of equation III.5 corresponds to matrix $\underline{A}_r$ in equation 5.3 and is given by:

$$\frac{\partial \Phi_{ij}^{k\ell}}{\partial \underline{r}^k} = -\underline{e}_j^k + \underline{e}_i^k \tag{III.6}$$

$$\frac{\partial \Phi_{ij}^{k\ell}}{\partial \underline{r}^{\ell}} = \underline{e}_j^{\ell} - \underline{e}_i^{\ell}. \tag{III.7}$$

The second part of the right-hand side of equation III.5 corresponds to matrix $\underline{B}^*$ in equation 5.3. It is partitioned into 2 parts:

$$\underline{B}^* = \left[\frac{\partial \underline{r}}{\partial \underline{\kappa}} \; \frac{\partial \underline{r}}{\partial \underline{p}} \right], \tag{III.8}$$

the first one with derivatives of the satellite position vector with respect to the initial Keplerian elements $\underline{\kappa}$ and the second one with derivatives with respect to the initial solar radiation parameters $\underline{p}$. The Keplerian part follows from *Langley et al.* [1984] and *Parrot* [1989]:

$$\frac{\partial r}{\partial a} = \underline{M}_0 \left\{ \frac{1}{a} \, \underline{r}^{OR} + \begin{bmatrix} -a \sin E \; E_a \\ a(1-e^2)^{1/2} \cos E \; E_a \end{bmatrix} \right\}, \tag{III.9}$$

$$\frac{\partial r}{\partial e} = \underline{M}_0 \begin{bmatrix} -a(1 + \sin E \; E_e) \\ -a[e/(1-e^2)^{1/2} \sin E + (1-e^2)^{1/2} \cos E \; E_e] \end{bmatrix}, \tag{III.10}$$

$$\frac{\partial r}{\partial i} = \underline{M}_i \underline{r}^{OR}, \tag{III.11}$$

$$\frac{\partial r}{\partial \Omega} = \underline{M}_\Omega \underline{r}^{OR}, \tag{III.12}$$

$$\frac{\partial r}{\partial \varpi} = \underline{M}_\varpi \underline{r}^{OR}, \tag{III.13}$$

$$\frac{\partial r}{\partial \tau} = \underline{M}_0 \begin{bmatrix} -a \sin E \; E_\tau \\ a \cos E (1-e^2)^{1/2} E_\tau \end{bmatrix}, \tag{III.14}$$

where:

$$\underline{r}^{OR} = \begin{bmatrix} a \cos E - ae \\ a\sqrt{1-e^2} \sin E \\ 0 \end{bmatrix}, \tag{III.15}$$

$$\underline{M}_0 = \begin{bmatrix} \cos\Omega\cos\varpi - \sin\Omega\cos i\sin\varpi, & \cos\Omega\sin\varpi - \sin\Omega\cos i\cos\varpi \\ \sin\Omega\cos\varpi + \cos\Omega\cos i\sin\varpi, & -\sin\Omega\sin\varpi + \cos\Omega\cos i\cos\varpi \\ \sin i\sin\varpi, & \sin i\cos\varpi \end{bmatrix}, \quad \text{(III.16)}$$

$$\underline{M}_i = \begin{bmatrix} \sin\Omega\sin i\sin\varpi, & \sin\Omega\sin i\cos\varpi \\ -\cos\Omega\sin i\sin\varpi, & -\cos\Omega\sin i\cos\varpi \\ \cos i\sin\varpi, & \cos i\cos\varpi \end{bmatrix}, \quad \text{(III.17)}$$

$$\underline{M}_\Omega = \begin{bmatrix} -\sin\Omega\cos\varpi - \cos\Omega\cos i\sin\varpi, & \sin\Omega\sin\varpi - \cos\Omega\cos i\cos\varpi \\ \cos\Omega\cos\varpi - \sin\Omega\cos i\sin\varpi, & -\cos\Omega\sin\varpi - \sin\Omega\cos i\cos\varpi \\ 0, & 0 \end{bmatrix}, \text{(III.18)}$$

$$\underline{M}_\varpi = \begin{bmatrix} -\cos\Omega\sin\varpi - \sin\Omega\cos i\cos\varpi, & -\cos\Omega\cos\varpi + \sin\Omega\cos i\sin\varpi \\ -\sin\Omega\sin\varpi + \cos\Omega\cos i\cos\varpi, & -\sin\Omega\cos\varpi - \cos\Omega\cos i\sin\varpi \\ \sin i\cos\varpi, & -\sin i\sin\varpi \end{bmatrix}, \text{(III.19)}$$

$$E_a = \frac{dE}{da} = -\frac{3}{2}\left(\frac{GM}{a^3}\right)^{1/2}\frac{1}{r}(t-\tau), \quad \text{(III.20)}$$

$$E_e = \frac{dE}{de} = \frac{a}{r}\sin E, \quad \text{(III.21)}$$

$$E_\tau = \frac{dE}{d\tau} = -\left(\frac{GM}{a^3}\right)^{1/2}\frac{a}{r}, \quad \text{(III.22)}$$

in which a, e, i, ϖ, Ω and τ are the initial Keplerian elements, r represents the geocentric distance of the satellite at time t, and E the eccentric anomaly given by:

$$E = \sqrt{\frac{GM}{a^3}}(t-\tau) + e\sin E. \quad \text{(III.23)}$$

The second part of $\underline{B}^*$ is computed by numerically integrating:

$$\frac{\partial \ddot{r}_i}{\partial p_k} = A_{ij}\frac{\partial r_j}{\partial p_k} + \frac{\partial \ddot{p}_i}{\partial p_k}, \quad \text{(III.24)}$$

where $r_{i,j} = 1, 2, 3$ correspond to the Cartesian components of $\underline{r}$, p_k the initial solar radiation pressure parameters, $\ddot{p}_i$ represents the x, y, z components of the solar radiation pressure contribution and $\underline{A}$ is the matrix $\underline{W}$ containing only the radial field contribution (cf. Chapter 5):

$$\underline{A} = -\frac{GM}{r^3}\left(\frac{\underline{I} - 3\ \underline{r}\ \underline{r}^T}{r^2}\right), \tag{III.25}$$

with $\underline{I}$ being a unit matrix of dimension 3 by 3 and r is the norm of $\underline{r}$.

The term $\partial\ddot{p}_i/\partial p_k$ in equation III.24 depends on the choice of p_k, or in other words on the choice of the solar radiation pressure model (cf. Chapter 4). If $p_k = (p_0, p_y)$ at t_0 then (replacing $\ddot{p}_i$ by the vector $\underline{\ddot{p}}$):

$$\underline{\ddot{p}} = \nu\ p_0\ \underline{n} + \nu\ p_y\ \underline{e}_y. \tag{III.26}$$

Hence:

$$\frac{\partial\underline{\ddot{p}}}{\partial p_0} = \nu\ \underline{n}, \tag{III.27}$$

$$\frac{\partial\underline{\ddot{p}}}{\partial p_y} = \nu\ \underline{e}_y, \tag{III.28}$$

If $p_k = (G_x, G_z, p_y)$ at t_0, then:

$$\underline{\ddot{p}} = \nu\frac{a_{ES}^2}{\|\ \underline{r} - \underline{r}_s\ \|^2}(G_x a_x \underline{e}_x + G_z a_z \underline{e}_z) + \nu G_y \underline{e}_y. \tag{III.29}$$

Therefore:

$$\frac{\partial\underline{\ddot{p}}}{\partial G_x} = \nu\frac{a_{ES}^2}{\|\ \underline{r} - \underline{r}_s\ \|^2} a_x \underline{e}_x, \tag{III.30}$$

$$\frac{\partial\underline{\ddot{p}}}{\partial G_x} = \nu\frac{a_{ES}^2}{\|\ \underline{r} - \underline{r}_s\ \|^2} a_z \underline{e}_z, \tag{III.31}$$

$$\frac{\partial\underline{\ddot{p}}}{\partial p_y} = \nu\ \underline{e}_y. \tag{III.32}$$

III.3 Tropospheric zenith delay correction

The partial derivatives with respect to the tropospheric delay are obtained by first writing the double difference tropospheric delay as a product of mapping functions and zenith delays:

$$d^{k\ell}_{trop_{ij}} = d^z_{trop_i}[mf(e^k_i) - mf(e^\ell_i)] + d^z_{trop_j}[mf(e^k_j) - mf(e^\ell_j)], \tag{III.33}$$

where d^z_{trop} represents the zenith tropospheric delay at a particular station, e the elevation angle at a particular station to a particular satellite and mf is the mapping function. The partial derivatives are then given as:

$$\frac{\partial \Phi^{k\ell}_{ij}}{\partial d^{k\ell}_{trop_i}} = mf(e^k_i) - mf(e^\ell_i) \tag{III.34}$$

$$\frac{\partial \Phi^{k\ell}_{ij}}{\partial d^{k\ell}_{trop_j}} = mf(e^k_j) - mf(e^\ell_j). \tag{III.35}$$

These partial derivatives, like the previous ones, are valid for either $L1$ and $L2$ or for any of their linear combinations.

III.4 Ambiguity

The partial derivatives with respect to the cycle ambiguities are formulated relative to a reference satellite whose ambiguity is set to zero. The derivatives are then derived using the between-receiver single difference ambiguities N^k_{ij} and N^ℓ_{ij}, being written as:

$$\frac{\partial \Phi^{k\ell}_{ij}}{\partial N^k_{ij}} = -\lambda_L \tag{III.36}$$

$$\frac{\partial \Phi^{k\ell}_{ij}}{\partial N^\ell_{ij}} = \lambda_L, \tag{III.37}$$

where the subscript L indicates that these partials depend on the wavelength of either $L1, L2$ or of a linear combination. In the case of the ionosphere-free linear combination DIPOP 2.1 has been using:

$$\lambda_{Lc} = \frac{77^2}{2329}\ \lambda_{L1}. \tag{III.38}$$

In DIPOP 3.0 this value has been modified to:

$$\lambda_{Lc} = \frac{c}{f_{Lc}} \approx 0.484 \text{ m}, \tag{III.39}$$

where f_{Lc} is the effective frequency of the ionosphere-free linear combination. This change only scales the value of the estimated ambiguities without affecting the final results. We have used the way expressed by eqn. (III.39).

III.5 Misclosure

The misclosure vector $\underline{w}$ may assume different forms depending on the use of $L1$ or $L2$ or any of their linear combinations. Each element of the misclosure vector relating stations i, j with satellites k, ℓ is written as:

$$w_{ij}^{k\ell} = \Phi_{ij\ L}^{k\ell} - (P_{ij}^{k} - P_{ij}^{\ell}), \tag{III.40}$$

where P_{ij}^{k} and P_{ij}^{ℓ} are the theoretical single-difference ranges computed as a function of the known (at the time of computation) receiver and satellite positions, corrected for tropospheric delay, via the tropospheric delay model, and antenna heights. The subscript L denotes $L1$ or $L2$. If the ionosphere-free linear combination is used, the misclosure is:

$$w_{ij}^{k\ell} = \left(\frac{\Phi_{ij\ L1}^{k\ell} f_{L1}^2 - \Phi_{ij\ L2}^{k\ell} f_{L2}^2}{f_{L1}^2 - f_{L2}^2}\right) - (P_{ij}^{k} - P_{ij}^{\ell}). \tag{III.41}$$

If the wide lane linear combination is used, the misclosure is:

$$w_{ij}^{k\ell} = \left(\frac{\Phi_{ij\ L1}^{k\ell} f_{L1} - \Phi_{ij\ L2}^{k\ell} f_{L2}}{f_{L1} - f_{L2}}\right) - (P_{ij}^{k} - P_{ij}^{\ell}). \tag{III.42}$$

If the narrow lane linear combination is used, the misclosure is:

$$w_{ij}^{k\ell} = \left(\frac{\Phi_{ij\,L1}^{k\ell} f_{L1} + \Phi_{ij\,L2}^{k\ell} f_{L2}}{f_{L1} + f_{L2}}\right) - (P_{ij}^{k} - P_{ij}^{\ell}). \tag{III.43}$$

VITA

Full Name: Marcelo Carvalho dos Santos

Place and Date of Birth: Rio de Janeiro, Brazil, 26th May 1959.

Permanent Address:
Rua Oliveira, 39 Apt. 102
CEP: 20725-400 – Rio de Janeiro, RJ, Brazil

Schools Attended:
Colégio Metropolitano
Rua Lopes da Cruz
Rio de Janeiro, RJ, Brazil

Universities Attended:
Department of Cartography
Rio de Janeiro State University
Rio de Janeiro, RJ, Brazil
1977-1982, B.Sc. in Cartographic Engineering

Department of Geophysics
National Observatory
Rio de Janeiro, RJ, Brazil
1986-1990, M.Sc. in Geophysics

Publications:

Santos, M. C. and Silva, G. N. (1987). "Processamento de dados basitmétricos." Anais Hidrográficos, Tomo XLIV, 1987, pp. 127-186.

Santos, M. C. and Silva, G. N. (1987). "Processamento de dados basitmétricos." Anais do XIII Congresso Brasileiro de Cartografia, Brasília, DF, pp. 347-389.

Amadeo, F. A. C. and M. C. Santos (1988). "Métodos de posicionamento hidrográfico e obtenção de profundidades." *Anais do V Encontro Nacional de Engenheiros Cartógrafos,* Presidente Prudente, SP. pp. 41-51.

Santos, M. C. (1989). "Estudo sobre a aplicação do NAVSTAR/GPS à gravimetria marinha, na correção Eötvös." *Anais Hidrográficos,* Tomo XLVI, 1989, pp. 55-59.

Santos, M. C. (1990). "NAVSTAR/GPS: aspectos teóricos e aplicações geofísicas." Publicação Especial No. 7, Observatório Nacional do Rio de Janeiro, 1990, 127 p.

Santos, M. C. (1991). "Análise espectral da duração do dia, através de 3 anos de dados diários do IERS." Anais do XV Congresso Brasileira de Cartografia, Vol. I, São Paulo, SP, pp. 53-60.

Santos, M. C. (1992). "Variações de alta frequência da duração do dia." Revista do Instituto Geográfico e Cadastral, Vol. 11, Lisboa, Portugal, pp. 51-56.

Vajda, P., M. C. Santos, P. Ong, M. Craymer and P. Vaníček (1992). "A comparison of geoidal deflections computed from UNB'91 geoid with observed astrodeflections." EOS Trans., AGU, April, p. 81 (Abstract only).

Santos, M. C. (1994). "On the principles of orbit improvement and the generation of ephemerides for GPS satellites." Presented at the Fifth Annual Atlantic Institute Research Conference, Fredericton, N. B., Canada, 13-14 May.

Santos, M. C. (1994). "Survey of scientific GPS software suites." Available through the Canadian Space Geodesy Forum (CANSPACE) File Archives, via anonymous ftp unbmvs1.csd.unb.ca, University of New Brunswick, Fredericton, N.B., Canada.

Santos, M. C., P. Vaníček and R. B. Langley (1995). "Real-time improvement of GPS satellite orbits: the approach and first results." Submitted to the 25th General Assembly, International Union of Geodesy and Geophysics, Boulder, Colo., U.S.A, 2-14 July.